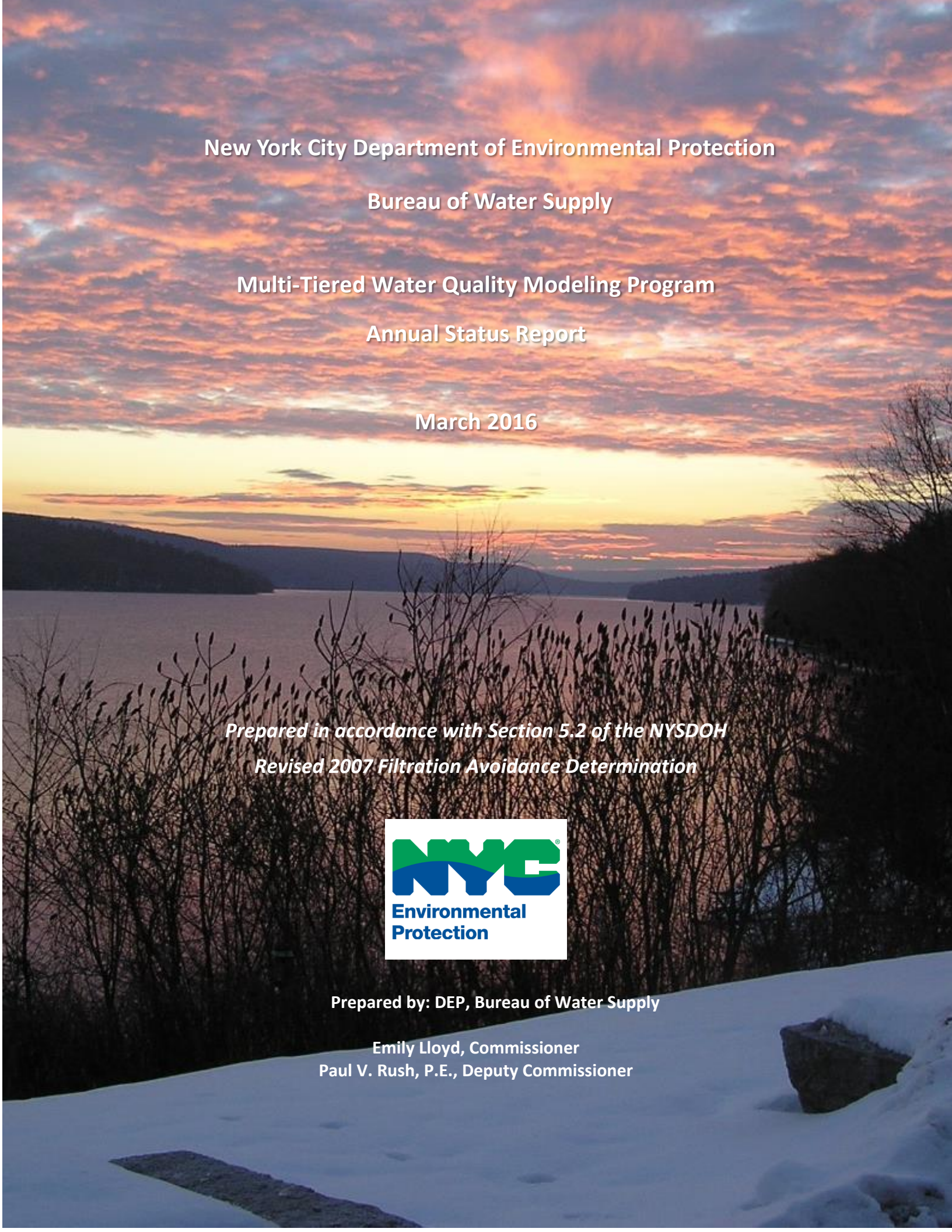

New York City Department of Environmental Protection

Bureau of Water Supply

Multi-Tiered Water Quality Modeling Program

Annual Status Report

March 2016

Prepared in accordance with Section 5.2 of the NYSDOH Revised 2007 Filtration Avoidance Determination

Prepared by: DEP, Bureau of Water Supply

Emily Lloyd, Commissioner
Paul V. Rush, P.E., Deputy Commissioner

Table of Contents

List of Figures

List of Tables

Acknowledgements

This report was produced by the Water Quality Modeling group of Water Quality Science and Research (WQSR), Directorate of Water Quality, in the Bureau of Water Supply at DEP.

During 2015, the Water Quality Modeling group was fortunate to have the services of 4 post-doctoral researchers who are employed by the City University of New York (CUNY), and worked day-to-day as a part of the Water Quality Modeling Group under contract with DEP (see Section 7.5). These individuals, and the report sections which they authored, are: Nachiketa Acharya, Ph.D. (Section 3.2), Linh Hoang, Ph.D. (Section 4.1), Yu Li, Ph.D. (Section 4.2), and Kyongho Son, Ph.D. (Section 4.5). These researchers are supported by the following faculty advisors: Allan Frei, Ph.D. (Hunter College, CUNY), Tammo Steenhuis, Ph.D. (Cornell University), Paul Hanson, Ph.D. (University of Wisconsin), and Larry Band, Ph.D. (University of North Carolina).

Rakesh Gelda, Ph.D., Research Scientist in the Water Quality Modeling group at DEP was the author of Section 4.3, while Jordan Gass, GIS Specialist in the Water Quality Modeling group was the author of Section 6. Emmet Owens, P.E., Section Chief of Water Quality Modeling, authored Sections 4.4, 5.1, and 5.2, and was responsible for overall report editing and production. Karen Moore, Ph.D., in the Program Evaluation and Planning group within WQSR, provided information on modeling simulations to support operational decisions made in early 2015 (Section 2), and on interactions with GLEON (Section 7.4). Lorraine Janus, Ph.D., Chief of Water Quality Science and Research, provided overall support and guidance for the Water Quality Modeling program and completed the final review of this report.

The cover photograph was taken by Michael Reid of NYCDEP.

Executive Summary

The New York City Department of Environmental Protection (DEP) has maintained a program of water quality modeling for its water supply system for over 20 years. The general goal of this program is to develop and apply quantitative tools, supporting data, and data analyses in order to evaluate effects of land use change, watershed management, reservoir operations, ecosystem health, and climate change on water supply quantity and quality. The quantitative tools include models that simulate future climate conditions in the watersheds of the water supply reservoirs (weather generators), terrestrial/watershed models that simulate the quantity and quality of runoff from the watersheds entering the reservoirs, reservoir models that simulate mixing, fate and transport of water, heat and pollutants within the reservoirs themselves, and operations models that consider alternative operations of DEP's system of reservoirs in the delivery of high quality water in sufficient quantities to meet demand. This linked collection of models is DEP's "multi-tiered" modeling system. This report describes the activities in DEP's water quality modeling group in the development and application of models and supporting data during 2015.

As in past years, DEP's reservoir turbidity model was used to evaluate the impact of runoff events on turbidity in Kensico Reservoir. Simulations were made during one period in late March, 2015 in anticipation of a snowmelt and runoff event and associated potential increases in turbitiy. This model was also used to evaluate the impact of the closure of the Rondout-West Branch tunnel on turbidity in Kensico. Closure of that major aqueduct for a period of several months is planned to occur in 2022.

DEP has reliable turbidity models for Schoharie, Ashokan and Kensico Reservoirs; that same model framework has recently been extended to Rondout Reservoir. In July 2015, DEP began the process of rapid drawdown of Cannonsville Reservoir in response to a turbid groundwater discharge occurring at the base of the Cannonsville dam; plans to continue the drawdown for as much as 10 weeks were considered. Shortly after the drawdown began, the Rondout turbidity model was used to evaluate the impact of potential increases in the turbidity of Cannonsville associated with sustained drawdown of that reservoir on the downstream Rondout Reservoir. The simulations showed that, due to dilution and settling of turbidity-causing particles in Rondout, the Cannonsville drawdown would not increase turbidity levels in the water supply from Rondout to levels of concern. The actual drawdown of Cannonsville proceeded for about 3 weeks, resulting in a drawdown of only about 20 feet in this 150-foot deep reservoir. The modeling exercise demonstrated that Rondout Reservoir has the ability to withstand a 10-week period of sustained turbid inflow from an upstream reservoir without significantly affecting the turbidity of the withdrawal from Rondout.

The Schoharie, Ashokan, and Kensico turbidity models have been integragted into the Operations Support Tool (OST), DEP's reservoir operations model. Integration into OST allows these models to be operated using "position analysis". This feature allows forecasts of water supply quantity and quality to be made for a range of future weather conditions. While DEP has plans for integrating the Rondout model into OST, as an interim measure the capability to make position analysis simulations was added to the Rondout turbidity model in 2015. The utility of turbidity forecasts for Rondout using position analysis is demonstrated.

Research was conducted in 2015 on the development of stochastic weather generators for the application to the watersheds of the West of Hudson reservoirs. These models generate synthetic time series of weather variables such as precipitation and air temperature that have statistical properties which closely resemble observations, but contain extreme events that may not be captured in historical weather records. Significant analyses were conducted to evaluate and compare various alternative approaches to develop these generators, and a specific generator for precipitation occurrence and magnitude was developed. In future, DEP will use this and other generators in the application of so-called "bottom-up" evaluations of the impact of extreme events on the quantity and quality of the water supply. The weather generators will be used to generate time series of weather conditions, and evaluate the impact of extrement events, for both current and future climate conditions.

Also in 2015, DEP made significant progress in the application and testing of two terrestrial/watershed models. The Soil Water Assessment Tool (SWAT) was applied to the Town Brook watershed which drains to Cannonsville Reservoir, and the Regional Hydro-Ecologic Simlation System (RHESSys) was applied to the Biscuit Brook and Shelter Creek watersheds draining to Neversink Reservoir. These two models are distributed-parameter watershed models which consider spatial variations in watershed characteristics such as slope, soil type, and land use in simulating runoff quantity and quality. These model applications represent a significant advancement in watershed modeling at DEP, where previous work involved use of the General Watershed Loading Function (GWLF) model which uses a simpler lumped parameter approach. The availability of detailed geographical information system (GIS) data at DEP to provide detailed characterization of spatial variability in the watersheds supports the application of SWAT and RHESSys. These models offer the promise of increased accuracy in simulating both current conditions and in the evaluation of changes in land use and climate change.

A major new modeling initiative at DEP is the development of watershed and reservoir models to predict the origins, fate and trasport of the organic compounds that are precursors of disinfection byproducts (DBPs). DEP has begun to apply the linked General Lake Model - Aquatic Eco-Dynamics (GLM-AED) model as a part of this effort. As a first step in that project, the hydrothermal model GLM was applied, tested and validated for Cannonsville and Neversink Reservoirs for observed historical conditions occurring in 2007 and 2008. Using this physical

model as a foundation, the AED framework will be applied and tested in simulating the cycling of organic carbon and associated disinfection byproduct precursors.

DEP continued to develop and organize data to support model development, testing, and applications in 2015. This data includes GIS, meteorology, hydrology, and stream, reservoir and aqueduct water quality. Field work to measure bathymetry of the West of Hudson reservoir basins was completed in 2015. DEP continued its collaboration with various outside groups in activities associated with the modeling program. These outside groups and activities include participation in several Water Research Federation (WRF) research projects, acting as a participating utility in the Water Utility Climate Alliance (WUCA), active cooperation with the Global Lake Ecological Observatory Network (GLEON) including attending meetings and sharing data, and working with the faculty advisors who are an important component of DEP's agreement with the City University of New York (CUNY) to support the water quality modeling program.

1. Introduction

This status report describes work completed as a part of DEP's Multi-Tiered Water Quality Modeling program for the period January through December, 2015. This report was prepared in accordance with Section 5.2 of the 2007 Revised Filtration Avoidance Determination (NYSDOH, 2014).

The Water Quality Modeling program at DEP consists of development, testing, validation, and application of an integrated suite of models which allow evaluation of a range of water quality issues (Figure 1.1). The overarching water supply issue is the delivery of high quality water in a sufficient quantity to meet demand, under both normal and infrequently-occurring environmental conditions, both now and in the future. Particular water quality issues are eutrophication, disinfection byproducts, and turbidity. These issues are evaluated under changing conditions in the watersheds, including land use, population, and wastewater and stormwater management. The effect of changing climate conditions on water quantity and quality are also evaluated in the water quality modeling program.

DEP uses a suite of weather, watershed/terrestrial, reservoir, and system operations models in the water quality modeling program. In 2015, development of weather generators was initiated. Weather generators are models that generate a synthetic time series of weather conditions, the statistics of which are similar to observed historical time series, but which contain a more complete representation of extreme or infrequently-occurring conditions than historical records. Synthetic time series which represent both current and future climate conditions are generated.

Both historical and generated weather data are used in driving three watershed/terrestrial models. These models are used to predict the quantity and quality of watershed runoff and streamflow entering the various reservoirs. The Generalized Watershed Loading Function (GWLF) model has been tested and validated for the West of Hudson watersheds, and has been applied in a variety of evaluations. DEP is currently testing two watershed models that have a stronger physical basis compared to GWLF, these being the Soil Water Assessment Tool (SWAT) and the Regional Hydro-Ecologic Simlation System (RHESSys). Historical or generated weather data, and streamflow quantity and quality predictions from watershed models are then used as inputs to reservoir models. DEP's reservoir models are all capable of predicting thermal structure and hydrodynamics and mixing in the water column, and selective withdrawal characteristics associated with reservoir outflows. The two-dimensional (vertical/longitudinal) model CE-QUAL-W2 (W2) has been extensively tested and validated for simulation of turbidity, and is used to evaluate the impact of reservoir operations on water supply turbidity. One-dimensional eutrophication models (UFI-1D and Protbas) have also been extensively tested and

validated. The one-dimensional model GLM-AED is currently being tested with in the simulation of organic carbon cycling and precursors of disinfection byproducts in the reservoirs. The W2 turbidity model has been linked with the OASIS water supply system model in DEP's Operations Support Tool (OST), which simulates the operation of the multiple reservoirs that comprise the water supply system.

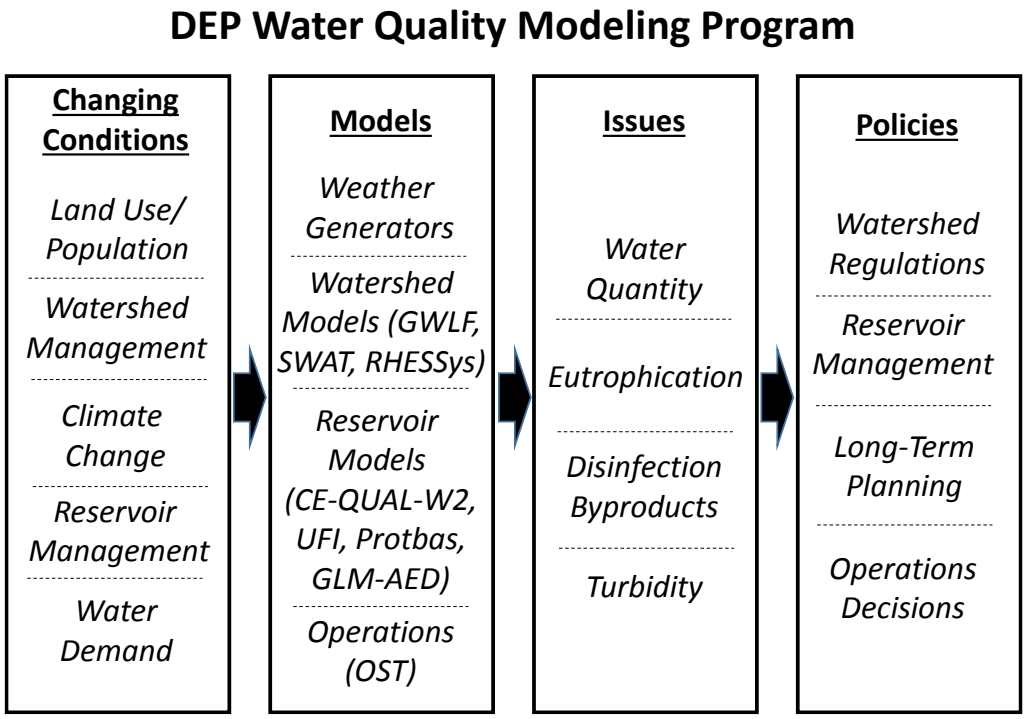

Figure 1.1. Overview of DEP's Water Quality Modeling Program.

This report focuses on activities in the Water Quality Modeling group at DEP in 2015, which includes the following:

- Use of reservoir turbidity models to support the operation of the City's water supply system during times of challenging turbidity conditions

- Developing model applications that simulate the impacts of future climate change on reservoir water quality and quantity; in particular, to develop and apply the "bottom-up" approach to investigate and identify potential vulnerabilities in the water supply system

- Continuing model development and testing based on ongoing model simulations, data analyses, and research results

- Development and testing of models which simulate the fate and transport of organic carbon and disinfection byproduct precursors in watersheds and reservoirs

- Updating and organizing of land use, watershed protection programs, and time-series data to support modeling

- Development and testing of models to support watershed management and long-term planning

- Continuing development of data analysis tools to support modeling

- Collaboration and outreach activities by DEP's Water Quality Modeling group

2. Use of Models for Support of Operational Decisions

In 2015, three separate CE-QUAL-W2 (W2) modeling analyses of turbidity were conducted, with all three involving simulations for Kensico Reservoir. Table 2.1 summarizes the model runs performed during this period. One model run in late spring was done in anticipation of a snowmelt and runoff event. The remaining model runs were carried out to aid in long-term planning in anticipation of a shutdown for repairs and bypass connection in the Rondout – West Branch Tunnel (RWBT) portion of the Delaware Aqueduct. The shutdown is scheduled for late 2022, and consequently, the normal method of reducing flow from the Catskill Aqueduct to mitigate the effects of elevated turbidity will not be available. The RWBT W-2 model runs in 2015 are a small part of the steps taken over the past few years in the analysis of Kensico effluent turbidity under a range of scenarios in preparation for the aqueduct shutdown.

Table 2.1. List of modeling analyses performed during the reporting period (January 1–December 31, 2015) including descriptions of each analysis.

Date	Background	Modeling Description	Results
01/23/2015	Planning for the future Rondout – West Branch Tunnel Shutdown necessitated W-2 model runs under a range of turbidity and flow scenarios. These modeling results are intended for discussion purposes.	Kensico reservoir positional analysis simulations were done to give insights on reservoir responses to low turbidity levels reduced by alum treatment. The simulation time period was 8 months (1 Oct – 31 May) and Catskill influent turbidity was set at 2.5, 3.0, and 4.0 NTU, and a flow of 636 MGD; Delaware influent turbidity was simulated at 1.5 NTU, and a flow of 175 MGD.	No exceedances of a 2.5 NTU internal guidance value threshold for the Kensico effluent occurred for the simulation period when the Catskill influent was at 3.0 NTU or less.

Date	Background	Modeling Description	Results
3/19/2015	Ongoing planning for the future Rondout – West Branch Tunnel Shutdown necessitated additional W-2 model runs. These modeling results are intended for discussion purposes.	Kensico Reservoir positional analysis simulations spanned an 8-month period (1 Oct – 31 May) and Catskill influent turbidity was set at 2.0, 2.5, 3.0, and 4.0 NTU, and a flow of 636 MGD; Delaware influent turbidity was simulated at 2.0 and 2.5 NTU, and a flow of 175 MGD.	For a constant Catskill input of 2.0 – 2.5 NTU, no exceedances are predicted for the entire shutdown period when the Delaware influent turbidity ranges from 1.5 – 2.5 NTU.
03/26/2015	Ashokan West Basin turbidity had risen to about 3 NTU due to spring snowmelt/rain events. Delaware System turbidity was less than 1 NTU. Kensico Reservoir turbidity ranged from 0.8 – 1.2 NTU in the reservoir on 3/11/15 based on transmissometer data and ranged from 1.1 – 1.4 NTU on 3/25/15 at the effluent. The reservoir was isothermal at this time.	Kensico Reservoir positional analysis simulations were run to provide guidance for aqueduct flow rates into Kensico Reservoir for the given current and possible future Ashokan effluent turbidity. The tested Catskill inflow rates were 400, 500, and 600 MGD with a Catskill Aqueduct turbidity of 4, 5, and 6 NTU for the period from March 25 – April 23.	The simulations indicated that Kensico effluent turbidity would remain below 2.5 NTU over a 30-day simulation period with input turbidity and flow in the following combinations: 4 NTU at 400, 500, and 600 MGD; 5 NTU at 400 and 500 MGD; and 6 NTU at 400 MGD. The maximum turbidity level of 2.5 NTU at the end of the simulation period occurred with a Catskill influent load of about 2700 NTU*MGD.

3. Modeling Applications of Climate Change Impacts

3.1. Climate Change Integrated Modeling Project

The Climate Change Integrated Modeling Project (CCIMP) encompasses the DEP Water Quality Modeling Section's effort to evaluate the effects of future climate change on the quantity and quality of water in the NYC water supply. The CCIMP is designed to address the following major issues: (1) overall quantity of water in the entire water supply; (2) turbidity in the Catskill System of reservoirs, including Kensico; (3) eutrophication in Delaware System reservoirs; and (4) disinfection byproducts in the West of Hudson reservoirs. The first phase of CCIMP was completed in 2013, so that 2015 was the second full year of work on Phase II.

Work completed in 2015 was mainly in two areas. First, research has been completed in the development and application of stochastic weather generators for the West of Hudson reservoir watersheds. This work is described in Section 3.2, and will be the basis for the application of the "bottom-up" approach to evaluation of climate change impacts. Application of the terrestrial model RHESSys to watersheds draining to Neversink Reservoir also continued in 2015, and is described in Section 4.5.

3.2. Evaluation of Stochastic Weather Generators (SWGs) for use in Simulating Precipitation

3.2.1. Introduction

Extreme hydrological events are in general responsible for a disproportionate loading of nutrients and sediment into the streams and reservoirs. Past studies suggest increasing trends in total precipitation and in the frequency and magnitude of extreme precipitation events in the watersheds of New York City's West of Hudson (WOH) reservoirs. Burns et al. (2007) analyzed precipitation trends for the period 1952 to 2005 and found that the regional mean precipitation for the Catskill Mountain region increased by 136 mm over the study period. Matonse and Frei (2013) found that warm season extreme precipitation events have been more frequent between 2002 and 2012 than any time during the 20th century. DeGaetano and Castellano (2013) found that the annual frequency of extreme Catskills precipitation (number of events that produce ≥50.8 mm precipitation per year) has an increasing trend over the last 60 years, with the time series dominated by year-to-year and decade-to-decade variability. They also analyzed the

climate model projections from the North American Regional Climate Change Assessment Program (NARCCAP) which suggests that extreme precipitation will increase at a rate of 2–3% per decade through 2069. The potential effects of these changes in precipitation include increased sediment erosion, increased nutrient loads, modifications to thermal stratification, and other factors that may pose challenges for water management.

As a part of the NYCDEP's ongoing program on Climate Change Integrated Modeling Project (CCIMP), a series of studies (Anandhi et al., 2011a; Anandhi et al., 2011b; Pradhanang et al. 2011; Anandhi et al., 2013; Matonse et al., 2013; Pradhanang et al., 2013) have examined the potential impacts of climate change on the availability of high quality water in the WOH reservoirs. These studies have followed the "top-down" approach, using downscaled climate scenarios from Global Climate Models (GCMs), to incorporate climate change into vulnerability analyses. The Change Factor Methodology (CFM), sometimes referred as a delta change factor, has been used to downscale the GCM's scenarios (baseline and future) which was further used as inputs to the NYCDEP's integrated suite of hydrological models including watershed hydrology, water quality, water system operations, and reservoir hydrothermal models (Anandhi et al., 2011a). The monthly change factor was calculated as the difference for air temperature or ratio for precipitation and wind speed between baseline and future simulation of GCM. This difference or ratio is then applied to local meteorological data to create future local climate scenarios (Anandhi et al., 2011a).

"Bottom-up" or vulnerability-based methods to climate change adaptation have recently been applied to water resources (Wilby and Desai, 2010; Brown et al., 2011). Such approaches can explore the climate vulnerabilities of a system over a wider range of plausible climate change scenarios than the more traditional "top-down" approaches in which GCM projections completely define the parameter space of future scenarios (Wiley and Palmer, 2008; Steinschneider and Brown, 2013). The bottom-up approach first determines the system vulnerabilities and then assesses different adaptation measures to find the most robust measure under future uncertainty (Steinschneider and Brown, 2013). While the bottom-up approach includes the results of GCM simulations, it also enables more quantifiable and flexible definition of uncertainty. An integral component of the bottom-up approach includes stochastic weather generators (SWGs).

SWGs are statistical models that produce synthetic weather time series based on observed statistical properties at a particular location. SWGs are often employed in bottom-up risk assessments to generate several scenarios of daily climate within which a water resource system can be tested (Ray and Brown, 2015). A SWG coupled with a single or series of response models facilitates a more complete identification of system vulnerabilities, and flexible, quantitative definitions of uncertainty, which can aid in the selection of robust adaption measures (Steinschneider and Brown, 2013). There has been limited application of SWGs for vulnerability assessments of the WOH supply system. Rossi et al. (2015) used a multivariate, multisite

weather generator for introducing incremental changes in mean precipitation and temperature to simulate a range of climate change scenarios to study the turbidity levels in Ashokan reservoir. However, the skill (accuracy) of weather generators to simulate the observed precipitation characteristic is not discussed. As there are a number of categories and types of SWGs available in the literature with different levels of complexity (number of model parameter), and their skill in simulating observed precipitation characteristics is very location specific (Chen and Brissette, 2015), there is a need to assess different SWGs for the WOH supply system prior to using them to generate future scenarios.

This section describes application of a variety of SWGs, including selections from different categories, for each of the WOH watersheds in order to assess their skill in simulating the overall statistical characteristics, as well as the extreme statistical characteristics, of daily precipitation.

3.2.2. Data

Observed daily precipitation data were obtained from Northeast Regional Climate Center (NRCC) at Cornell University. A total of 18 National Climate Data Center (NCDC) rain gage stations are non-uniformly distributed across the WOH watersheds (Figure 3.1). To ensure a uniform comparison period for each station, the precipitation data for the period of 1950 to 2009 were used. As the focus of the study is to analyze the average precipitation over each watershed, the weighted mean of nearby stations was calculated to get a single time series for each watershed. The Thiessen polygon method, a graphical technique, was used to estimate the weights based on the relative areas of each measurement station in the Thiessen polygon network. Individual weights were multiplied by the station observation and the values are summed to obtain the areal average precipitation. Table 3.1 describes the nearest stations and their corresponding weights for each watershed. Anandhi et al (2011) gives details about the construction of the area average precipitation data for WOH watersheds.

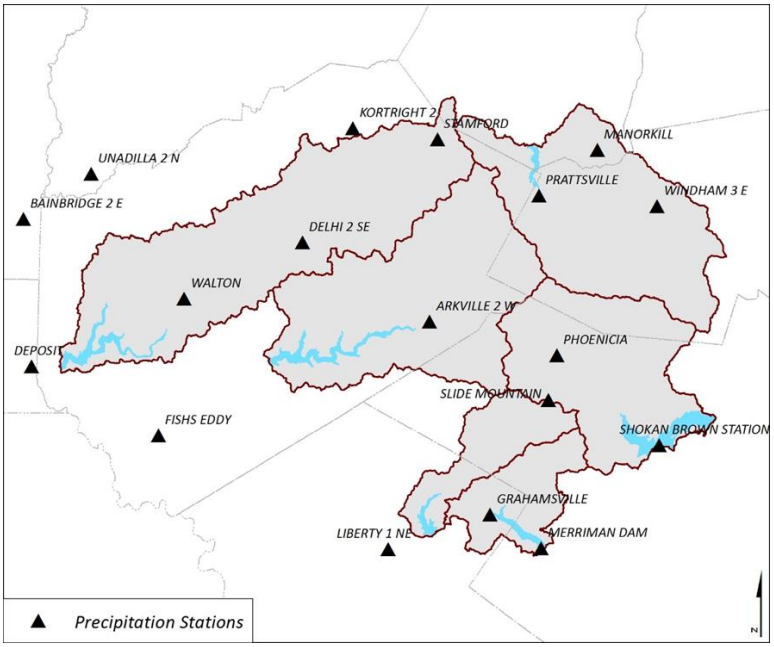

Figure 3.1. Precipitation gage stations over the study region.

Table 3.1. Description of the nearest stations and associated weights for estimating weighted mean precipitation for each of WOH watersheds

Watershed	Stations
Schoharie	Windham 3E (0.4434), Prattsville (0.2992), Manorkill (0.1694), Stamford (0.0468), Phoenicia (0.0389), Shokan Brown (0.0024).
Ashokan	Phoenicia (0.4985), Shokan Brown (0.3401), Slide Mountain (0.1413), Windham 3E (0.02)
Cannonsville	Walton (0.3526), Delhi 2SE (0.2948), Kortright 2 (0.1143), Stamford (0.1532), Arkville 2W(0.0068),Bainbridge 2E (0.0085),Deposit (0.0568), Fish Eddy (0.0013), Unadilla 2N (0.0118),
Pepacton	Arkville 2W(0.5564), Delhi 2SE (0.1876), Prattsville (0.1282), Stamford (0.0523), Phoenicia (0.0397), Slide Mountain (0.0181), Walton (0.0175), Fish Eddy (0.0002)
Neversink	Slide Mountain (0.5013), Grahamsville (0.3640), Liberty 1 NE (0.1347),
Rondout	Grahamsville (0.5796), Merriman Dam (0.2118), Slide Mountain (0.2084),Shokan Brown (0.0002),

Weights corresponding each station are in parentheses. All the weights add up to 1 for each watershed.

3.2.3. Stochastic Weather Generators

Stochastic weather generators (SWGs) are statistical models that produce synthetic time series of any desired length of weather variables. These time series have statistical properties (example mean, standard deviation, skewness coefficient etc.) resembling those of a specified station record. SWGs have wide applications in the modeling of weather and climate-sensitive systems such as crop growth and development, hydrological process and ecological systems where the observed climate records are inadequate in terms of length or completeness (Wilks and Wilby, 1999). A plethora of early studies dedicated to the development and advancement of SWGs (Gabriel and Neumann, 1962; Todorovic and Woolhiser, 1975; Katz, 1977; Richardson, 1981) have been summarized in several review articles (Wilks and Wilby, 1999; Srikanthan et al., 2001; Alliot et al., 2015). SWGs can be broadly classified into four groups: two-part model (first part is dedicated to precipitation while the second part deals with other meteorological variables such as temperature or solar radiation), resampling model, transition probability model and auto regressive moving average (ARMA) model (Srikanthan et al., 2001). The first two approaches are most popular in the literature. In this study, we only discuss the precipitation generation in two-part model, and the resampling model.

Precipitation can be measured as both a discrete (occurrence) and continuous (amount) variable, has always been a key variable of interest in the construction of SWGs (Wilks and Wilby, 1999). In the two-part model, SWGs analyze precipitation as a chain-dependent model, first simulating precipitation occurrence (wet or dry day) and then precipitation amount. Occurrence is usually simulated using either a Markov Chain (MC) based model or a renewal process, sometimes referred to as a spell - length model. Two-state (i.e., precipitation occurs or does not occur) MC models based on the occurrence or non-occurrence of precipitation relate the state of the current day to the states of preceding days, where the number of preceding days considered as the order of the MC (Boulanger et al., 2007). Although, the first-order MC model (depends only on the previous day) has been found satisfactory in most of the cases (Katz, 1977; Richardson, 1981, Wilks, 1992), the higher order is better to simulate long wet and dry spells (Wilks, 1999; Chen and Brissette, 2014). The alternating renewal process, rather than simulating occurrence for each day, fits a probability distribution to the sequence of alternating wet and dry spells which are assumed to be independent (Buishad, 1978; Roldan and Woolhiser, 1982; Semenov and Barrow, 2002). Various probability distributions have been evaluated for the best fit of wet and dry spells such as logarithmic series, truncated negative binomial distribution, truncated geometric distribution, and semi-empirical distribution (Wilks and Wilby, 1999).

Given the occurrence of a wet day, the daily precipitation amount is then modeled, typically using a parametric distribution. The distributional pattern of daily precipitation is strongly skewed to the right as very small daily precipitation events occur frequently, while heavy daily precipitation events are relatively rare (Wilks and Wilby, 1999; Chen and Brissette,

2014). Numerous studies have compared several probability distributions for simulating daily precipitation, including both single and compound distributions such as exponential (Todorovic and Woolhiser, 1975; Roldan and Woolhiser, 1982), gamma (Ison et al., 1971; Richardson and Wright, 1984), Weibull (Stöckle et al., 1999), skewed normal (Nicks and Gander, 1994), mixed exponential distribution (Roldan and Woolhiser, 1982; Wilks, 1999b) and hybrid exponential and Pareto distributions (Li et al., 2012; Chen and Brissette, 2014). In addition to the probability distribution, some other theoretical constructs have been applied to generate precipitation amount. For example, Boulanger et al (2007) introduced multi-layer perceptron-based neural network to generate synthetic time series of precipitation. Chen et al (2015) proposed the use of a 2^{nd} degree polynomial curve fitting approach to fit a Weibull experimental frequency distribution of observed daily precipitation constrained on the probable maximum precipitation (PMP) for the generation of precipitation amount.

The resampling model, a data driven method, provides an alternative to the above discussed two-part model. The k-nearest-neighbor (k-NN) conditional bootstrap approach, the most popular resampling scheme for SWG, generates daily weather variables by resampling (with replacement) historical records associated with the wet-dry day series (Rajagopalan and Lall; 1999). The "k - nearest neighbors" for each date are chosen by considering all historical dates within a specified time window. Subsequently, the k – nearest neighbor with a higher probability to closer neighbors is chosen (King et al., 2015). After the pioneering work by Young (1994) and Sharma and Lall (1997), a number of studies extended and improved the k-NN approach (Rajagopalan and Lall; 1999; Buishand and Brandsma, 2001; Yates et al., 2003; Sharif and Burn, 2007; Apipattanavis et al., 2007, Steinschneider and Brown, 2013; King et al., 2015). Following the aforementioned concepts, several SWGs have been developed and widely used for precipitation generation over the last few decades (Table 3.2).

3.2.4. Implementation of SWGs

In this study, we applied a chain-dependent model which first generate precipitation occurrence and then simulate precipitation amount in wet days. We used MC based model to generate precipitation occurrence, while parametric probability distributions, resampling method and curve fitting techniques are used to generate precipitation amount. The overall methodology to implement SWG in this study is shown in Figure 3.2.

To generate precipitation occurrence, we adopted a first-order two-state (i.e., wet or dry day) MC model which has advantage over alternating renewal process to handle the seasonality in the rainfall occurrence process (Sirkanthan and McMahon, 2001). As discussed in earlier section, MC based on the relationship between the states of the present day with previous days.

While MC models of orders 1, 2 and 3 (MC1, MC2 and MC3) were applied, in this study, wet and dry day are discriminated by a precipitation threshold of 0.1 mm.

To generate precipitation amount, seven distribution models including five parametric distributions, one resampling method (k-NN), and one curve fitting method, were investigated. Parametric distributions include three single distributions: exponential (1-parameter), gamma (2-parameter), and skewed-normal (3-parameter) - and two compound distributions - mixed exponential distribution (3-parameter) and a hybrid exponential and generalized Pareto (3-parameter) distribution. The 2nd order polynomial-based curve fitting method used in this study, fit a Weibull experimental frequency distribution of observed daily without constrained on the PMP. More details of each model are found in Table 1.3.

Table 3.2. Description of some popular SWG with their precipitation occurrence and amount components and respective reference.

Name	Precipitation occurrence and amount component	Reference
WGEN	First-order MC for Precipitation occurrence and Gamma distribution for precipitation amount	Richardson, 1981; Richardson and Wright, 1984
SIMMETEO	Same as WGEN but use monthly data as input instead of daily	Geng et al., 1988; Soltani and Hoogenboom, 2003; Elshamy et al., 2006
CLIGEN	First-order MC for Precipitation occurrence and skew-normal distribution for precipitation amount	Nicks & Gander (1994)
GEM	First-order MC for Precipitation occurrence and mixed exponential distribution for precipitation amount	Hanson and Johnson, 1998
CLIMGEN	Second-order MC for Precipitation occurrence and Weibull distribution for precipitation amount	Stockle et al., 1999
WGENK	Modification of WGEN by introducing seasonality	Kuchar, 2004
WeaGETS	Third-order MC for Precipitation occurrence and mixed exponential distribution for precipitation amount	Chen et al., 2012b
LARSWG	semi-empirical distribution to simulate precipitation occurrence and daily precipitation amounts	Semenov and Barrow, 2002
KnnCAD	Precipitation occurrence and amount generated by Resampling the historical data based on k-NN method.	Prodanovic and Simonovic,2008; King et al., 2015

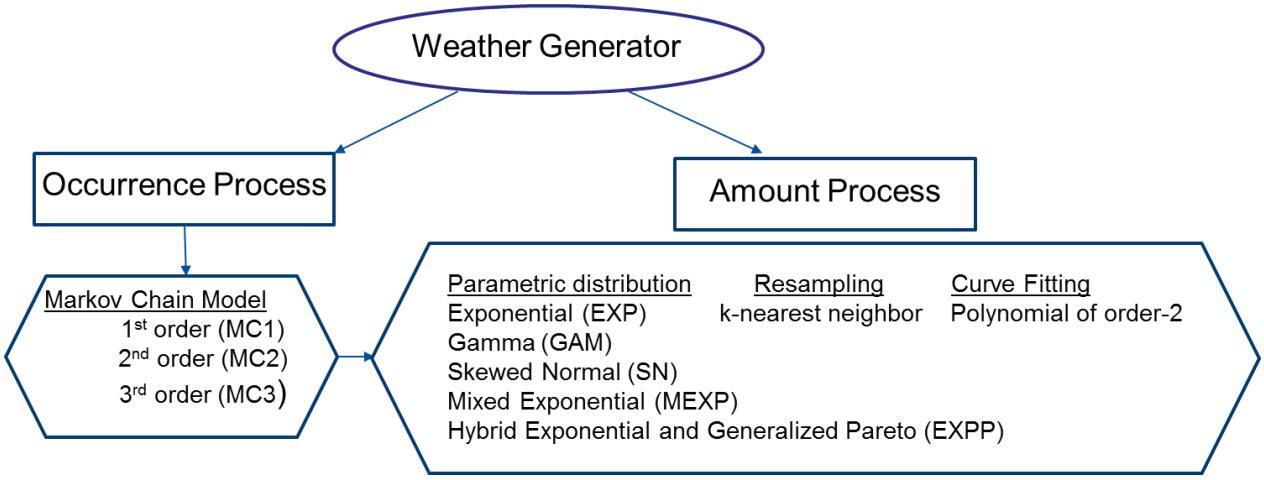

Figure 3.2. Flow chart showing the methodology of calibration of SWG.

Table 3.3. Seven models evaluated for generating daily precipitation amounts.

Model	Name	Abbreviation	Reference
Parametric	Exponential	EXP	Todorovic & Woolhiser (1975)
	Gamma	GAM	Ison et al. (1971), Richardson & Wright (1984)
	Skewed-normal	SN	Nicks & Gander (1994)
	Mixed exponential	MEXP	Woolhiser & Roldán (1982), Wilks (1999b)
	Hybrid exponential and generalized Pareto	EXPP	Li et al. (2012)
Resampling	k-nearest-neighbor conditional bootstrap	k-NN	Rajagopalan and Lall (1999)
Curve-fitting	2nd order polynomial	PN	Chen et al. (2015)

3.2.5. Statistical Evaluation of SWGs for daily precipitation characteristic

In this section, we examined the skill of SWGs, in terms of simulating the statistical characteristics of the full distribution of daily precipitation. To simulate daily precipitation, A SWG has to simulate both the occurrence and then the amount, each of which is evaluated independently.

3.2.5.1. Precipitation Occurrence

As discussed above, we discriminated wet and dry day using a precipitation threshold of 0.1 mm. Markov chain models of first order (MC1), second order (MC2) and third order (MC3), were compared with observations with respect to reproducing the frequency of wet days per month and the distribution of wet and dry spells.

To estimate the frequency of wet days per month, we first calculate the number of days which is equal or greater than the threshold (0.1 mm/day) for each month, and determine the mean and standard deviation for all twelve months (Figure 3.3). To calculate the distribution of wet and dry spells, we first define wet (dry) spells as the consecutive days with precipitation more (less) than threshold values. The mean and standard deviation of the number of wet days, and wet and dry spells, were predicted equally well by all three models (Figure 3.3, Figure 3.4, Figure 3.5). The models also performed well for extreme values (Figure 3.4, Figure 3.5).

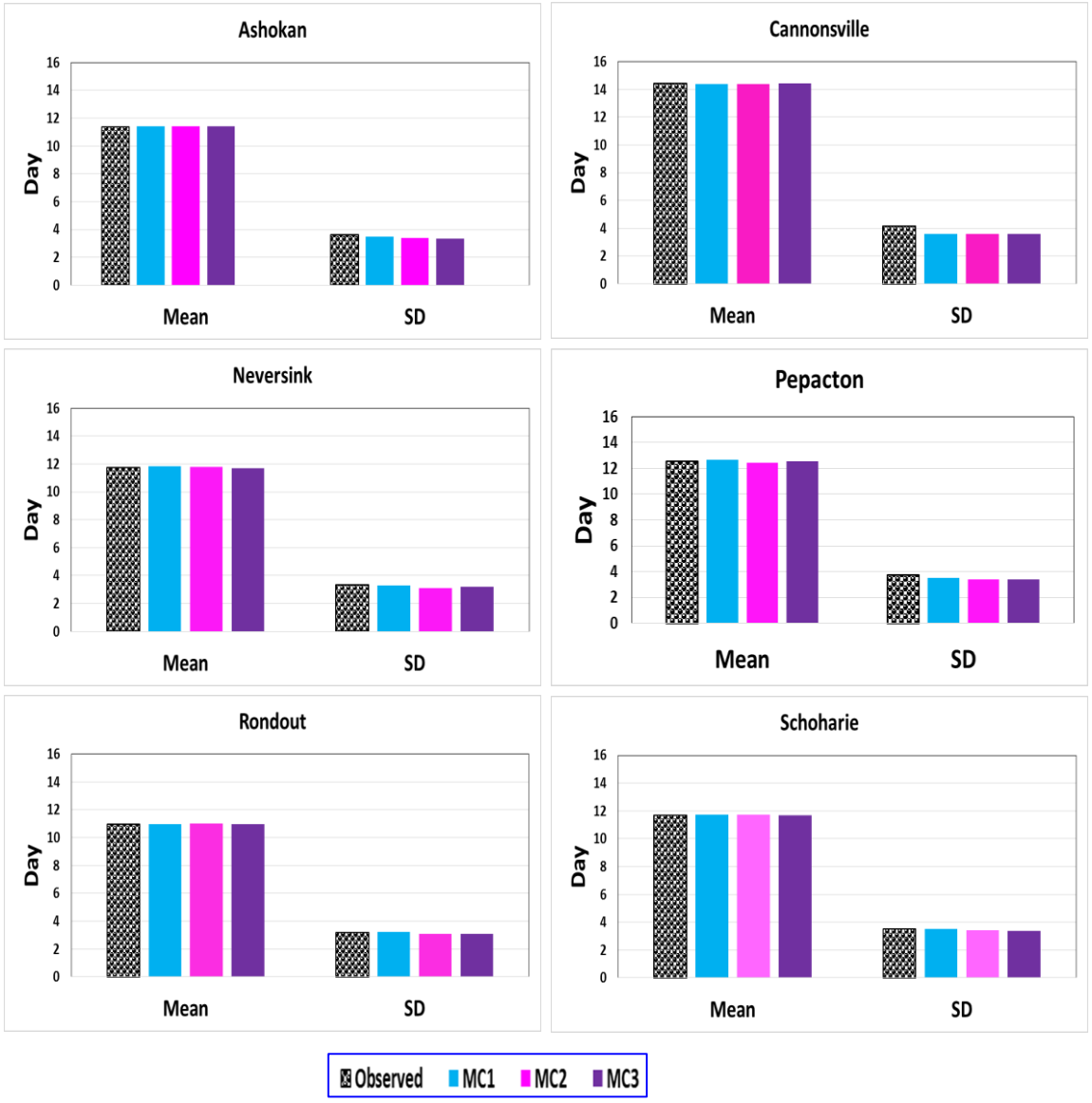

Figure 3.3. Mean and standard deviation of the observed and generated counter part of wet days per month from MC1, MC2 and MC3.

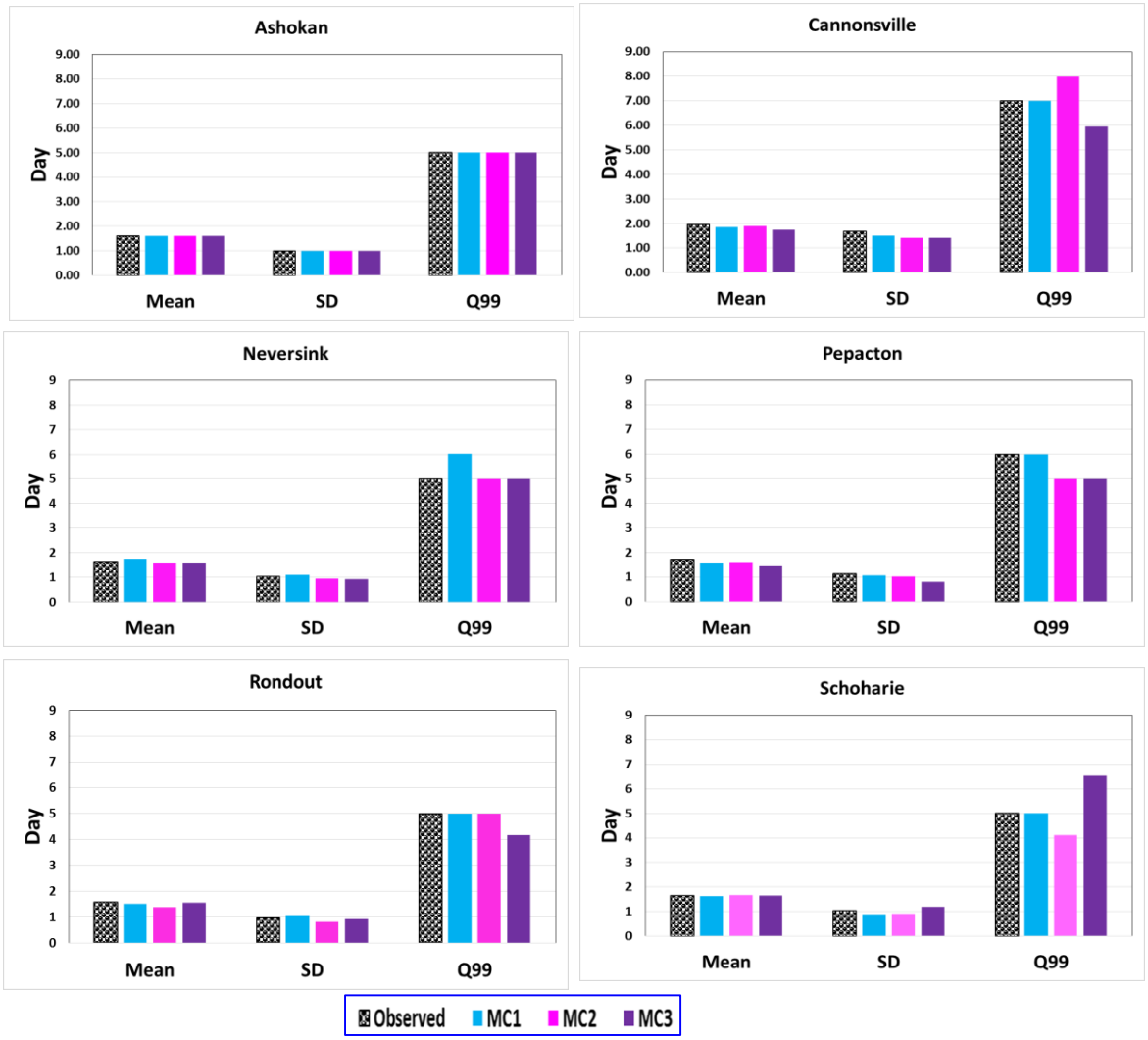

Figure 3.4. Mean, standard deviation and extreme (Q99) of wet spells of the observed and generated counterpart from MC1, MC2 and MC3.

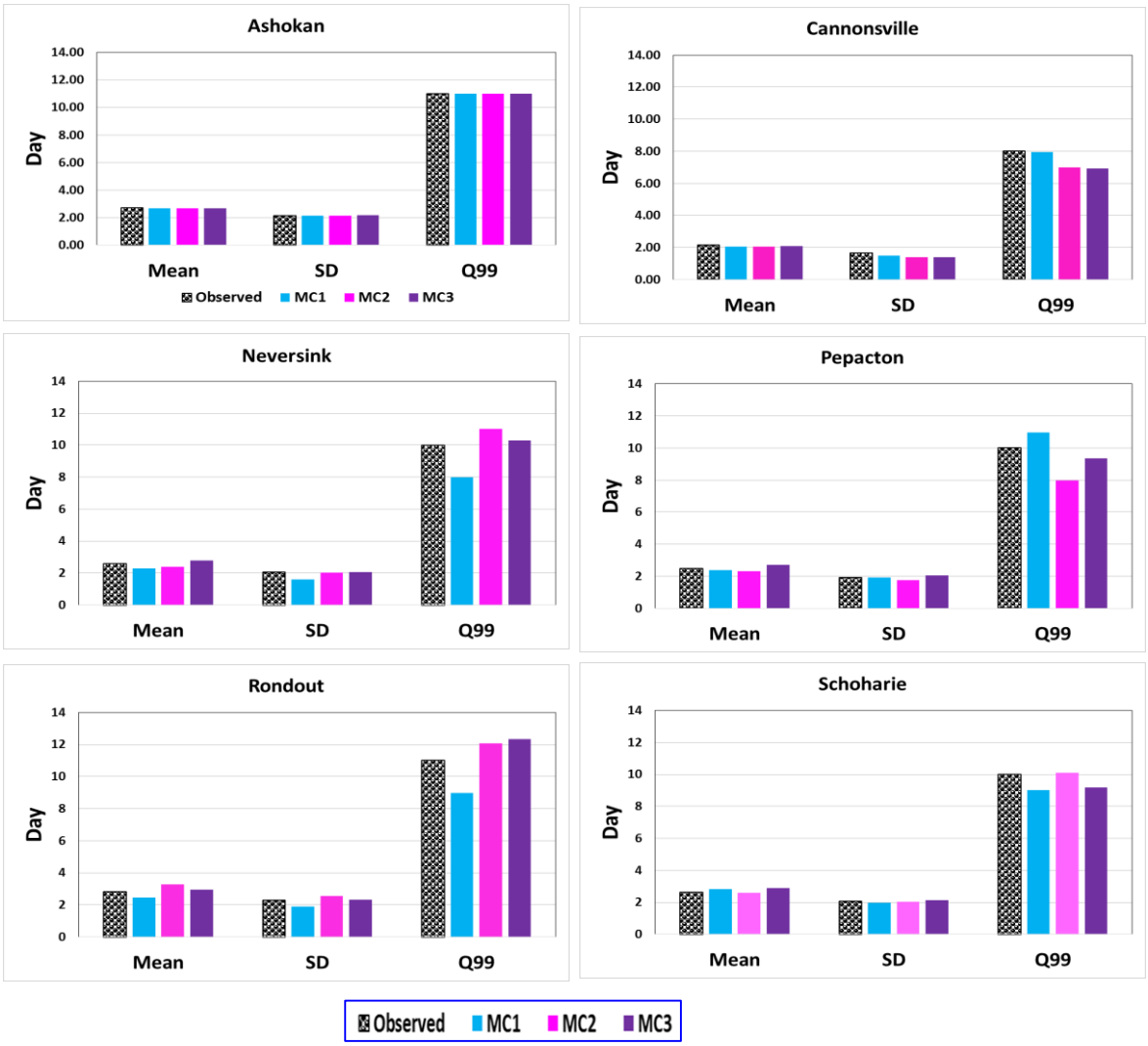

Figure 3.5. Mean, standard deviation and extreme (Q99) of dry spells of the observed and generated counterpart from MC1, MC2 and MC3.

3.2.5.2. Precipitation Amount

Daily precipitation amounts simulated by the seven models described in the methodology section were evaluated. The mean, standard deviation and skewness coefficients of daily precipitation amount (precipitation equal to or more than 0.01 mm/day) was calculated for observation and generated counterpart for each watersheds (Figure 3.6). All seven models simulate the mean of daily precipitation very well for all watersheds. However, the skills of the models in reproducing the observed standard deviation and skewness coefficients vary. The EXP and GAM distributions (for abbreviations, see Table 3.3) consistently underestimate the standard deviation, while the SN, MEXP and k-NN-based models perform well. EXPP and PN considerably overestimates the standard deviation for most watersheds.

The skewness coefficient of daily observed precipitation exceeds 3.0 for most of the watershed, implying the distribution of daily precipitation is extremely skewed to the left. EXP and GAM consistently underestimate the skewness coefficient while SN, k-NN, and MEXP adequately simulate the skewness. EXPP and PN overestimate the skewness coefficient for all six watersheds especially for the Schoharie watershed. Similar results for these distributions have been reported on for other watersheds (e.g. Chen and Brissette, 2014). Moreover, skewness coefficients are poorly simulated by the EXP, GAM, EXPP and PN models, indicating that they poorly preserve the shape of the daily precipitation distribution. To understand this issue in more detail, we plotted the probability density function (pdf) for observed data along with each of the seven models to understand the probabilistic structure of the daily precipitation. Figure 3.7 shows the result for the Ashokan watershed, where it is seen that SN, MEXP and k-NN's are very close to the observed pdf. The pdf plot of EXPP and PN indicates that these two approaches generate unreasonably high values which is likely the reason for their overestimation of the statistical characteristics of the entire time series. This results are very similar for the remaining watersheds.

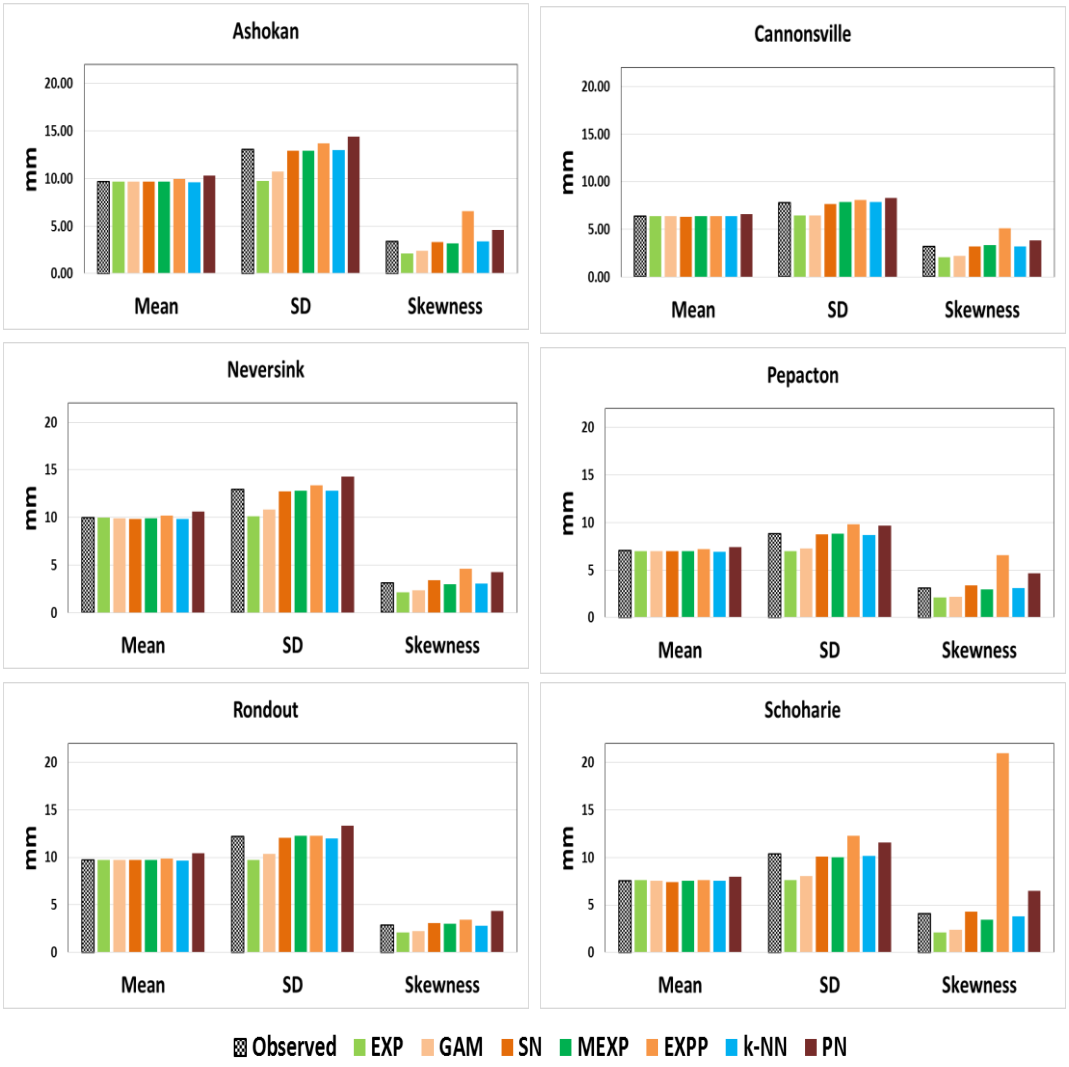

Figure 3.6. Mean, standard deviation and skewness coefficients of observed and generated daily precipitations from seven models (EXP, GAM, SN, MEXP, EXPP, k-NN and PN).

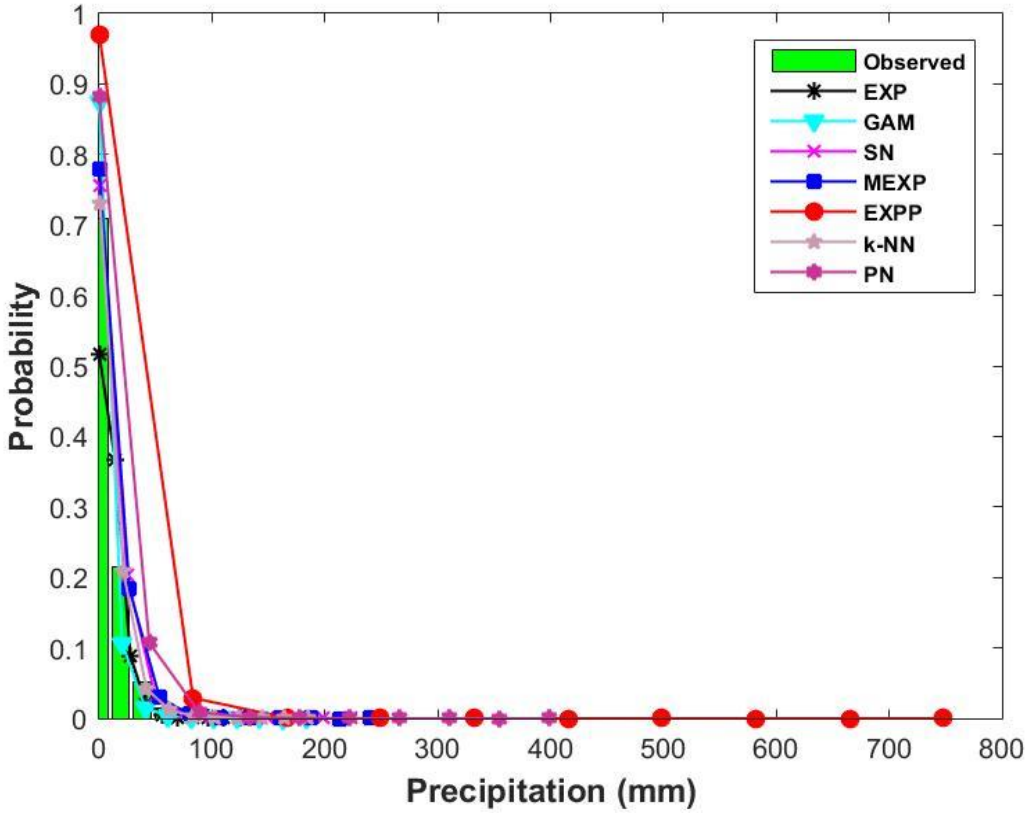

Figure 3.7. Probability distribution functions of observed and generated daily precipitations from seven models (EXP, GAM, SN, MEXP, EXPP, k-NN and PN) for Ashokan watersheds.

3.2.6. Performance of SWGs for Extreme Precipitation Events

In addition to the metrics considered above, it is important to evaluate the SWGs regarding their capacity to represent extreme event probabilities. In the present section, we examined each seven precipitation amount models with respect to their capacity to reproduce the observed extremes. To define the extreme events, both non-parametric and parametric approaches are employed.

3.2.6.1. Non-parametric Approach

A set of 27 climate extremes indices based on daily temperature and precipitation has been proposed by The Expert Team on Climate Change Detection and Indices (ETCCDI) (Klein Tank et al., 2009). Due to their robustness and fairly straightforward calculation and interpretation, these indices have become popular in recent decade for multiple applications in climate research. A complete description of the indices, including definitions and computation methods, is provided by Zhang et al. (2011). Following this work, the four extreme event indices associated with large precipitation events were computed. These indices are:

- RX1day: Maximum 1-day precipitation per year.
- RX5day: Maximum consecutive 5-day precipitation per year.
- R95p: Annual total precipitation due to events exceeding the 95th percentile of the entire data period (1950-2009).
- R99p: Annual total precipitation due to events exceeding the 99th percentile of the entire data period (1950-2009).

The indices were computed each year both for the observation and generated counter part by using "RClimDex", an R-based software application which was developed by Xuebin Zhang and Feng Yang at the Climate Research Branch of Meteorological Service of Canada. The mean of each index over the study period is shown in Figure 3.8. All seven models overestimate R95p and R99p for the Cannonsville and Rondout watersheds. For the Neversink and Pepacton watersheds, all models overestimate R95p and R99p except EXP and GAM (whose simulations are reasonable). For Ashokan and Schoharie, SN, MEXP, EXPP and k-NN adequately reproduce R95p and R99p, while EXP and GAM underestimate and PN overestimate R95p and R99p.

3.2.6.2. Parametric Approach

In order to evaluate the abilities of SWGs to simulate the probabilistic structure of observed extreme precipitation events, extreme value theory (EVT) was applied. The general extreme value (GEV) distribution was fitted to the annual maximum precipitation to estimate precipitation values associated with return periods of 50, 75, and 100 years of observed and generated counterpart by the seven models for each watershed (Figure 3.9). In GEV, the return level associated with the extreme events can be calculated by the quantiles of GEV (Coles, 2001). The detailed procedure of such technique consists of three steps: 1) calculate the annual maximum rainfall; 2) fit the GEV distribution; and 3) estimate the return level by calculating the quantiles of GEV distribution (Figure 3.9). SN, MEXP and k-NN are superior to the other distributions in simulating extreme value statistics, though their skills also not perfect. EXP and GAM models consistently underestimate precipitation amount corresponding to all return

periods. EXPP and PN do not accurately reproduce the upper tail of the observed daily precipitation.

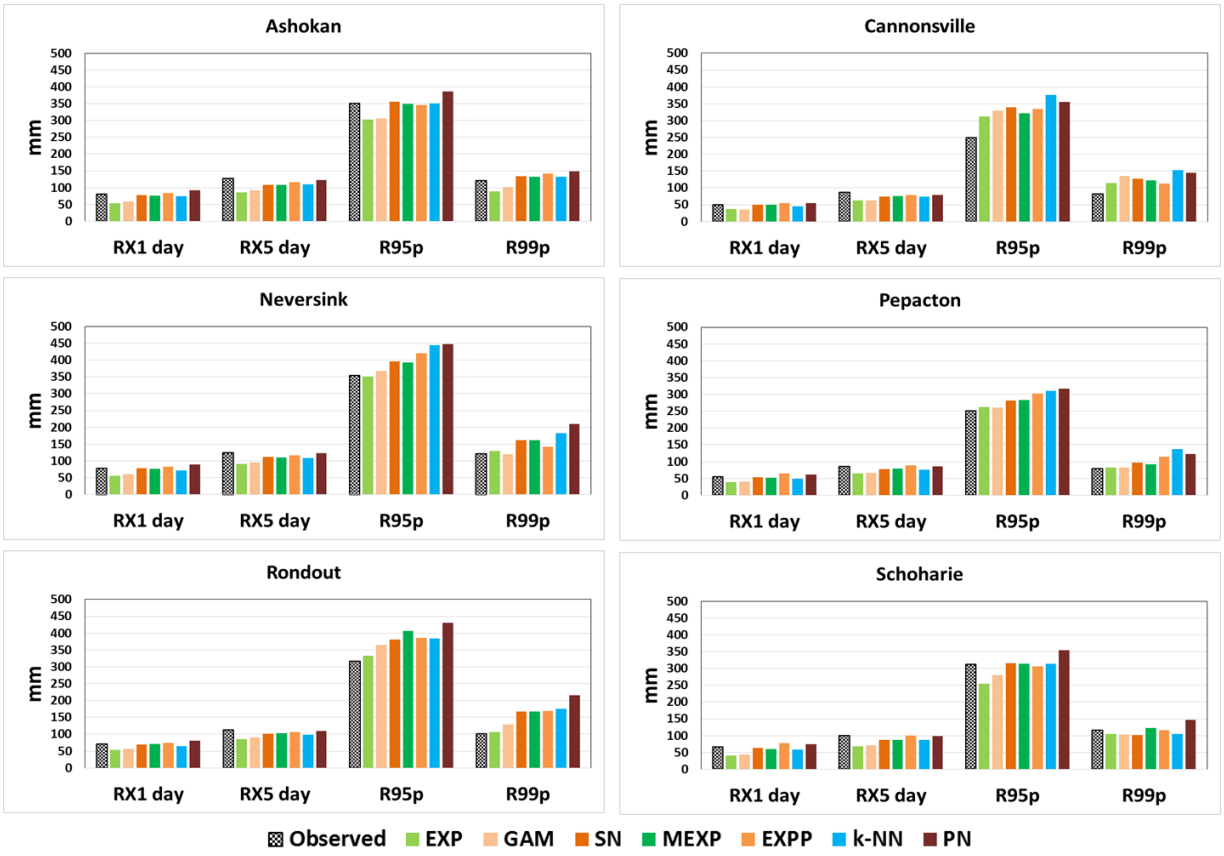

Figure 3.8. RX1day, RX5day, R95p and R99p of observed and generated daily precipitations from seven models (EXP, GAM, SN, MEXP, EXPP, k-NN and PN).

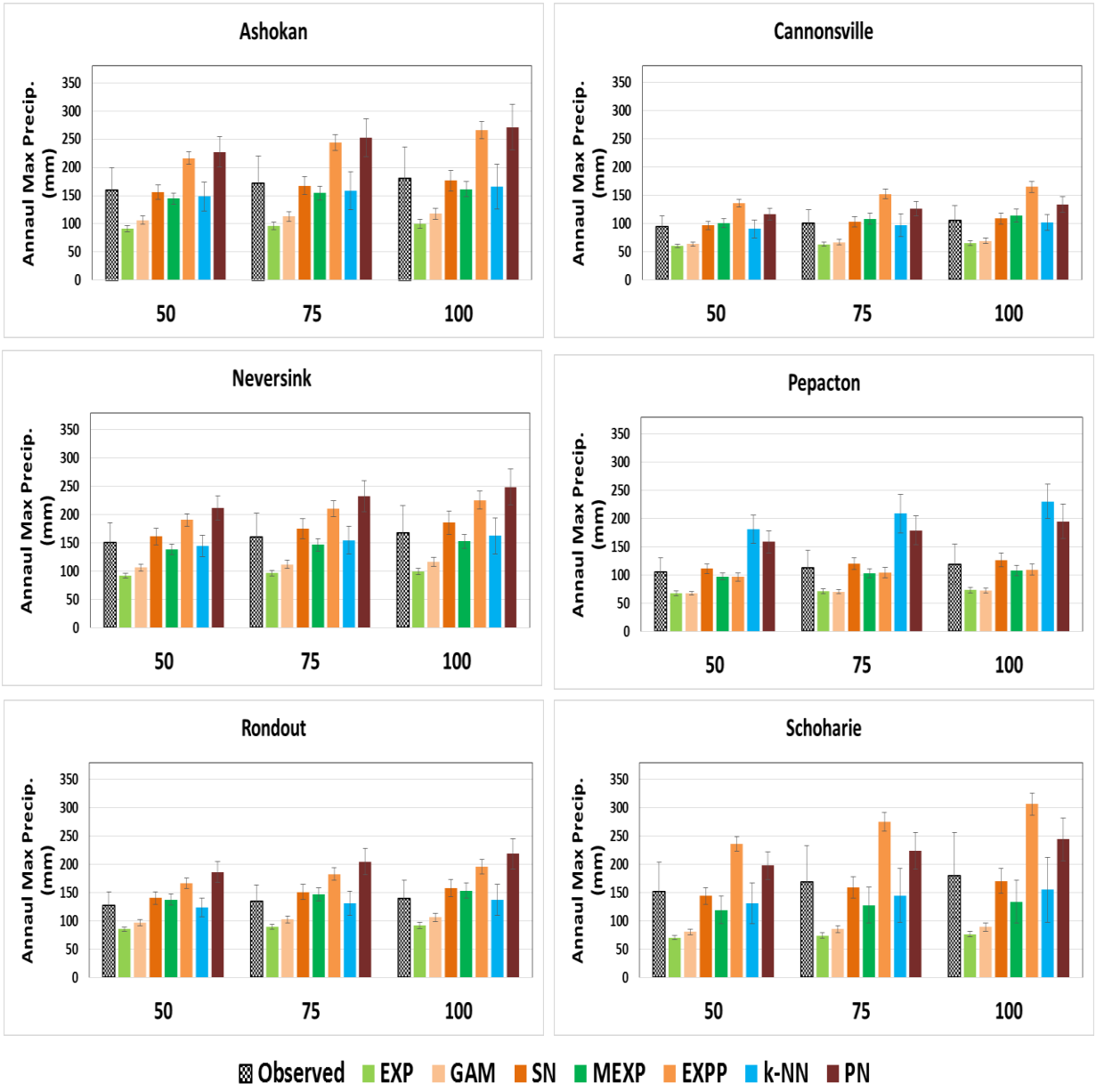

Figure 3.9. Annual maximum daily precipitation levels at the 50, 75 and 100 year return periods of observed and generated daily precipitations from seven models (EXP, GAM, SN, MEXP, EXPP, k-NN and PN). The error bars refers the 95% confidence interval for each return levels.

3.2.7. Discussion

This work compares the skill of three models for generating precipitation occurrence and seven models for simulating precipitation amount for six watersheds. Precipitation occurrence is adequately simulated by each of the three MC (MC1, MC2 and MC3) models for all watersheds. Considering the fact that the number of parameters in an MC model increases exponentially with each increase in order (Wilks, 1999), under the principle of parsimony the first order MC model (MC1) is chosen to simulate precipitation occurrence.

Of the seven models evaluated for generating daily precipitation amount, 5 are based on parametric distributions, one is based on a semi-parametric k-nearest neighbor bootstrapping technique, and one is based on a 2nd degree polynomial curve-fitting approach. Parametric distribution models include 3 single distributions (1-parameter EXP, 2-parameter GAM and 3-parameter SN), 1 compound distribution (3-parameter MEXP) and 1 hybrid distribution (3-parameter EXP-GP). While all these models reasonably reproduce mean daily precipitation for all the watersheds, their skills differ with regard to the standard deviation, skewness coefficient and extreme characteristics of daily precipitation. With the exception of SN, all the other single distributions (EXP and GAM) consistently underestimate the standard deviation and skewness coefficient of daily precipitation for all watersheds, suggesting that these 2 distributions underrated the high frequency variability of precipitation and are unable to preserve the shape of the daily precipitation distribution. These 2 distributions also underestimate the extreme indices and return values of annual maxima. The performance of SN is consistently better than the other single distributions in all respects. Such better performance may be partly due to the inclusion of additional parameters which increases the model's flexibility and use of method of moment rather than maximum likelihood to estimate model parameters (Chen and Brissette, 2014). The compound distribution MEXP also performed better than the single distributions except SN. This result is consistent with earlier studies (Wilks,1999; Chen and Brissette, 2014) where it is found that the MEXP is generally better represent the daily precipitation distribution than the EXP and GAM as the compound distribution specifically takes the entire range of precipitation distribution into account, not just the bulk. As the hybrid distribution includes heavy-tailed functions (such as the Pareto distribution) which explicitly take into account the upper tail of precipitation distributions, it is expected that it will do better at representing extreme precipitation.

The EXPP distribution has the unfortunate tendency to overestimate extremes, sometimes by an order of magnitude. This is due to the fact that when the generalized Pareto distribution is used to simulate the tail of the daily precipitation distribution, a few cases of unreasonably large values are typically generated (Li et al., 2013). Chen and Brissette (2014) described this issue in detail in their study. The resampling k-NN consistently performs better in terms of reproducing the observed precipitation characteristics for all the watersheds. However, as the k-NN method is

based on a resampling technique, the distributional properties of the generated series are exactly the same as those of the observations, limiting extrapolation ability of this method to generate the new extremes outside the observed range; this limits its applicability in climate change impact studies (Chen and Brissette; 2014). PN methods also overestimate the precipitation amount in terms of standard deviation, skewness and extreme events. The likely reason is that the fitting of 2nd degree polynomial is not the perfect choice to fit the Weibull experimental frequency distribution of observed daily precipitation for this study location.

3.2.8. Conclusions and Future Work

The results of SWGs model evaluations for the WOH watersheds are fairly typical in the sense that some models perform better with regard to some metrics, while others are superior with regard to other metrics; no one model performs best for all metrics. Overall, it is our preliminary conclusion that MC1 model along with the three models perform best in our region: SN, MEXP, and k-NN. The basis for this conclusion, its preliminary nature, and how this information will be used in the next phase of the analysis, are explained in the following paragraphs.

The most important criteria is that a model adequately simulate mean hydrological conditions. All models evaluated here adequately reproduce mean daily precipitation in all basins, indicating that with regard to this metric, all models are potential candidates for use in simulating the mean or background precipitation regime. This is also critical for simulating hydrological extremes because large streamflow events are determined by both the precipitation amount during an event as well as by antecedent conditions. During the cold season this is related to snow accumulation, which subsequently causes floods during melt and/or rain-on-snow events. During the warm season this is related to antecedent soil moisture conditions, which subsequently determine the flooding potential of large precipitation events.

During the warm season (when snow is not a factor) large precipitation events are important factors in flooding. Many of the metrics evaluated in this analysis reflect some aspect of the ability of these models to simulate extreme daily events. For precipitation occurrence, this includes the number of wet days and wet / dry spell lengths. For daily amount this includes standard deviation, skewness, a suite of extreme precipitation indices, as well as the magnitudes of the 50, 75, and 100 year recurrence intervals. The results discussed in the previous section all suggest that the three models such as SN, MEXP, and k-NN combine with MC1 model chosen more consistently (between basins and between indices) reproduce the observed statistics of extreme daily precipitation, though k-NN can't be a good choice for climate change impact studies due to its inability to generate the new extremes.

The next steps in evaluating the abilities of these models to reproduce extreme hydrological events include: (1) evaluation of the models' abilities to reproduce the interannual variability on the monthly time scales, for event lengths up to five days; and (2) the evaluation of

extreme streamflow statistics simulated by a hydrological model forced by the simulated precipitation time series. Ultimately, these models will be used to develop tools such as response surfaces (e.g. Prudhomme et al 2010, Brown et al 2011) that will support NYCDEP efforts to evaluate the vulnerability of the water supply system to extreme events (and to drought as well as to other changes in hydrology) during the coming decades.

4. Model Development and Applications

4.1. Realistically predicting saturation-excess runoff with SWAT-Hillslope

4.1.1. Introduction

The Soil and Water Assessment Tool (SWAT) (Arnold et al., 1998) is a widely used watershed model for predicting flow and pollutant loads from watershed nonpoint sources to receiving waters under varying scenarios of land use, management, and climate change (Arnold et al., 2010; Bosch et al., 2010; Gassman et al., 2007). However, its usefulness is limited because SWAT does not simulate saturation-excess runoff (Easton et al., 2008;White et al., 2011; Woodbury et al., 2014). SWAT simulates surface runoff essentially as an infiltration-runoff process by the SCS curve number (CN) method (USDA-SCS, 1972), using curve numbers that relate land use, soil and slope characteristics of hydrologic response units (HRUs) to soil infiltration rates (Neitsch et al., 2011). Infiltration-excess runoff occurs when precipitation intensity exceeds soil infiltration capacity and occurs in areas where soil crust forms in soils with low organic matter (Horton, 1933, 1940). In contrast, saturation-excess runoff is common in humid, well-vegetated areas (Dunne and Leopold, 1978) where soils are well structured and infiltration capacity is high. Saturation-excess runoff is generated in "variable source areas" (VSAs) where a perched groundwater table rise to the ground surface (USDA-SCS, 1972). The location of VSAs depends on topographic position in the landscape and soil transmissivity, and varies over time with landscape wetness (Dunne and Black, 1970). Since surface runoff is the primary mechanism to transport sediments and materials that accumulate on or near the ground surface to receiving waters, it is essential to identify appropriate runoff processes in the landscape in order to correctly estimate pollutant fluxes and properly apply conservation practices to improve water quality (Rode et al., 2010).

Several efforts have been carried out to add saturation-excess runoff to SWAT. In SWAT-VSA, Easton et al. (2008) used topographic wetness index to redefine HRUs, which distributed overland flow in ways consistent with VSA hydrology by modifying the definition of Curve number and available water content. White et al. (2011), in SWAT-WB, defined saturation deficit based on soil wetness classes classified by the values of soil topographic index, and applied a water balance instead of the Curve Number method to calculate runoff as water in excess of local soil water storage. While both SWAT-VSA and SWAT-WB were found to capture the spatial distribution of saturation excess runoff, the underlying mechanism of a perched water table that rises to the surface creating saturated conditions and saturation-excess runoff was not incorporated in either model.

Recent attempts to incorporate landscape routing into SWAT in order to represent realistic transport processes in the watershed may improve SWAT's ability to simulate VSA hydrology. Arnold et al. (2010) introduced a hillslope approach for SWAT which allows flow routing between three landscape units, i.e. divide, hillslope and valley bottom, from the furthest to the nearest one to the streams. Bosch et al. (2010) tested this SWAT landscape model in a low-gradient coastal plain watershed and showed that average annual surface runoff agreed satisfactorily with observations, but monthly simulated results differed significantly from measurements; and estimates of groundwater flow were greater than what would be expected. Therefore, it was concluded that the landscape model may require additional details to properly describe the interactions between the soil surface, vadose zone and groundwater. Currently, the SWAT landscape model is undergoing development and testing. Recently, Rathjens et al. (2015) introduced a fully distributed grid-based version of the SWAT landscape model, which incorporated the hillslope approach by Arnold et al. (2010) in simulating landscape flow routing between grids. The model testing in Little River Watershed near Tifton, Georgia showed good agreement between simulated results and flow observations both at daily and monthly time steps and reasonable spatial distribution of different flow types over the watershed. However, due to the large number of spatial units, the grid-based SWAT model is not computationally efficient, which limits its application to small-scale watersheds and impedes the ability of auto-calibration.

A modification to the SWAT model so that it can be used realistically for management purposes in humid areas where saturation excess runoff is common is described here. The modified SWAT version, referred as SWAT-Hillslope, redefines HRUs to include landscape position; replaces the SCS curve number method for predicting surface runoff with a variable bucket approach of Sivapalan et al. (1997) and Boughton (2004) for simulating saturation-excess runoff; and introduces a perched water table with the ability to route interflow from "dryer" to "wetter" HRU wetness classes. The SWAT-Hillslope model is tested in application to the Town Brook watershed in the upper reaches of the West Branch of the Delaware River in the Catskill Mountains, where rainfall intensities rarely exceed infiltration rates and saturation-excess runoff is common (Walter et al., 2003). The sensitivity of Digital Elevation model (DEM) resolution on SWAT-Hillslope modeled results was tested to select the appropriate DEM resolution. Then the model performance was evaluated by comparing with temporal and spatial observations.

4.1.2. Methodology

4.1.2.1. The modified version of SWAT for simulating saturation excess runoff (SWAT-Hillslope)

Three main modifications have been made to SWAT to simulate saturation-excess runoff. First, HRUs are redefined by classifying them according to a wetness index based on a statistical distribution of soil water storage capacity. In SWAT-Hillslope, the wetness index is user-

defined, and can be based on any suitable method for classifying moisture storage capacity across the catchment. A variety of methods are used in hillslope hydrology models to define the statistical distribution of soil water storage capacity, including the topographic index (TI) of TOPMODEL (Beven and Kirkby, 1979); a pareto distribution as in the Variable Infiltration Capacity (VIC) model (Liang and Lettenmaier, 1994; Wood et al., 1992), the Probability Distributed Model (PDM) (Moore, 2007) and the XINANJIANG model (Zhao et al., 1995); a statistical soil moisture distribution based on the USDA Curve Number equation interpreted as a saturation excess runoff process (Steenhuis et al., 1995; White et al., 2011); or an empirical distribution as in the AWBM model (Boughton, 2004). In the example model application presented, the TI distribution is used. The TI is the quotient of the amount of water delivered to a point in the landscape and the ability to transmit through the soil at that point (Beven, 1986; Beven and Kirkby, 1979)

$$\lambda = \ln\left(\frac{\alpha}{\tan(\beta)K_s D}\right) \tag{4.1}$$

where λ is the soil topographic index (STI) [unit: ln(d m $^{-1}$)], α is upslope contributing area per unit contour length (unit: m), $\tan(\beta)$ is the local surface topographic slope, K_s is the mean saturated hydraulic conductivity of the soil (unit: m d^{-1}), and D is the soil depth (unit: m).

Second, the SCS curve number method for predicting surface runoff is replaced by the variable bucket approach of Sivapalan et al. (1997) and Boughton (2004) that generates runoff when the storage capacity of a wetness class is exceeded. The ability to calculate infiltration-excess runoff using the Green-Ampt method is retained. Additional information is provided below.

Last, a perched aquifer is introduced to control soil saturation which generates saturation excess runoff as the perched water table rises above the soil surface; and laterally route interflow from "dryer" to "wetter" wetness classes. Water not lost is stored the wettest wetness classes, thereby distributing upslope water downstream. The modifications made in SWAT2012 to obtain SWAT-Hillslope are described below. SWAT2012 was used as the basis for all modifications.

Calculating runoff with the perched water table

Up to 10 wetness classes of increasing storage capacity can be taken into account in SWAT-Hillslope. The maximum storage capacity (before surface runoff occurs) in each wetness class is referred as Effective Depth Coefficient *edc(i)* where *i* is the wetness class number. Figure 4.1 presents two simple examples of storage capacity distribution of a watershed covering 5 wetness classes with increasing soil water storage capacity. The *x* axis shows areal proportion while the *y* axis specifies the maximum storage capacity of wetness classes. Wetness 1, which has the greatest likelihood of producing surface runoff during a rainfall event, has very small value of *edc*, while Wetness 5 which has a high value of *edc* and will be very rarely be saturated

unless there is extreme rainfall. Example (a) in Figure 4.1 presents a watershed dominated by dry areas while example (b) illustrates a watershed dominated by perennial wetlands with large areas of small storage capacity. Figure 4.2 summarizes the hydrology of an HRU the original SWAT and the SWAT-Hillslope models. Flows from all HRUs within a sub-basin are summed in order to obtain the total flow of the sub-basin.

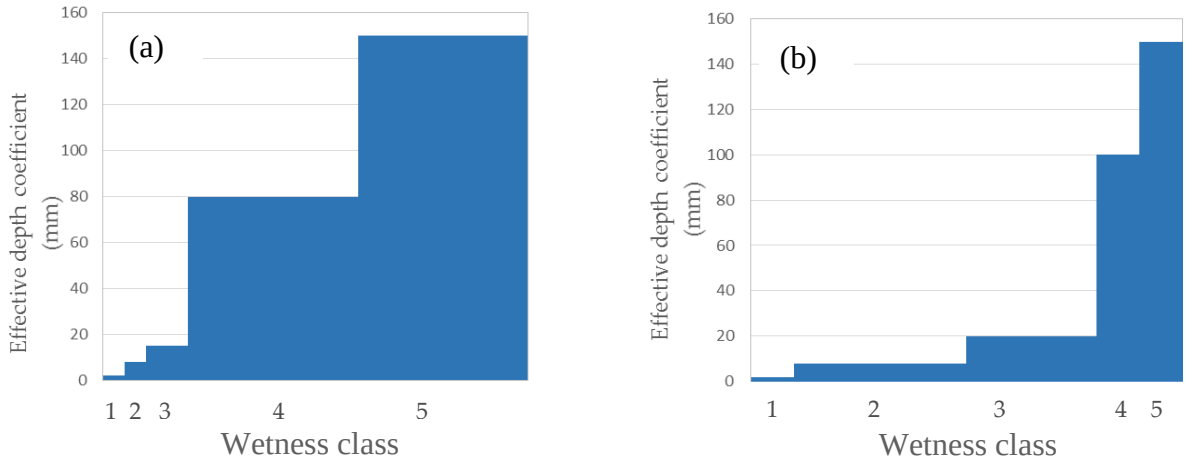

Figure 4.1. Examples of storage capacity distribution of a watershed: (a) watershed dominated by dry areas, and (b) watershed dominated by perennial wetlands.

In the original SWAT, the water moves through three aquifers: soil profile, shallow aquifer and deep aquifer. When there are precipitation and snowmelt inputs, surface runoff is calculated by SCS curve number based on the current soil moisture. The amount of water that is not surface runoff becomes infiltration to the soil profile. The water goes through soil layers from which lateral flow is generated. The seepage from the bottom of soil profile enters shallow aquifer from which groundwater flow is generated. A small amount of water may enter the deep aquifer and then contributes to streamflow somewhere outside of the watershed.

SWAT-Hillslope adds a perched aquifer between the soil profile and shallow aquifer. The perched aquifer represents a part of the soil profile above an impervious layer that transmits subsurface flow laterally through the hillslope, controls soil saturation as the perched water table approaches the surface, provides water for plant use and influences biogeochemical transformation related to saturated soil conditions. With this modification, SWAT-Hillslope creates a pathway for hillslope processes to transport water and pollutants from the upslope areas corresponding to "dryer" wetness classes to downslope areas with "wetter" wetness classes. For simplicity, it is assumed that the depth of perched aquifer from soil surface equals to the depth of the soil profile. The seepage from the bottom of soil profile contributes to both perched aquifer and shallow aquifer based on a recharge fraction parameter (*rchrg_paf*). The amount of water entering the perched aquifer raises the water table which rise into the root zone making the

aquifer available for plant use, and may rise above soil surface causing saturated areas and producing saturated excess runoff.

Mathematically, the perched aquifer is treated as a non-linear reservoir that can generate rapid subsurface stormflow as the water table rises, with return flow occurring at the saturated areas.

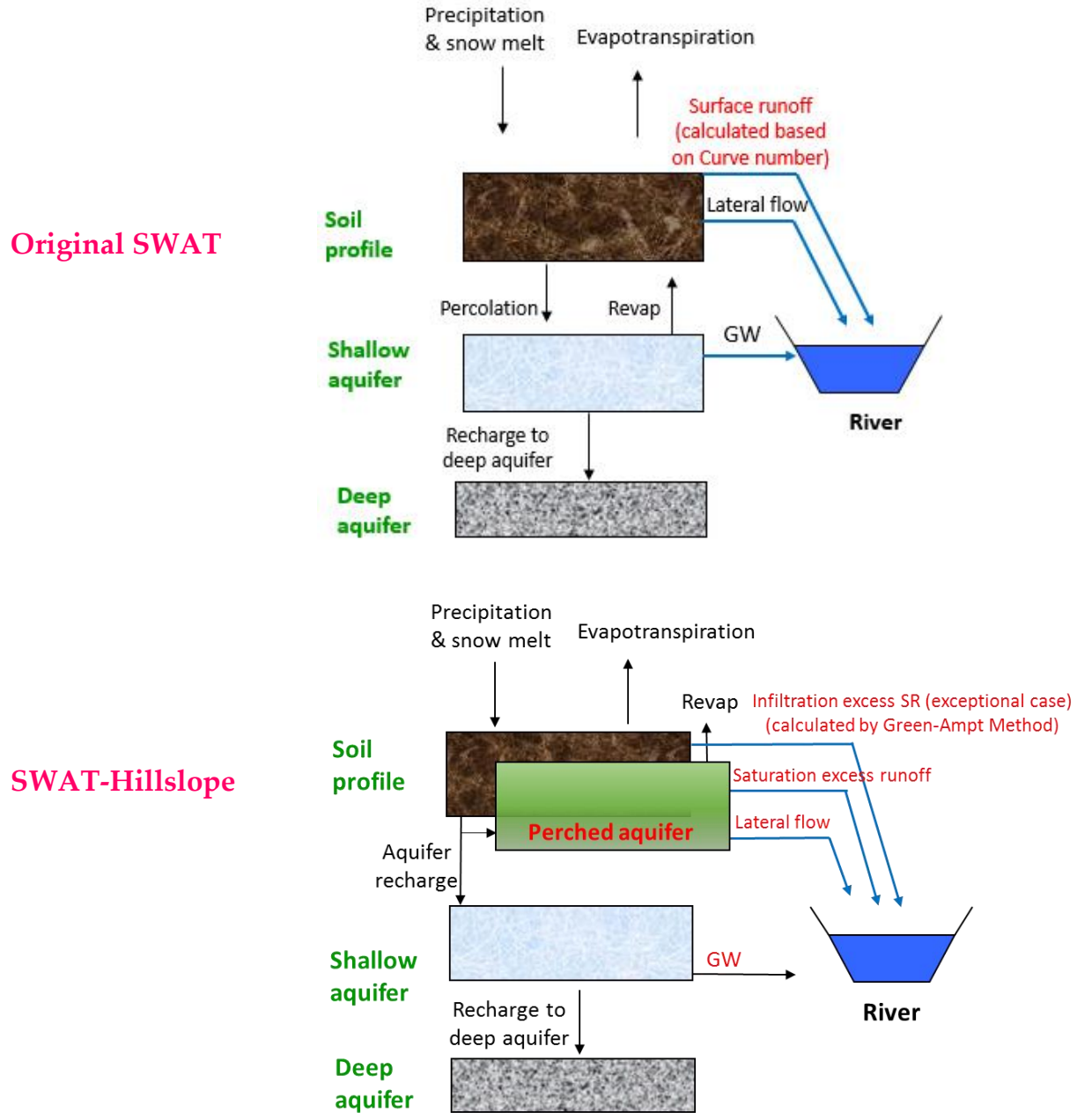

Figure 4.2. Difference in hydrological processes between the original SWAT and SWAT-Hillslope

New parameters added to SWAT-Hillslope

The runoff calculation with a perched aquifer in SWAT-Hillslope requires an addition of a number of parameters. Table 4.1 presents the added new parameters and the corresponding processes, their definitions and value ranges. *Weti* is the wetness class index for each HRU. *Edc* and *edc_factor* define the water storage capacity for wetness classes. *Rchrg_paf* defines the recharge of perched aquifer while *effporfactor* affects the rise of water table in perched aquifer. *Perchst_datum* defines the depth of perched aquifer from where the lateral flow starts to contribute to streamflow whereas *latA* and *latB* are coefficient for generating lateral flow based on non-linear reservoir concept.

Table 4.1. New parameters added to SWAT-Hillslope

Name	Unit	Definition	Range
edc(weti)	mm	Effective Depth Coefficient: Maximum drainable water storage capacity defined at wetness class level	0-1000
edc_factor	-	Calibration factor adjusts all *edc* values	0 - 10
effporfactor	-	Fraction of effective porosity that can hold water under saturated conditions	0 - 1
latA		Perched aquifer non-linear reservoir coefficient	0 - 1
latB		Perched aquifer non-linear reservoir coefficient	1 - 3
perchst_datum	mm	Mean depth of perched aquifer drawn down just to point where lateral flow from aquifer ceases	
rchrg_paf	-	Fraction of root zone percolation that recharges the perched aquifer	0 - 1
weti(i)	-	Wetness class (1-10) assigned to HRU *i*	1-10

4.1.2.2. Study area: Town Brook watershed, Delaware County, New York

The Town Brook watershed covers an area of 37 km^2 and is located in the Catskill Mountains of New York State. The climate in this area is humid with average temperature of 8ºC and average annual precipitation of 1123mm/year. The region is characterized by steep to moderate hillslopes of glacial origins with shallow permeable soils. Elevation ranges from 493 to 989 m. The majority of soil is silty loam and silty clay loam belonging to soil hydrologic group C ratings (USDA-NRCS, 2000). The upper terrain of the watershed is characterized by shallow soil (average thickness 80 cm) overlaying fractured bedrock, steep slope (average slope 29%) and deciduous and mixed forests (60% of the watershed). The lowland areas of the watershed have deeper soils (average thickness 180 cm) underlain by a dense fragipan restricting layer,

more gentle slope (average slope 14%) and are predominantly occupied by pasture and row crops (20%) and shrub land (18%). Water and wetland comprise only 2% of the watershed and impervious surface is insignificant. Dairy farming is the main agricultural land use.

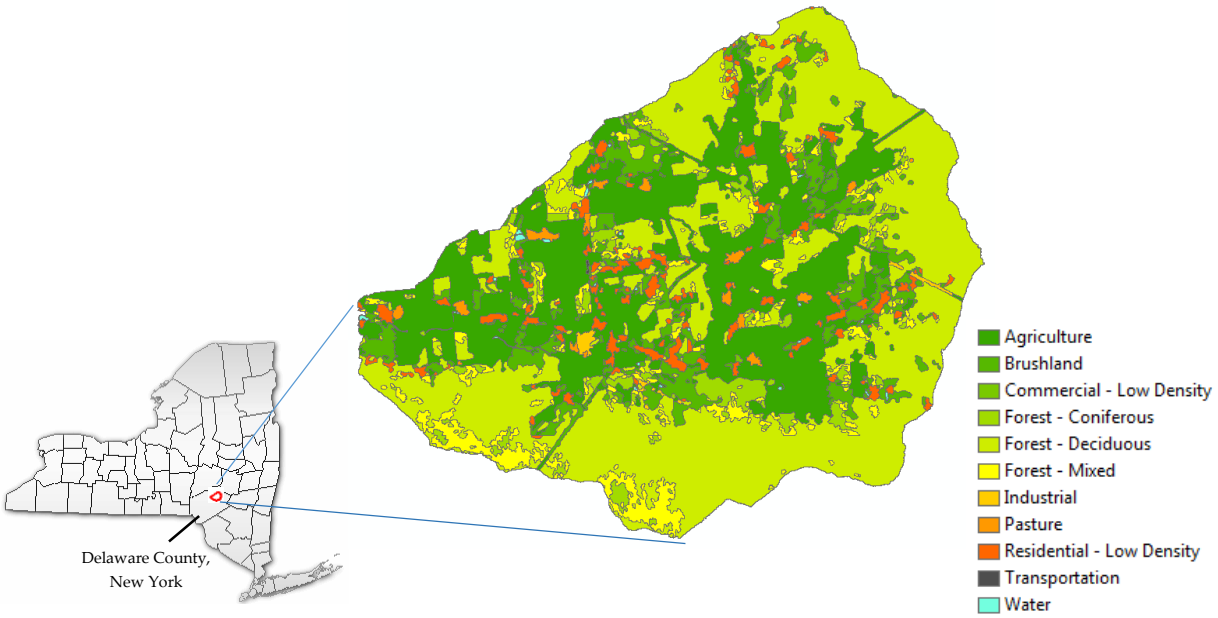

Figure 4.3. Town Brook watershed, Delaware County, New York

4.1.2.3. SWAT-Hillslope model set up for the Town Brook watershed

Watershed delineation

A 10-meter DEM (digital elevation model) was used to delineate the watershed and for calculating slopes and flow paths. The 10m resolution was chosen based on a sensitivity analysis on DEM resolution suggesting that courser resolution (30m) resulted in unusual representation of saturated conditions, while very fine resolution (1m, 3m) gave a very broad distribution of highly disconnected saturated areas and diminished the importance of topography in the calculation of topographic index. The 37 km^2 Town Brook watershed is quite small, thus the watershed was not split into sub basins. Instead, the watershed was split into multiple HRUs based on soil, land use and wetness maps.

HRU definition

Wetness map

A wetness map was created based on soil topographic index (STI) defined in Equation (4.1). The upslope contributing area, α, was determined by the Terrain Analysis Using Digital Elevation Models (TAUDEM) (Tarboton, 1997; Tarboton and Mohammed, 2010). The saturated conductivity and soil depth were respectively extracted from two variables: *saturated hydraulic conductivity* and *depth to restricted layer* in soil SSURGO database.

Based on the results from the Soil Moisture Routing (SMR) model of the Town Brook watershed, Agnew et al. (2006) developed a relationship between STI and probability of saturation (P_{sat}) for April, August and October representing spring, summer and fall conditions. The study found that STI is a reliable parameter to identify and quantify the risk of saturation excess runoff due to the clear, regionally consistent relationship between STI and P_{sat} with strong correlation throughout the year. Based on the average results in the 3 seasonal conditions, Figure 4.4 shows that the areas with STI < 7.6 have almost no chance to be saturated; the areas with STI > 17.7 are always saturated.

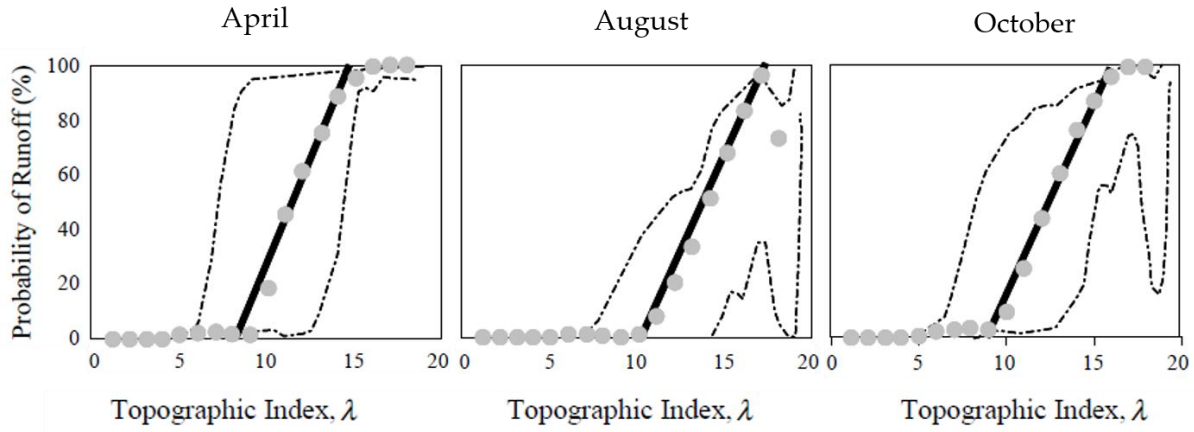

Figure 4.4. Relationship between topographic index (λ) and probability of saturation (P_{sat}) in April, August and October (Agnew et al., 2006). The symbol are the average P_{sat} for corresponding λ. The dashed lines correspond to 25th and 75th percentiles.

The Town Brook watershed was broken up into 5 wetness classes. Based on the results from Agnew et al. (2006), we grouped the areas with STI < 7.6 as the "driest" wetness class (wetness 5) with very high water storage capacity (1000mm) and the areas with STI > 17.7 as the "wettest" wetness class (wetness 1) with no water storage capacity (0 mm). This means that when there is hydrological input, the wetness 1 is always saturated while wetness 5 is constantly dry. The rest of the watershed was classified into wetness class 2, 3 and 4 and their water storage capacity were assigned by a trial method while running the model and comparing the results of

saturated areas with our available observations in 28-30 April 2006 which is shown in Figure 4.10a. The final classification of 5 wetness classes in the Town Brook watershed is shown in Figure 4.5. With this classification, only wetness 1, 2 and 3 can be saturated while wetness 4 and 5 are always dry. The maximum area of saturation is the summation of wetness 1, 2 and 3 which equals to approximately 10% of the watershed. Harpold et al. (2010), from 6 field surveys in 2007, also reported 9.9% as the maximum saturated areas in a small study watershed in the southwest corner of the Town Brook watershed.

Table 4.2. Classification of wetness classes for the Town Brook watershed.

STI	**Wetness**	**% of watershed area**	**Water storage capacity**	**Characteristics**
< 7.6	5	5.1	1000	Dry
7.6 – 12.2	4	84.98	50	
12.2 – 14.5	3	8.2	6	
14.5 – 17.7	2	1.12	3	
> 17.7	1	0.59	0	Wet

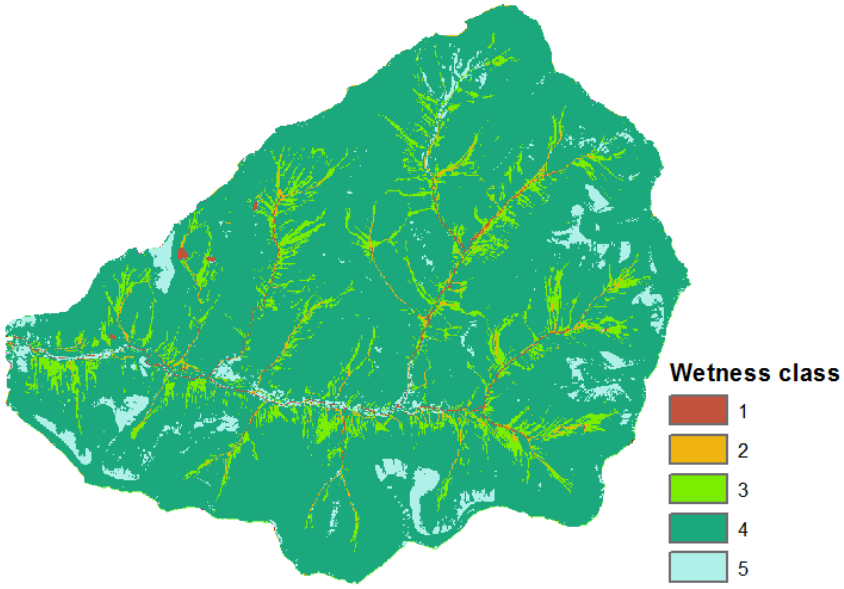

Figure 4.5. Wetness map for the Town Brook watershed

Soil

The soil map of Town Brook watershed was extracted from the SSURGO soil database. There are 17 soil types in the watershed. The data of soil properties that are necessary for the SWAT model are taken from the SSURGO database and the soil survey of Delaware County (USDA, 2006). The soil map is then combined with the wetness map to redefine soil types in different wetness classes in order to include wetness class assignment for each HRU in the final discretization, which is an essential step for running SWAT-Hillslope.

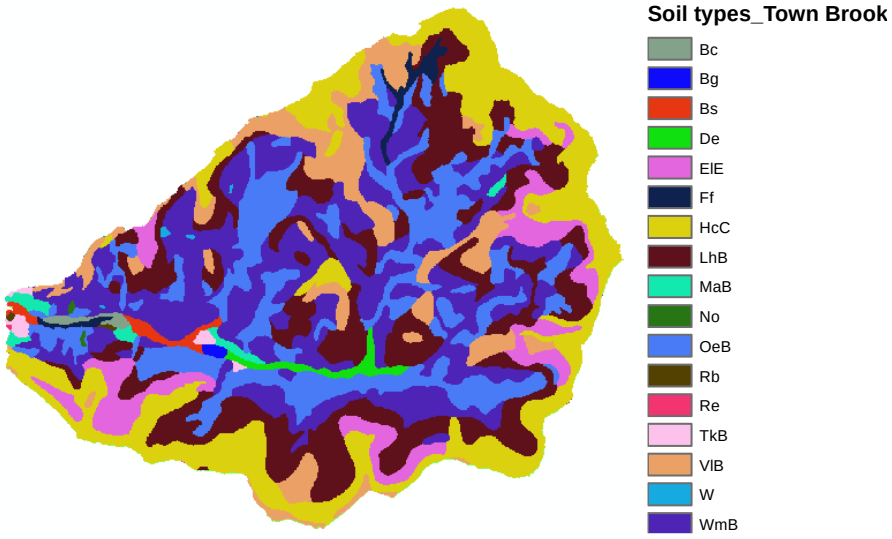

Figure 4.6. Soil types in the Town Brook watershed (*Source: SSURGO soil database*)

Land use

The land use map was derived from classified 2009 aerial photography data obtained from NYCDEP. The watershed was divided into 11 land use types which are shown in Figure 4.6 and Table 4.3. The main land use types are forest (54%), agriculture (32%) and brushland (9%). Residential area covers a very small part of the watershed (4%).

Table 4.3. Land use types in the Town Brook watershed

No.	Land use type	Percentage of area (%)
1	Forest - Coniferous	3.55
2	Forest - Deciduous	44.39
3	Forest - Mixed	5.83
4	Agriculture	32.10
5	Pasture	0.87
6	Brushland	8.94
7	Industrial	0.35
8	Commercial - Low density	0.02
9	Residential - Low density	3.73
10	Transportation	0.01
11	Water	0.21

Meteorological inputs

Daily precipitation and temperature data are available in a 4km x 4km gridded climate dataset from the Applied Climate Information System (ACIS) which was developed using the Parameter-Elevation Relationships on Independent Slopes Model (PRISM) interpolation method (Daly et al., 2008). Thiessen polygons were created based on the available grid points to choose the grid points that would be used for Town Brook watershed (Figure 4.7). As the Town Brook watershed was setup as a single subbasin, precipitation and temperature data was assumed to be taken at the centroid of the watershed by interpolating from data of surrounding PRISM grid points by inverse distance weighting method.

Solar radiation was averaged from the data at the Albany and Binghamton airport locations is available from 1926 to 2012. Relative humidity and wind speed were generated from the weather generation method built in SWAT.

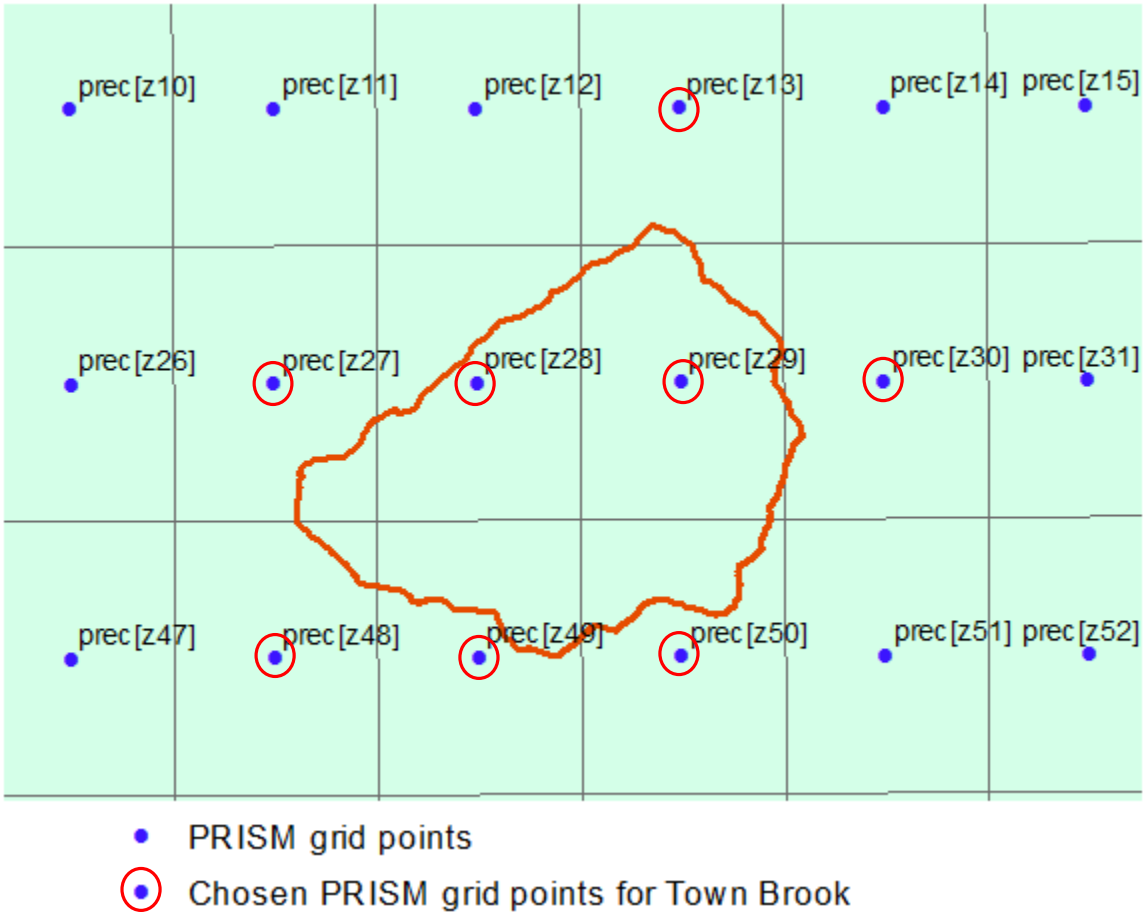

Figure 4.7. Meteorological grid points used for the Town Brook watershed

4.1.2.4. Model calibration and validation

Calibration was carried out at the outlet of the Town Brook watershed for the period 1998–2007 in which the first 3 years served as warming up period. The period of 2008–2012 was the validation period. To evaluate the SWAT-Hillslope performance for the simulated flow, we used three following criteria, each of which was calculated for daily and monthly time steps:

a. Nash Sutcliffe efficiency (NSE) (Nash and Sutcliffe, 1970): ranges between -∞ and 1.0, with NSE = 1 being the optimal value.

$$NSE = 1 - \left[\frac{\sum_{i=1}^{n} (Y_i^{obs} - Y_i^{sim})^2}{\sum_{i=1}^{n} (Y_i^{obs} - Y^{mean})^2} \right] \quad (4.2)$$

where Y_i^{obs} is the i^{th} observation, Y_i^{sim} is i^{th} simulated value, Y_i^{sim} is the mean of observed data and n is the total number of observations.

b. Percent bias (PBIAS): the optimal value of PBIAS is 0.0, with low magnitude values indicating accurate model simulation. Positive values specify underestimation bias and negative values indicate overestimation bias (Gupta et al., 1999).

$$PBIAS = \left[\frac{\sum_{i=1}^{n} (Y_i^{obs} - Y_i^{sim}) * 100}{\sum_{i=1}^{n} Y_i^{obs}} \right] \quad (4.3)$$

c. RMSE – observations standard deviation ratio (RSR): RSR standardizes RMSE using the observations standard deviation (Singh et al., 2004). It varies from the optimal value of 0, which indicates zero RMSE to +∞. The lower RSR, the lower RMSE, the better the model performance.

$$RSR = \frac{RMSE}{STDEV_{obs}} = \left[\frac{\sum_{i=1}^{n} (Y_i^{obs} - Y_i^{sim})^2}{\sum_{i=1}^{n} (Y_i^{obs} - Y^{mean})^2} \right] \quad (4.4)$$

The SWAT-Hillslope model was calibrated by applying the Monte Carlo sampling method. We randomly generated 10,000 parameter sets within the ranges of the chosen parameters for calibration. Then 10,000 simulations were run with SWAT-Hillslope. Finally, the best performance parameter sets were chosen. Table 4.4 shows the detailed parameters that were used for calibration and their values that were used to evaluate SWAT-Hillslope performance by comparing with observations. The calibration is performed in the following 3 steps, with steps 2 and 3 iterated:

1. Snow melt calibration: Five parameters related to snowmelt simulation were calibrated. In the Town Brook watershed, snowmelt is a very important process. The snow melt calibration helped to adjust the timing of flow peak when snow melt occurs.
2. Flow calibration: The best parameter set from the snowmelt calibration was used. Then eleven flow parameter were taken into account in the Monte Carlo calibration (Table 4.4). The flow calibration affected the partition of flow components and flow magnitude.
3. Adjust storage capacity of wetness classes: The best parameter sets from snowmelt and flow calibration were applied. Then the values of *edc* for wetness classes were calibrated manually. This step influences the distribution of saturated areas caused by saturation excess runoff.

4.1.3. Results

4.1.3.1. Performance of SWAT-Hillslope on flow simulation

The performance of SWAT-Hillslope on flow simulation was evaluated for simulation of the hydrograph at the watershed outlet; flow components (runoff, lateral flow, baseflow); and the spatial distribution of simulated runoff. The simulated results from the SWAT-Hillslope model were compared with observations as well as the results from the original SWAT2012 model.

4.1.3.1.1. Comparison with measured hydrograph data at watershed outlet

The statistical evaluation of SWAT-Hillslope daily predictions versus measurements at the outlet of Town Brook watershed (Table 4.5) resulted in *NSE* values at 0.68 and 0.52, *PBIAS* values at 7.17 and -3.61, and *RSR* at 0.57 and 0.69 for calibration and validation periods, respectively. These values are all within the range of "*good*" model performance for the calibration period while *NSE* is rated as "*satisfactory*", *PBIAS* as "*very good*" and *RSR* as "*satisfactory*" performance in the validation period, based on Moriasi et al. (2007) guidelines for evaluation of model performance. *NSE* improved significantly to 0.6 in the validation period if we excluded the year 2011 in which an extreme flood occurred in August that could not be captured very well by SWAT-Hillslope. The SWAT-Hillslope monthly predictions obtained better fit to measurements with significantly improved NSE value at 0.87 and 0.78 for calibration and validation periods, respectively. Monthly PBIAS values were comparable to daily ones while monthly RSR values has improvement from daily values to be ranked as "*very good*". Based on statistical results on monthly streamflow, the performance of the SWAT-Hillslope model is classified as "*very good*", "*good*" and "*very good*" respectively corresponding to NSE, PBIAS and RSR while it is classified as "very good" for all three indices in the validation period whether the year 2011 was excluded or not.

Table 4.4. Parameters for calibration using Monte Carlo sampling method

Name	Unit	Definition	Range	Calibrated value
Snowmelt calibration				
SFTMP	^{o}C	Snowfall temperature	-5 - 5	-0.58
SMTMP	^{o}C	Snowmelt temperature	-5 - 5	1.10
SMFMX	mm/ ^{o}C	Maximum snowmelt factor	5 - 10	7.62
SMFMN	mm/ ^{o}C	Minimum snowmelt factor	0 - 5	2.68
TIMP	-	Snow pack temperature lag factor	0 – 1	0.022
Flow calibration				
RCHRG_PAF	mm	Fraction of root zone percolation that recharges the perched aquifer	0-1000	0.626
latA		Perched aquifer non-linear reservoir coefficient	0 - 1	0.022
latB		Perched aquifer non-linear reservoir coefficient	1 - 3	1.72
ALPHA_BF	-	Baseflow alpha factor	0 - 1	0.23
GW_DELAY	days	Groundwater delay	0 - 200	28
EFFPORFACTOR	mm	Fraction of effective porosity that can hold water under saturated conditions	0 - 1	0.718
EDC_FACTOR	-	Calibration factor for adjusting *edc* values	0.5 - 5	1.78
EPCO		Plant water uptake compensation factor	0 - 1	0.567
ESCO		Soil evaporation compensation factor	0 - 1	0.102
CANMX	mm	Maximum canopy storage	0 - 5	4.73
SURLAG	days	Surface runoff lag time	0.05 - 24	8.79
Storage capacity of wetness classes (5 wetness classes were defined in this case study				
EDC01	mm	Storage capacity of wetness class 1	0-1000	0
EDC02	mm	Storage capacity of wetness class 2	0-1000	3
EDC03	mm	Storage capacity of wetness class 3	0-1000	6
EDC04	mm	Storage capacity of wetness class 4	0-1000	50
EDC05	mm	Storage capacity of wetness class 5	0-1000	1000

Table 4.5. Performance criteria for SWAT-Hillslope in daily and monthly time step

Period	**Time steps**	**Criteria**				
		NSE	*PBIAS*	*RSR*	*Average streamflow (mm/a)*	
					Simulated	*Observed*
Calibration	Daily	0.68	7.17	0.57	302.76	326.14
	Monthly	0.87	7.25	0.36		
Validation	Daily	0.52	-3.61	0.69	331.61	320.05
	Monthly	0.78	-3.38	0.46		
Validation (excluding 2011)	Daily	0.60	0.73	0.63	238.49	252.84
	Monthly	0.82	1.03	0.43		

The comparison between the SWAT-Hillslope and the original SWAT2012 models was based on two calibrated models for Town Brook watershed. Figure 4.8 shows the comparison on daily and monthly discharge values simulated by SWAT-Hillslope and SWAT2012 versus observations for the period 2001-2003 which is within the calibration period. It is clearly observed that SWAT-Hillslope was able to capture the variation of streamflow in both summer (May – October) and winter (November to April) periods. However, SWAT-Hillslope underestimated the flow in winter where snow melt occurred frequently and did not capture the winter flow peaks excellently while it gave relatively comparable predictions of summer flows. Compared to SWAT-Hillslope, although SWAT2012 was better in capturing the winter peaks, it over-predicted the summer flows with simulated flow fluctuations in summers which had not been observed during these periods. Moreover, it can be seen from month flow comparisons in Figure 4.8 that SWAT2012 did not capture the flow trend as well as the SWAT-Hillslope model.

Figure 4.9 presents the scatter plots of the streamflow simulated by SWAT2012 and SWAT-Hillslope versus measurements in daily and monthly time steps, relative to a 1:1 line plot. It again shows the closer fit of both daily and monthly simulated streamflow from SWAT-Hillslope to observed flow compared to SWAT2012. For daily time steps, SWAT-Hillslope particularly showed better prediction for low flows. Generally, both models did not capture the peak flows very well although SWAT2012 gave closer prediction to some extremely high flows. Both models gave better performance for monthly predictions than daily ones. However, for all the simulated months, SWAT-Hillslope gave closer fit to observations.

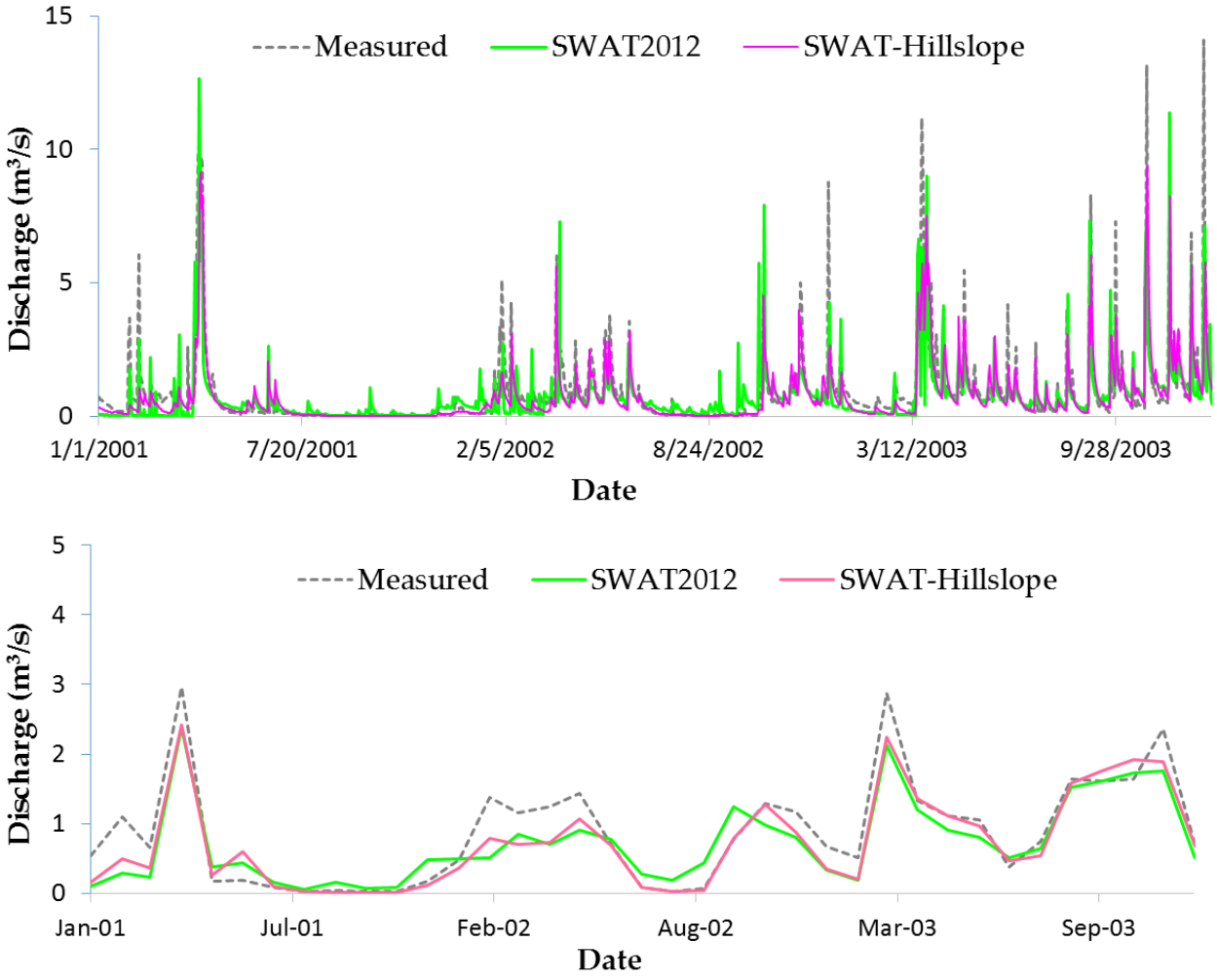

Figure 4.8. Comparison of simulated daily and monthly discharge values between SWAT-Hillslope, SWAT2012 and measured data

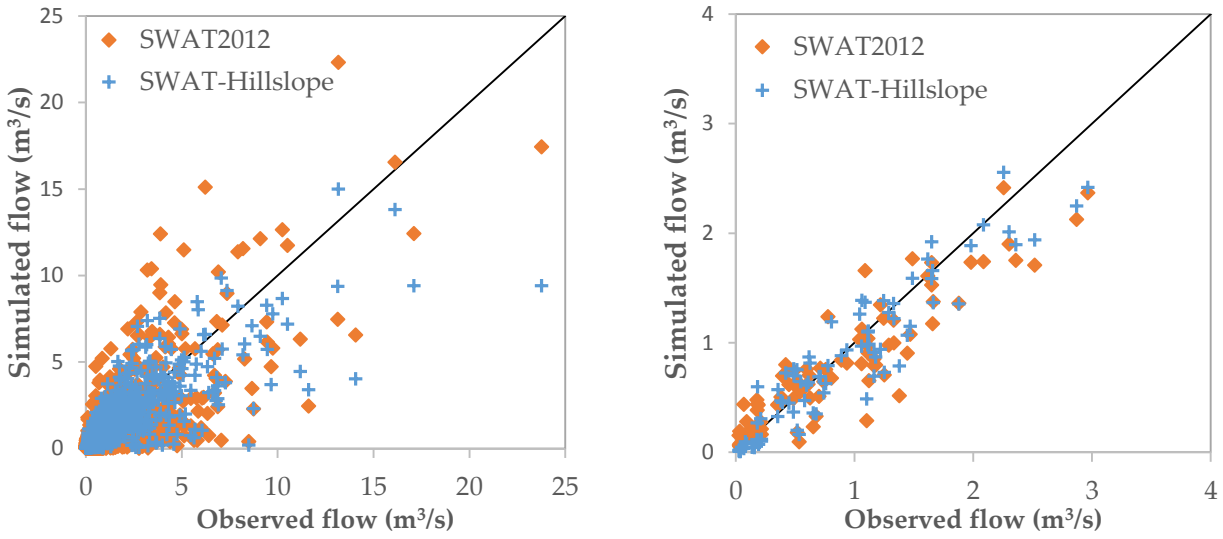

(a) Daily (b) Monthly

Figure 4.9. Scatter plot of daily and monthly simulated flow by SWAT-HS and SWAT2012 versus observed flow

4.1.3.1.2. Comparison of simulated flow components

The estimated time series of three flow components: surface runoff, lateral flow and groundwater flow by SWAT-Hillslope and SWAT2012 for the year 2003 are illustrated in Figure 4.10. Surface runoff was the dominant flow in SWAT2012 while lateral flow dominated in SWAT-Hillslope. For the Town Brook watershed, SWAT-Hillslope predicted all surface runoff coming from saturation excess process, the infiltration-excess runoff was estimated at 0, which is reasonable for the Catskill Mountains area with infiltration rates often exceeding the medium rainfall intensity. Lateral flow deriving from the perched aquifer in SWAT-Hillslope occurred most of the time of the year except the period of snowfall (Jan – Feb). SWAT-Hillslope estimated very stable groundwater flow which contributed to streamflow throughout the year, but with small contribution at the beginning of the year when snowpack was accumulated. Different from SWAT-Hillslope, surface runoff in SWAT2012 which is implicitly considered as infiltration-excess runoff occurred in high rainfall except the snowfall period (Jan – Feb). Lateral flow in SWAT2012 which derived from soil moisture excess from field capacity, occurred throughout the year whenever there was rainfall. Groundwater flow had the same trend in the two models with slightly more fluctuation in the SWAT2012 model because of high volume and the difference in calibrated values for the groundwater-related parameters.

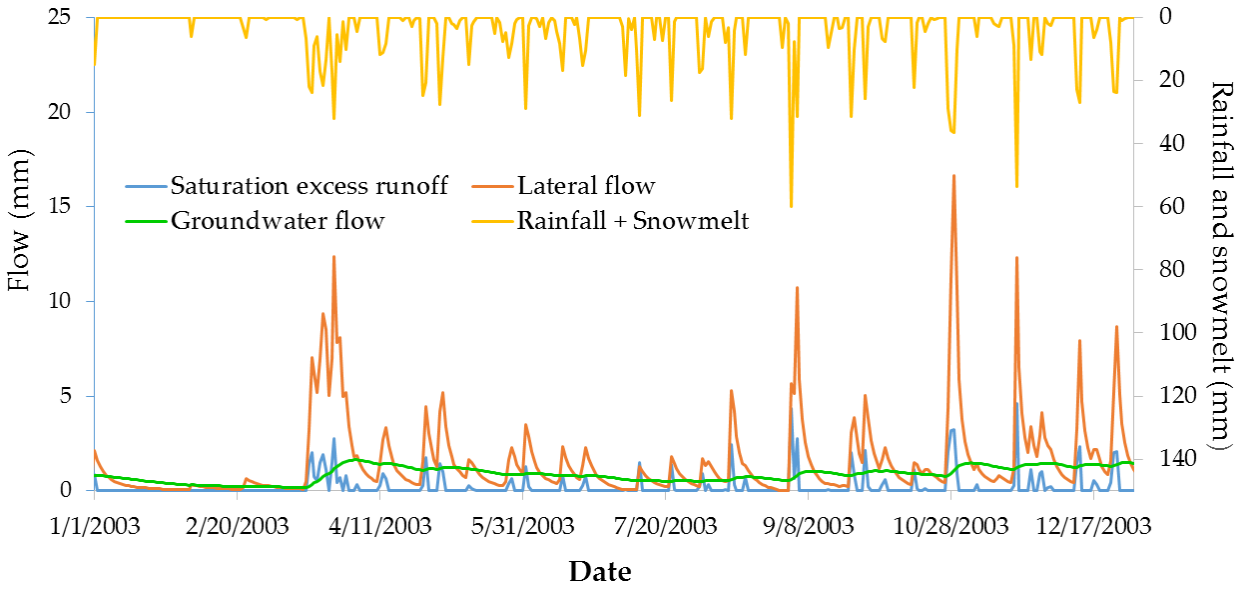

(a) SWAT-Hillslope

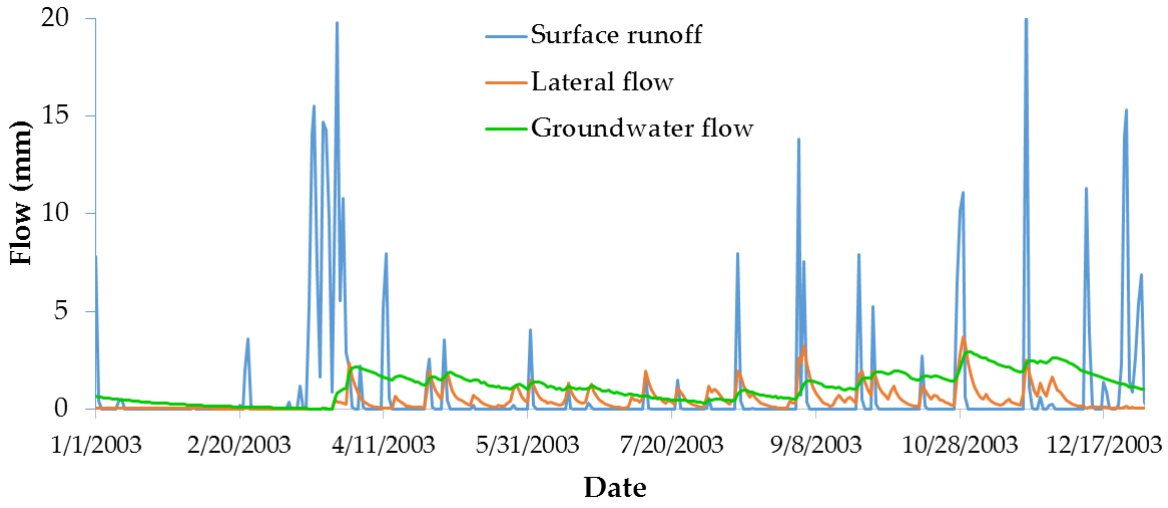

(b) SWAT2012

Figure 4.10. Time series of flow components simulated by SWAT-Hillslope in comparison with SWAT2012

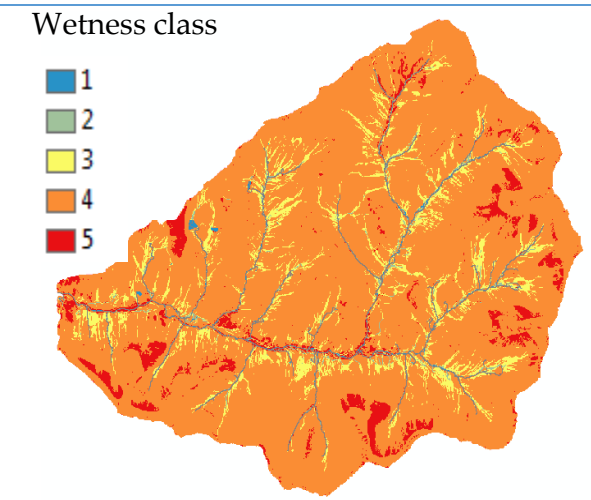

(a) Wetness map

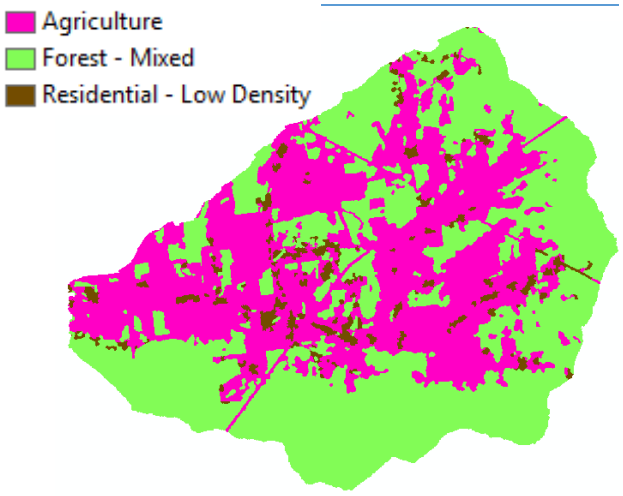

(b) Land use

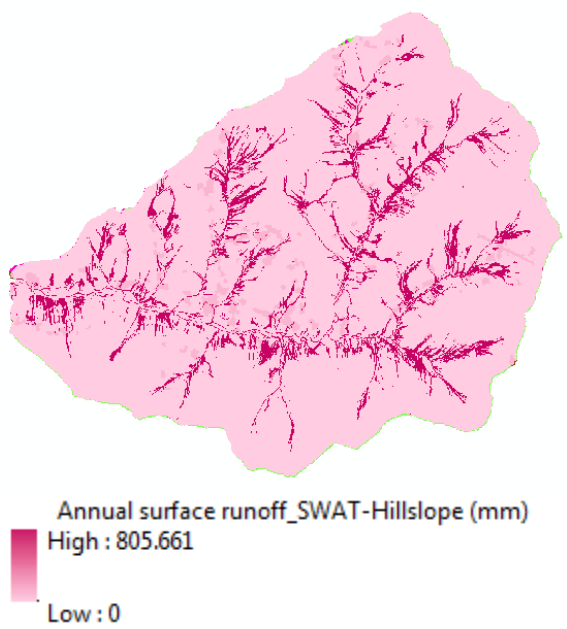

(c) Annual surface runoff in SWAT-Hillslope

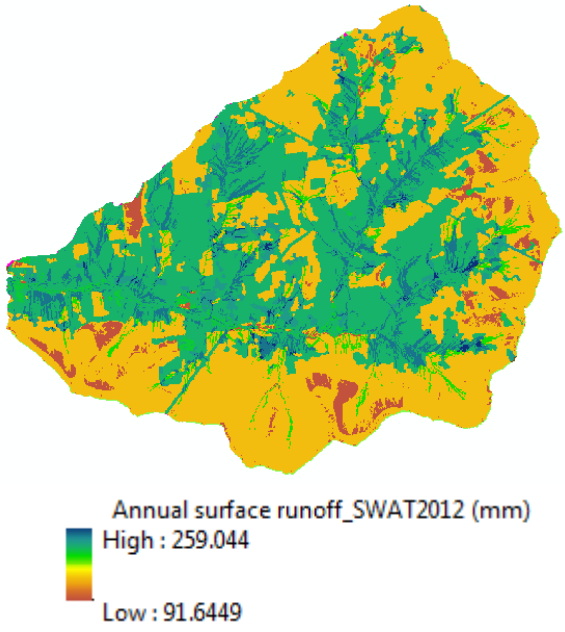

(d) Annual surface runoff in SWAT2012

Figure 4.11. Spatial distribution of annual surface runoff simulated by SWAT-Hillslope and SWAT2012.

4.1.3.1.3. Comparison of Spatial Distribution of Runoff

The spatial distribution of annual surface runoff during the calibration period generated by SWAT-Hillslope and SWAT2012 model was compared in Figure 4.11. Figure 4.11a and Figure 4.11b depict the wetness and land use map of the Town Brook watershed while Figure 4.11c and Figure 4.11d present a striking difference in the spatial locations of surface runoff production between SWAT-Hillslope and SWAT2012. The distribution of surface runoff

predicted by SWAT2012 followed the distribution of land use in which forest contributed the least runoff and agriculture was the most significant contribution. Residential areas had high amount of surface runoff, however they covered very small area in the watershed. Surface runoff was generated all over the watershed in SWAT2012 because it closely depended on land use due to the concept of Curve number. Unlike SWAT2012, runoff predicted by SWAT-Hillslope was only found in the areas corresponding to wetness class 1, 2 and 3 which were considered to be prone to saturation and were set with low water storage capacity.

Moreover, the spatial distribution of simulated saturated areas by SWAT-Hillslope was compared with available observations in 28-30/4/2006 in a small area in Town Brook watershed (Figure 4.12). Figure 4.12a and Figure 4.12b respectively show the observed and simulated saturated areas by SWAT-Hillslope in the three observed days while Figure 4.12b presents the variation of rainfall in April, 2006. From Figure 4.12c, no rainfall was observed from 28-30/4/2006 while there was a big storm happening on 23/04/2006. Due to no rainfall event, SWAT2012 predicted no surface runoff from 28-30/04/2006. In contrast, SWAT-Hillslope predicted the presence of saturation areas in these three days which is compatible with the observations. The saturation was caused by the high water level in perched aquifer resulting from the big storm event on 23/04/2006 and lateral flow contribution from the upslope areas to the downslope areas which are prone to saturation.

4.1.4. Discussion

Correctly identifying surface runoff source areas is particularly important for SWAT model applications to support watershed management. An effective watershed management strategy for pollution control is to target areas on the landscape where surface runoff and transportable pollutants co-occur (Gburek et al., 2002; Walter et al., 2000; Zollweg et al., 1996). Two runoff generation mechanisms - infiltration excess runoff and saturation excess runoff - can produce very different spatial distributions of runoff (Easton et al., 2008; Schneiderman et al., 2007). Infiltration excess runoff occurs where rainfall rates exceed infiltration capacity of the soil, while saturation-excess runoff occurs on variable source areas (VSAs) that saturate from below. Overland flow is generated at VSAs by a combination of rainfall and return flow (lateral flow in SWAT terminology), and return flow may be the dominant source of stormflow in catchments where VSAs occur but are limited in extent (Walter et al., 2000). Different areas in the same catchment may exhibit infiltration excess runoff, saturation excess runoff, and return flow in various combinations. It is thus important in watershed pollutant export modeling applications to explicitly account for these hydrological processes.

SWAT-Hillslope improves upon SWAT's ability to identify runoff source areas and hydrologic flow paths by replacing the runoff curve number method with explicit calculation of infiltration excess runoff, saturation excess runoff, and return flow at saturated areas. The curve number equation represents an empirical relationship between rainfall and runoff on a watershed

scale but does not account for the underlying processes of runoff generation. SWAT-Hillslope proceeds in the following order for each HRU: i) estimate infiltration-excess runoff and infiltration using Green-Ampt method (Green and Ampt, 1911; Mein and Larson, 1973; Neitsch et al., 2011), ii) determine saturation-excess runoff and saturated areas using a statistical-dynamical approach to simulating the perched aquifer, and 3) estimate return flow at saturated areas as a non-linear function of perched aquifer storage.

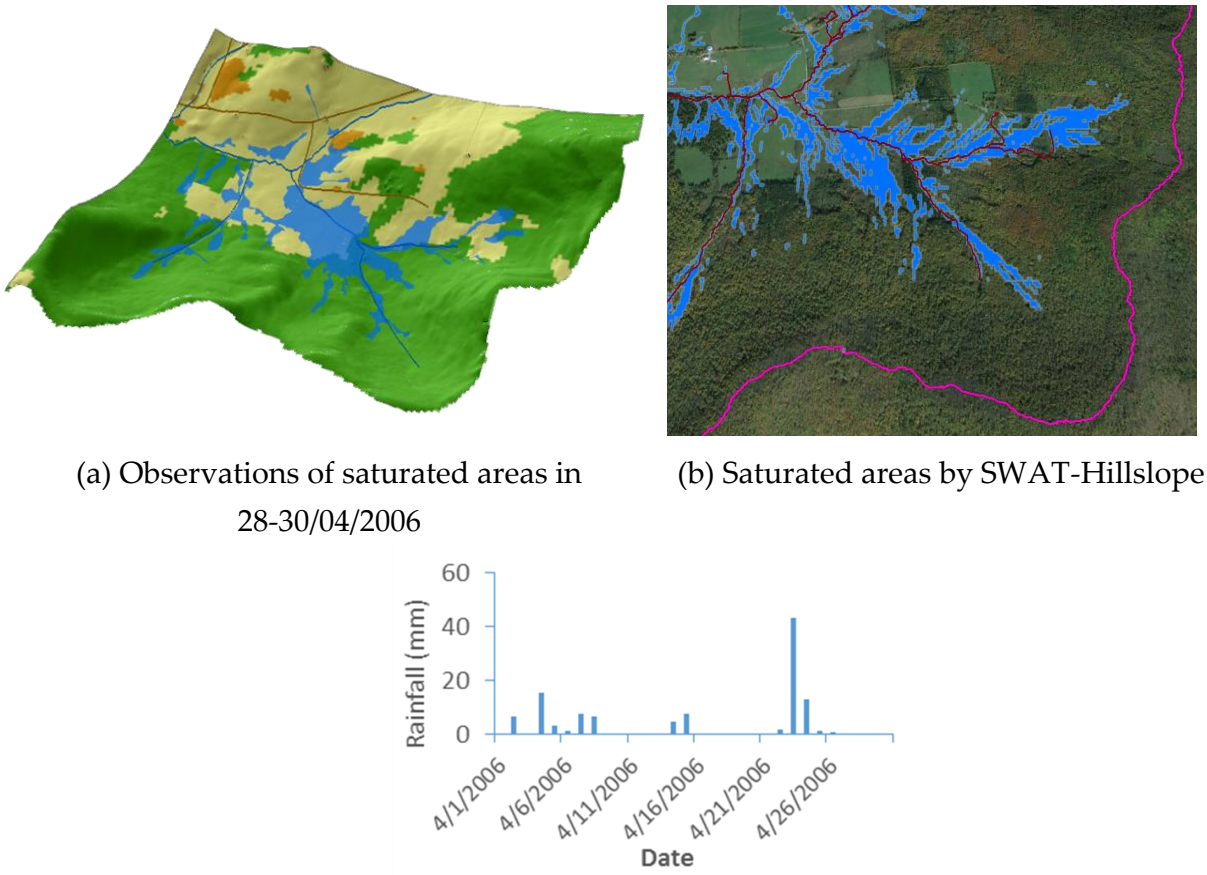

(a) Observations of saturated areas in 28-30/04/2006

(b) Saturated areas by SWAT-Hillslope

(c) Rainfall in April 2006

Figure 4.12. Saturated areas simulated by SWAT-Hillslope compared with observations.

The statistical-dynamical (SD) approach to simulating the behavior of a perched aquifer (Wigmosta and Lettenmaier, 1999) treats the mean height of a perched water table as a time-varying dynamic process while the shape of the water table (i.e., the spatial distribution of depth

to water table) within the hillslope is based on a statistical distribution of soil water storage capacity. The water table as a whole moves up and down as the average depth of water in the perched aquifer changes, while the shape of the water table remains constant over time (Figure 4.13). A number of models utilize this approach, including TOPMODEL (Beven and Kirkby, 1979; Sivapalan et al., 1997), the Variable Infiltration Capacity (VIC) model (Liang and Lettenmaier, 1994; Wood et al., 1992), the Probability Distributed Model (PDM) (Moore, 2007), the XINANJIANG model (Zhao et al., 1995), and the Australian Water Balance Model (AWBM) (Boughton, 2004). The efficiency of this approach has been studied most for TOPMODEL. The topographic wetness index (TWI) which defines the soil water storage capacity distribution in TOPMODEL has been shown to be fairly well correlated with observed soil moisture patterns in a number of studies including for the Town Brook watershed (Agnew et al., 2006; Buchanan et al., 2014; Grabs et al., 2009; Harpold et al., 2010; Lyon et al., 2004; Moore and Thompson, 1996; Troch et al., 1993), but others have found that the TWI may not fully describe the observed soil moisture patterns and that other factors not captured by the index may significantly influence wetness distributions (Buttle et al., 2001; Güntner et al., 2004; Hjerdt et al., 2004; Iorgulescu and Jordan, 1994; Seibert et al., 2003).

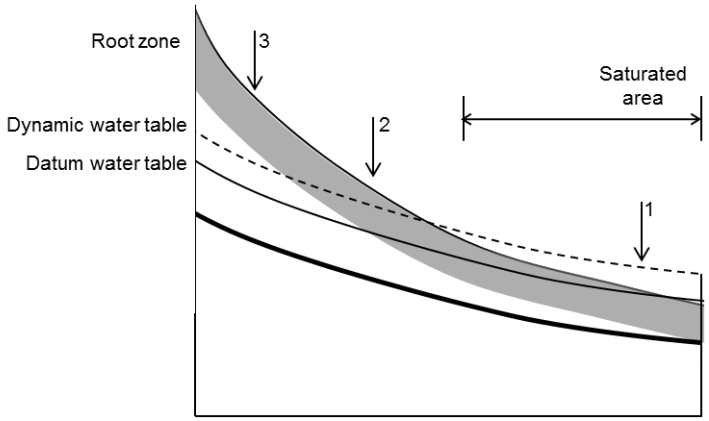

Figure 4.13 Idealized hillslope profile according to statistical dynamic approach. Water table saturates at location 1, intersects the root zone at location 2, and is below the root zone at location 3.

SWAT-Hillslope adopts the variable bucket approach of Sivapalan et al. (1997) and Boughton (2004) and others for defining the distribution of soil water storage capacity. A user-defined distribution is input by dividing the catchment into a set of subareas of increasing storage capacity and specifying the area and maximum storage capacity of each areal wetness class. The moisture distribution may be parametric, as in TOPMODEL, VIC, PDM and XINANJIANG models; or empirically derived as in AWBM model. In the application of SWAT-Hillslope in the

Town Brook watershed, the latter approach was taken. A previous analysis of observed soil moisture distribution in relation to the TWI was used to define 5 wetness classes and associated maximum soil moisture storage capacity distribution (Table 4.2). The resultant model performed well in simulating VSAs with a maximum extent of ~10% in accordance with observations as well as the hydrograph at the basin outlet, with hydrograph peaks being composed of substantial return flow.

For catchments where soil moisture data is not available to inform the storage capacity distribution, it may be useful to consider defining catchment wetness classes at least initially according to a basic wetness classification scheme (from wet to dry), for example: 1) perennial stream channel; 2) perennial wetlands; 3) seasonally-saturated wetlands; 4) intermittently saturated areas; 5) rarely or never saturated. A basic wetness classification may be parametrized using a variety of information, including soil survey hydrologic data, wetland maps, farmer/landowner observation knowledgebase. It may also be useful to consider the shape of a storage capacity distribution developed from soft data as falling between two extreme cases (Figure 4.14): (a) a catchment with limited benches and floodplains, limited maximum extent of VSAs, and characterized by a TWI storage capacity distribution, vs. (b) one with extensive floodplains, extensive extent of VSAs, and characterized by a pareto distribution with b>1 (Moore 2007). Alternatively, the moisture capacity distribution can be derived directly from the TWI distribution as in the variable bucket representation of TOPMODEL of Sivapalan (1997). The TWI distribution is transformed to a storage capacity distribution (S) by:

$$S = edc\_factor * (TWI_{\max} - TWI) \tag{4.5}$$

where TWI_{max} is the maximum TWI value for the catchment, and *edc_factor* serves as the TOPMODEL's 1/f hydrogeological parameter, a measure of the assumed exponential decrease of soil hydrologic conductivity with depth. Use of distribution (x) effectively equates the saturation-excess runoff algorithm in SWAT-Hillslope with a TOPMODEL application.

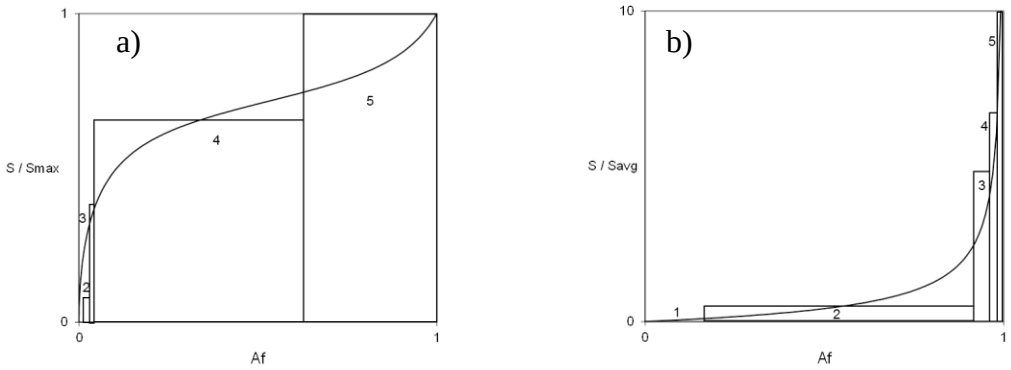

Figure 4.14. Water capacity distribution functions for two different topographic regimes. a) with limited benches and floodplains, limited maximum extent of VSAs, and characterized by a TWI storage capacity distribution. b) catchment with extensive floodplains, extensive extent of VSAs, and characterized by a pareto distribution with b>1 (Moore 2007).

4.1.5. Conclusions

When applied to the Town Brook watershed, the modified version of SWAT, SWAT-Hillslope, successfully separates the infiltration excess runoff and saturation excess runoff. SWAT-Hillslope performed well in flow simulation for both daily and monthly time steps. Moreover, the comparison on spatial distribution of saturated areas with available observation in the three days with no precipitation showed that SWAT-Hillslope model was able to correctly predict the locations of saturated areas while the original SWAT could not predict any surface runoff in these dry days. SWAT-Hillslope allows the transportation of interflow laterally from upslope to downslope areas, providing water to saturate the wet HRUs. In addition, the perched aquifer has close interaction with the soil profile, which keeps the water level stay high in wet HRUs. Based on the good performance of SWAT-Hillslope both on streamflow simulation and spatial runoff distribution, it can be confidently concluded that with the incorporation of topography characteristics and the adding of the perched aquifer, SWAT-Hillslope gives a realistic representation of hydrological processes and is expected to lead to better water quality models where the source of the surface runoff matters.

4.2. Application of the General Lake Model (GLM) to Cannonsville and Neversink Reservoirs

A major new modeling initiative at DEP involves disinfection byproducts (DBPs) in the water supply. DBPs are formed when chlorine is added to water as a disinfectant in order to inactivate bacteria, viruses, and other pathogens. A portion of the naturally-occurring organic compounds found in tributary streams and water supply reservoirs reacts with chlorine to form DBPs; this group of compounds which form DBPs are collectively known as the DBP precursors (DBPP). DEP seeks to better understand the role of both external watershed loading and internal reservoir production of dissolved organic carbon (DOC) and DBPPs, and the effect of watershed, terrestrial, and reservoir processes which act as sources and sinks for these chemicals. The role of climate change on levels of DOC and DBPPs in the water supply is also of significant interest. A goal of this work is to develop a predictive model for DOC and DBPP that may be used in guiding watershed protection activities, evaluating impacts of climate change, and integrated into DEP's Operations Support Tool (OST) to guide operations to minimize DBPPs in the water supply and DBPs in the distribution system.

The General Lake Model (GLM), linked with the Aquatic Ecodynamics model (AED), has been selected for application and testing in predicting DOC and DBPPs in DEP reservoirs. GLM/AED is an open source community lake and reservoir model that has been developed as an initiative of the University of Western Australia and the Global Lake Ecological Observatory Network (GLEON), and has been applied to numerous lakes and reservoir within the GLEON network and beyond. In its current form, GLM/AED is capable of simulating the organic carbon cycle, but is not capable of predicting DBPP. Working with postdoctoral researchers and associated university faculty advisors, DEP modeling staff will be developing enhancements to this model to allow prediction of DBPP. Cannonsville and Neversink Reservoirs have been selected for initial development and testing of this model.

Here the application and testing of the hydrothermal component of GLM to Cannonsville and Neversink is described. Hydrothermal testing and validation is a critical first step in the process of model application and testing, as the predictions of water temperature and internal reservoir mixing and transport that are a part of the hydrothermal predictions affect the subsequent predictions of all water quality parameters.

4.2.1. Methods

4.2.1.1. Study sites

Cannonsville and Neversink Reservoirs, two NYC reservoirs with different catchment characteristics, were chosen to test if GLM is capable of simulating in NYC reservoirs (Figure 4.15). The Neversink Reservoir watershed is 91% forested with very little agriculture (1.4%) and developed land (3%). In contrast, land use in the Cannonsville Reservoir watershed is about 19% agricultural with an additional 7% categorized as developed. The GLM model was applied to these two reservoirs for the historical conditions that occurred in 2007 and 2008.

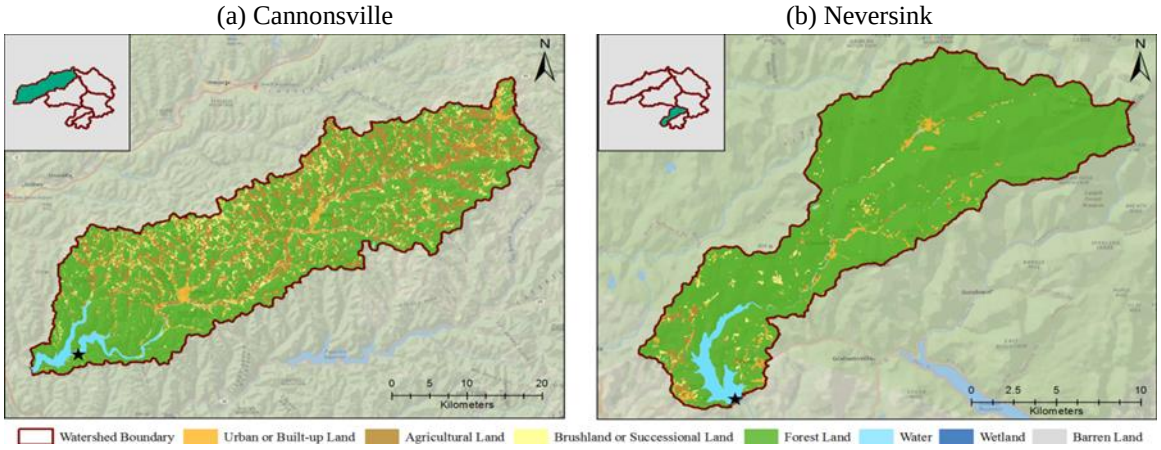

Figure 4.15. Land use within the watersheds of (a) Cannonsville Reservoir, and (b) Neversink Reservoir.

4.2.1.2. GLM Model set up

Bathymetric curves relating reservoir surface area and storage volume to water surface elevation are required for operation of GLM. The bathymetric curves for Cannonsville (Figure 4.16) and Neversink Reservoirs (Figure 4.17) contained in The New York City Water Supply Atlas were used in GLM simulations. In addition, the elevation of the spillway, and elevations of drinking water intakes as used in the GLM model are given in Table 4.6.

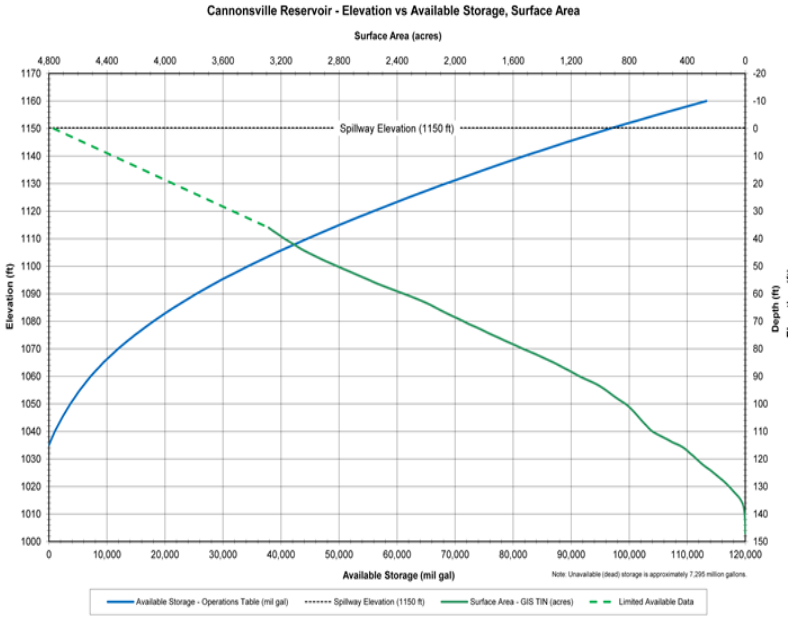

Figure 4.16. Bathymetric curves for Cannonsville Reservoir.

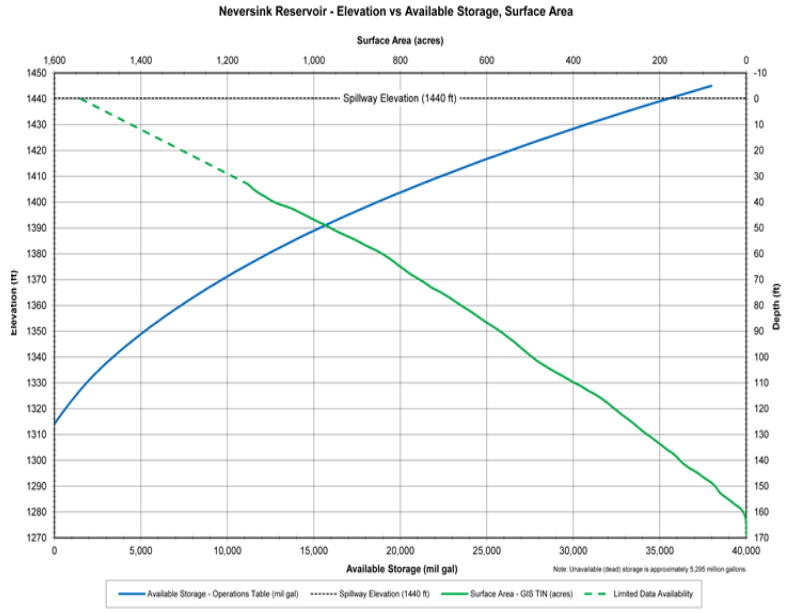

Figure 4.17. Bathymetric curves for Neversink Reservoir.

4.2.1.3. Meteorological inputs

The GLM model requires daily values of various meteorological data, including solar radiation, air temperature, relative humidity, wind speed, rain and snow. Daily values of these quantities for 2007 and 2008 taken from DEP records, are shown in Figure 4.18 for Cannonsville Reservoir, and Figure 4.19 for Neversink Reservoir.

4.2.1.4. Water budget calculation

A water budget calculation was performed independently and prior to GLM simulations. The goal of the water budget calculation was to determine daily values of the ungaged inflow to a reservoir, so that, when used as a model input for a historical period, the predicted reservoir water surface elevation closely matches the observed elevation. The water balance or budget equation used was:

$$\frac{dV}{dt} = Q_{IG} + Q_{IU} - Q_O \tag{4.6}$$

where V is reservoir volume, t is time, Q_{IG} is the gaged surface inflow, Q_{IU} is the ungaged surface inflow, and Q_O is the total outflow. This is the same water budget equation described in Section 5.1 of this report. For Cannonsville Reservoir, USGS streamflow records for the West Branch of the Delaware River at Beerston, and for Trout Creek at Trout Creek, represented the gaged inflows. For Neversink, USGS observations of the Neversink River at Claryville was the single gaged inflow to the reservoir. For both reservoirs, the outflow Q_O is the sum of drinking water withdrawal, dam release, and spill. Using these observations and Equation (4.6), daily values of the ungaged inflow Q_{IU} were determined as described in Section 5.1. The reservoir inflows and outflows for Cannonsville Reservoir for 2007-2008 are shown in Figure 4.20, while the inflows and outflow for the same years for Neversink Reservoir are shown in Figure 4.21.

Table 4.6. Spillway and Intake Elevations of Cannonsville Reservoir and Neversink Reservoir.

Site		Elevation	
		(ft)	(m)
Cannonsville	Cannonsville Reservoir Spillway Elevation	1150.00	350.52
	Cannonsville Reservoir Elevation Tap 1 (CR1)	1032.00	314.55
	Cannonsville Reservoir Elevation Tap 2 (CR2)	1077.75	328.50
	Cannonsville Reservoir Elevation Tap 3 (CR3)	1113.65	339.44
Neversink	Neversink Reservoir Spillway Elevation	1440.00	438.91
	Neversink Reservoir Elevation Tap 1 (NR1)	1314.00	400.51
	Neversink Reservoir Elevation Tap 2 (NR2)	1344.00	409.65
	Neversink Reservoir Elevation Tap 3 (NR3)	1374.00	418.80
	Neversink Reservoir Elevation Tap 4 (NR4)	1404.00	427.94
Note: elevations use Bureau of Water Supply (BWS) datum			

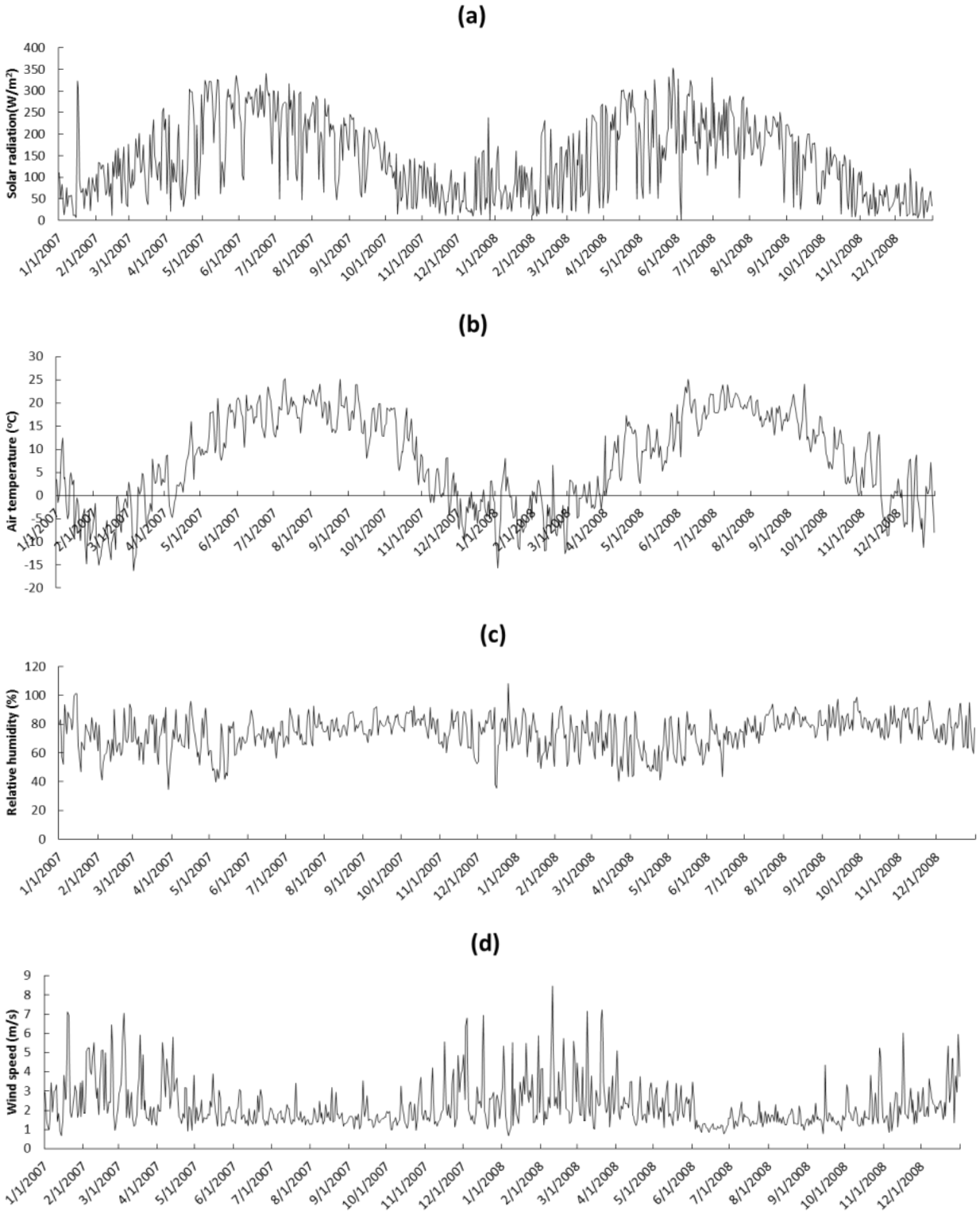
(a)
Solar radiation(W/m²)
(b)
Air temperature (°C)
(c)
Relative humidity (%)
(d)
Wind speed (m/s)

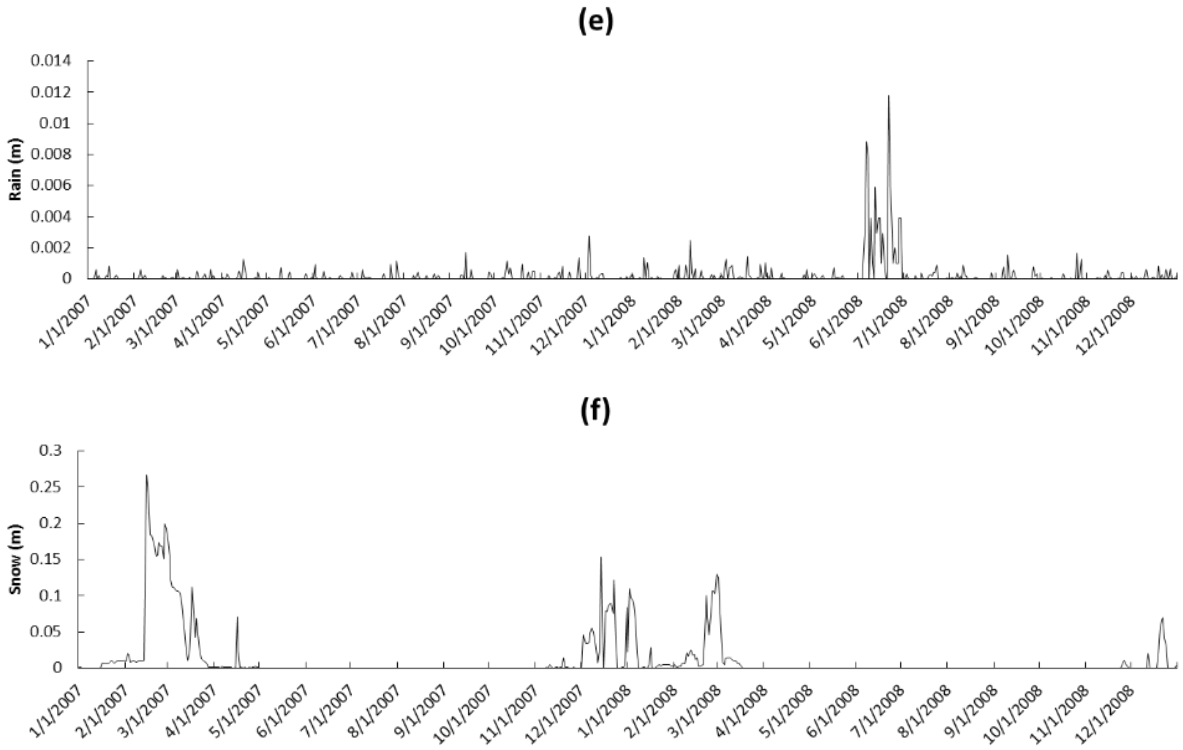

Figure 4.18. Meteorological data for Cannonsville Reservoir, 2007-08.

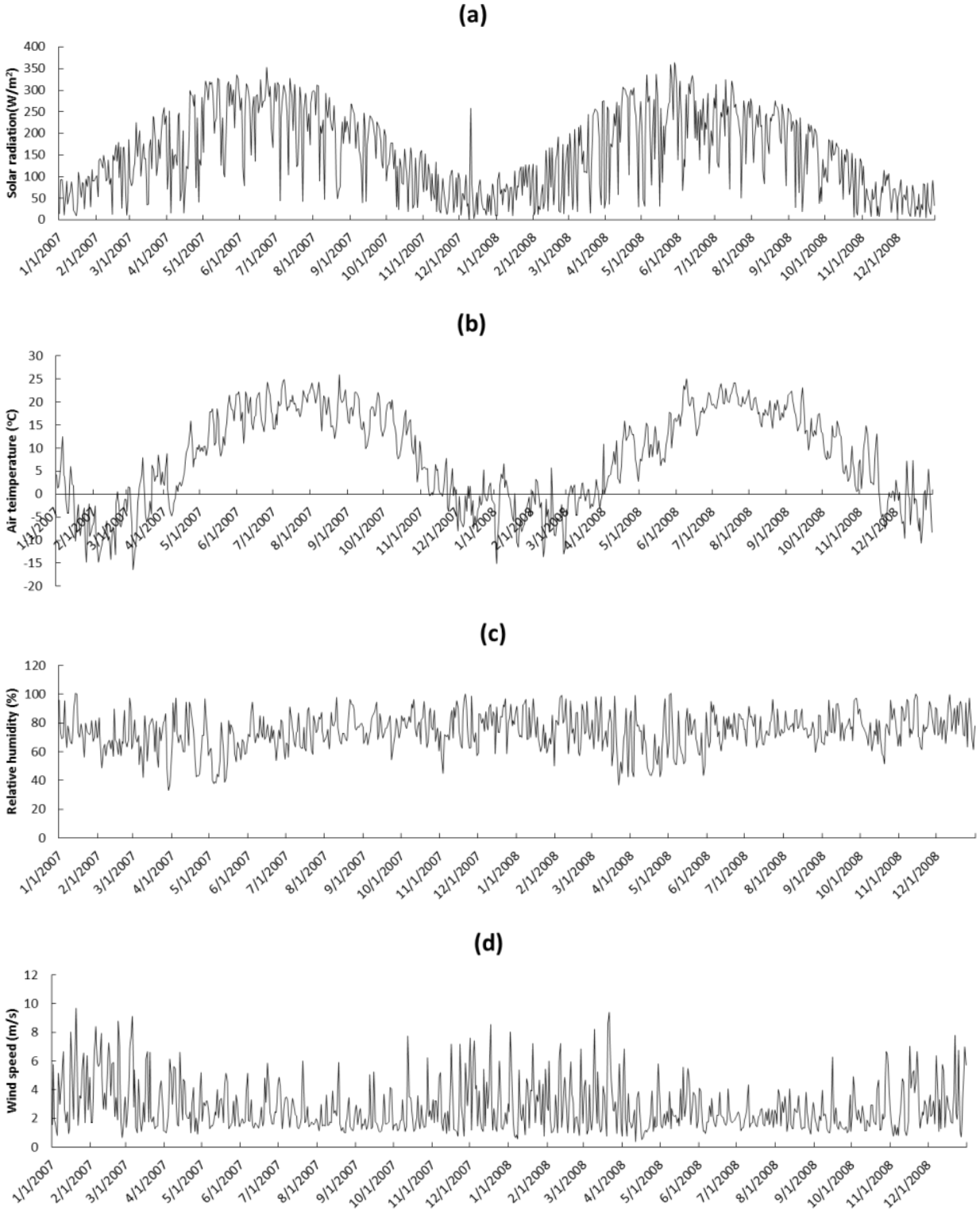
(a)
Solar radiation(W/m²)
(b)
Air teimperature (°C)
(c)
Relative humidity (%)
(d)
Wind speed (m/s)

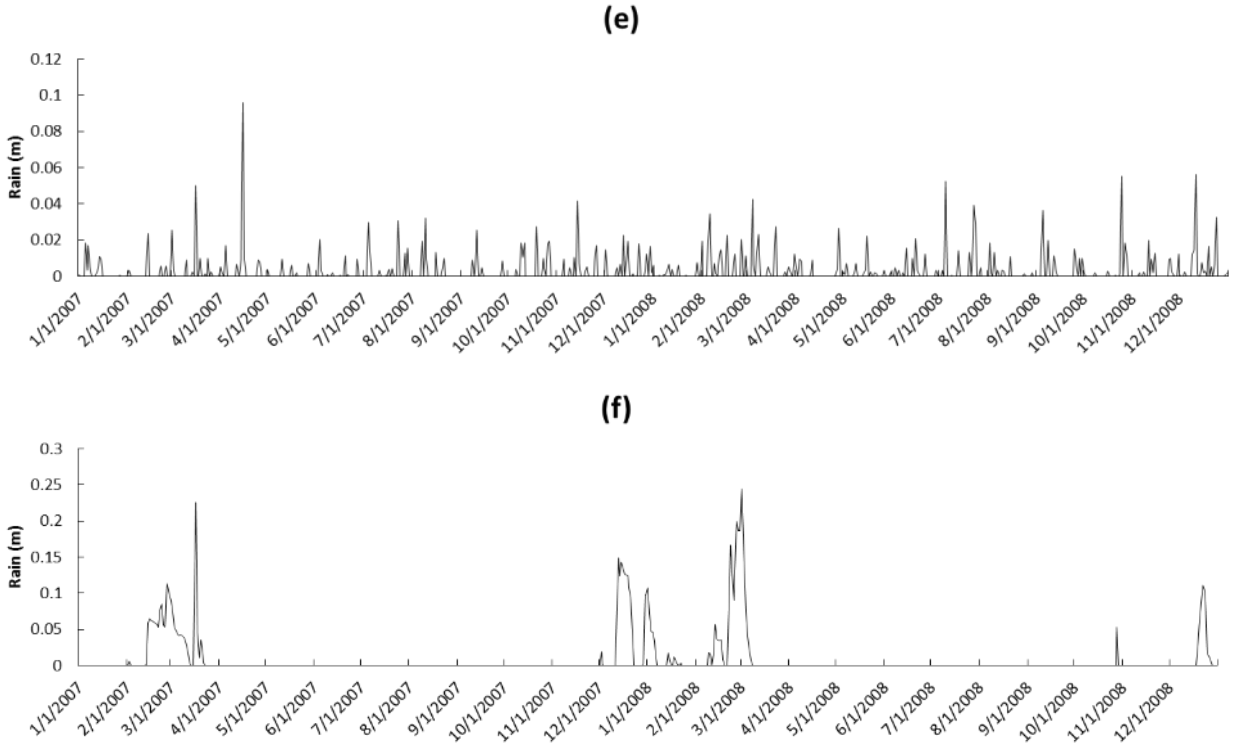

Figure 4.19. Meteorological data for Neversink Reservoir, 2007-08.

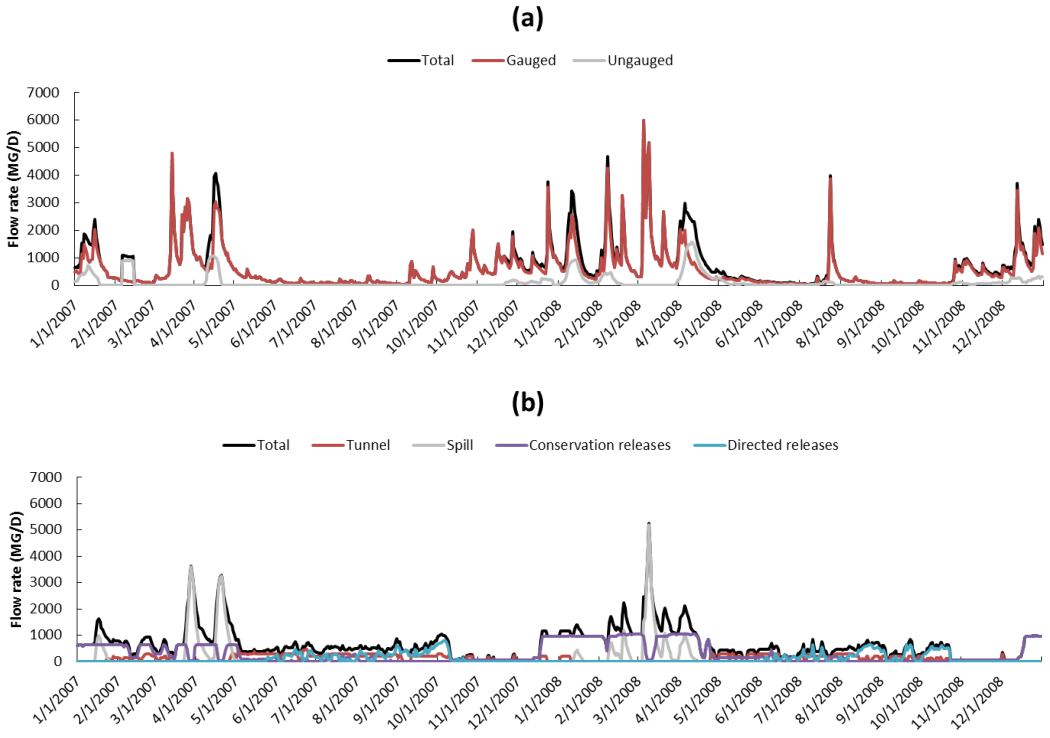

Figure 4.20. Components of the water budget for Cannonsville Reservoir, 2007-2008: (a) inflows, and (b) outflows.

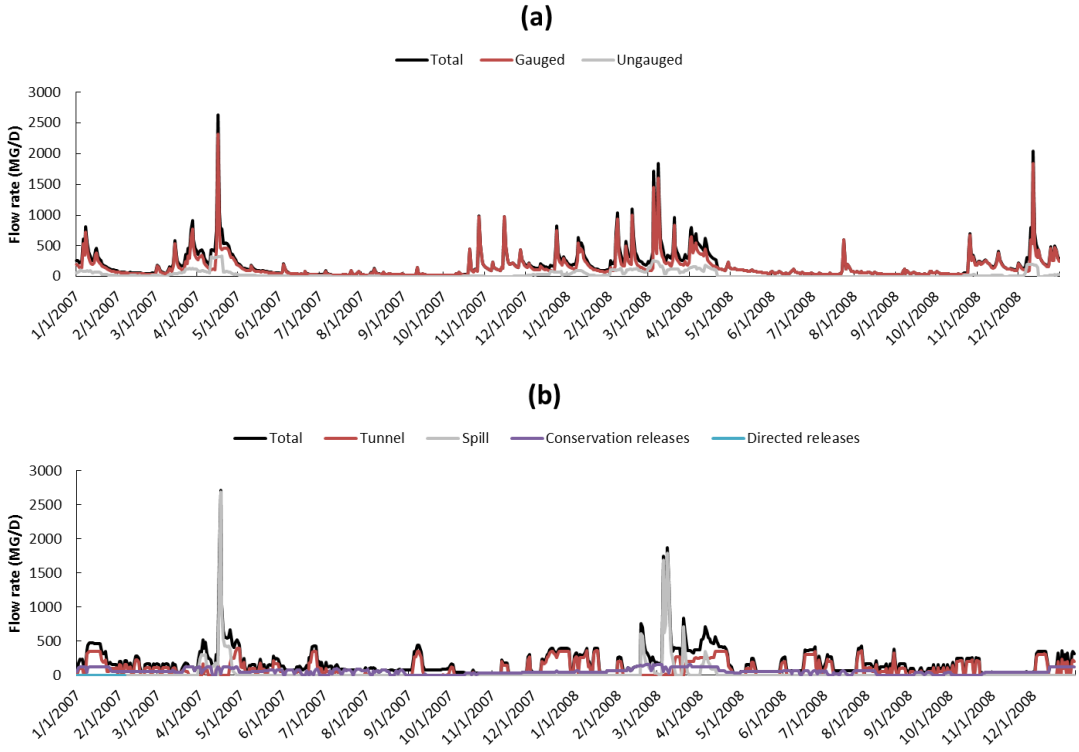

Figure 4.21. Components of the water budget for Neversink Reservoir 2007-2008: (a) inflows, and (b) outflows.

4.2.1.5. Tributary Stream Temperature

The temperature of tributary streams is a required input for GLM. Using DEP records, the temperature of stream inflows to for Cannonsville and Neversink Reservoirs in 2007 and 2008 are shown in Figure 4.22.

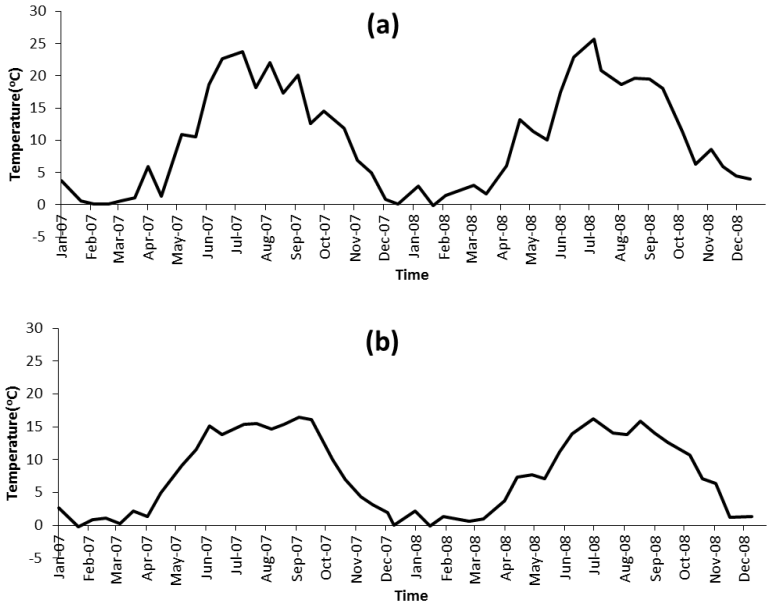

Figure 4.22. Inflow temperatures of Cannonsville Reservoir (a) and Neversink Reservoir (b).

4.2.1.6. Model calibration and validation

The primary goal in this application of the GLM hydrothermal model is the accurate simulation of the temperature of the entire water column, including the surface temperature (0-3m) and the bottom water layer (at variable depth) for the entire whole simulation period. Model simulations began on first date of water column temperature measurements in each of two years, for each reservoir, and continued to the end of year (Table 4.7). The predicted water column temperatures were compared to routine DEP temperature observations. The whole water column was first manually calibrated and then an auto calibration procedure was applied to reduce root mean square errors (RMSE) in the predicted water column temperature. The key hydrothermal model parameters coefficients that were adjusted as a part of the calibration process are given in Table 4.8.

Table 4.7. The simulation period for Cannonsville Reservoir and Neversink Reservoir.

		Cannonsville	Neversink
Calibration	Start	4 April 2007	24 April 2007
	End	31 December 2007	31 December 2007
Validation	Start	4 April 2008	14 April 2008
	End	31 December 2008	31 December 2008

Table 4.8. GLM hydrothermal model coefficients that were adjusted during model calibration.

Symbol	Parameter Description	Default	Cannonsville	Neversink
h_{min}	Minimum layer thickness (m)	0.5	0.25	0.25
h_{max}	Maximum layer thickness (m)	1.5	0.5	0.5
C_K	Mixing efficiency – convective overturn	0.2	0.125	0.125
C_W	Mixing efficiency – wind stirring	0.23	0.1033	0.1033
C_S	Mixing efficiency – shear production	0.3	0.0407	0.4868
C_T	Mixing efficiency – unsteady turbulence	0.5	0.51	0.51
C_{KH}	Mixing efficiency – Kelvin-Helmholtz turbulent billows	0.3	0.285	0.285
C_{HYP}	Mixing efficiency – hypolimnetic turbulence	0.5	0.52	0.47
K_W	Extinction coefficient for PAR Radiation (m^{-1})	0.2	0.7396	0.5023
A_C	Critical area below which wind sheltering may occur (m^2)	10^7	10^7	10^7
Wind factor	Wind multiplication factor	1.0	1.2676	1.0648
C_E	Bulk aerodynamic coefficient for latent heat transfer	0.0013	0.0014	0.0022
C_M	Bulk aerodynamic coefficient for transfer of momentum	0.0013	0.0013	0.0013
C_H	Bulk aerodynamic coefficient for sensible heat transfer	0.0013	0.0013	0.0013
λ	Latent heat of evaporation (J/Kg)	2.453×10^6	2.453×10^6	2.453×10^6
σ	Stefan-Boltzmann constant ($W/m^2/K^4$)	5.67×10^{-8}	5.67×10^{-8}	5.67×10^{-8}
ε_a	Emissivity of the water surface	0.985	0.985	0.985
C_D	Streambed drag	0.016	0.016	0.016
G	Seepage rate (m/d)	0	0	0

4.2.2. Results and Discussion

4.2.2.1. Water balance

The GLM simulated water surface elevation for Cannonsville Reservoir is shown in Figure 4.23. The good agreement between predictions and observations reflects the accurate calculation of ungaged inflows, and the accuracy of the bathymetric curves. The results for Neversink Reservoir (Figure 4.24) as similarly good. During the calibration and validation period, the simulated water surface elevation was generally highest in the spring and lowest in the fall both in Cannonsville Reservoir and Neversink Reservoir, which reflected the observed water surface elevation.

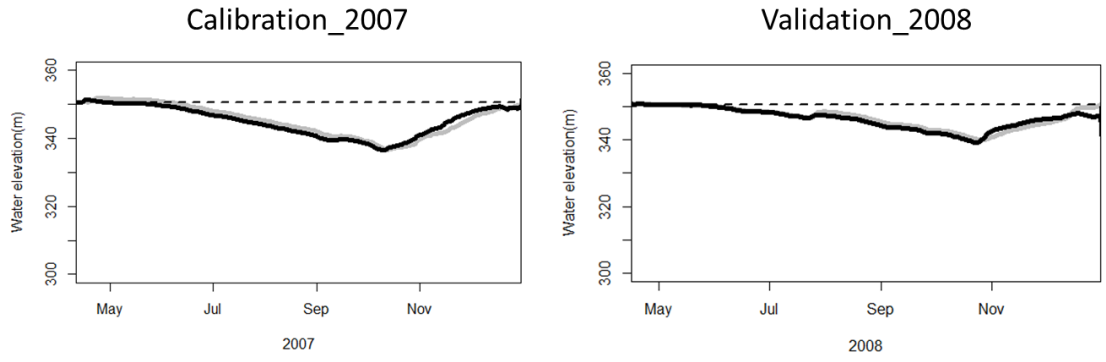

Figure 4.23. Simulated water level (grey) and observed water level (black) of Cannonsville Reservoir (dash line is the spillway elevation).

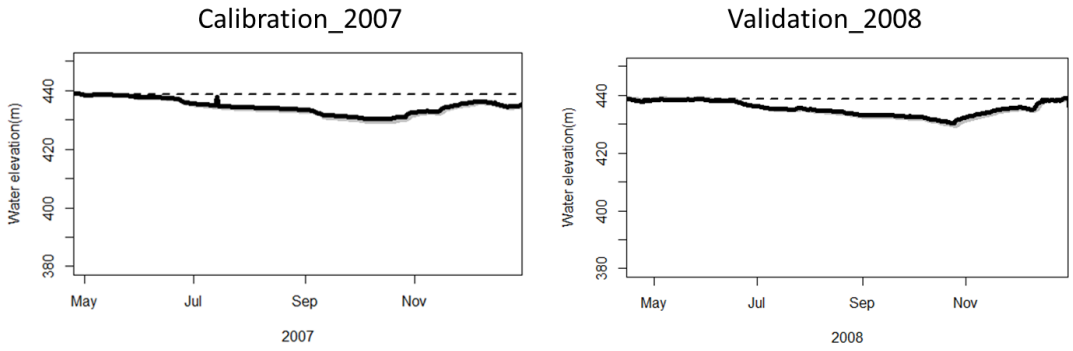

Figure 4.24. Simulated water level (grey) and observed water level (black) of Neversink Reservoir (dash line is the spillway elevation).

4.2.2.2. Temperature simulation

Calibration on the hydrothermal component of GLM was based comparison on predicted and observed temperatures for 2007 only. Once the calibration step was completed, the calibrated model was then applied to each reservoir for 2008, in order to separately validate the calibrated model.

The thermal structure of Cannonsville and Neversink Reservoirs as simulated by GLM is shown in Figure 4.25 and Figure 4.26, respectively. Comparison of predicted and observed temperatures in the surface and the bottom water layers of Cannonsville and Neversink Reservoirs are shown in Figure 4.27 and Figure 4.28, respectively. The seasonal variation in the temperatures of both water layers was captured well. The RMSE values for simulated temperatures over the entire water column for each reservoir for 2007 (calibration) and 2008 (validation) are summarized in Table 4.9. As expected, the temperature errors were modestly larger for the validation period (2008) relative to the calibration period (2007). Moreover, the accurate prediction of bottom water temperature is an indication that vertical mixing between the surface and bottom waters is simulated accurately.

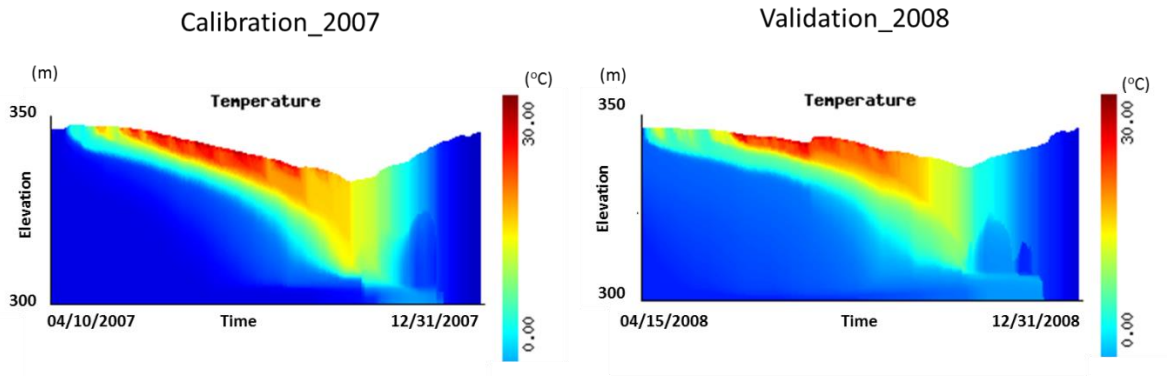

Figure 4.25. GLM simulated temperature in Cannonsville Reservoir.

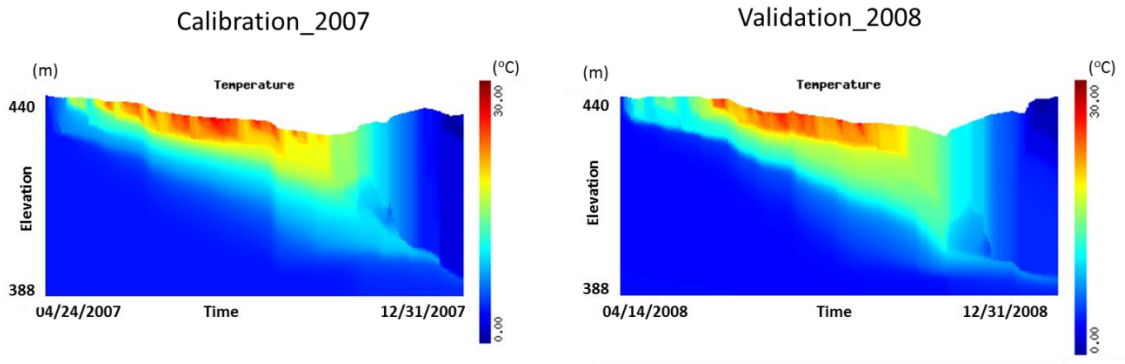

Figure 4.26. GLM simulated temperature in Neversink Reservoir.

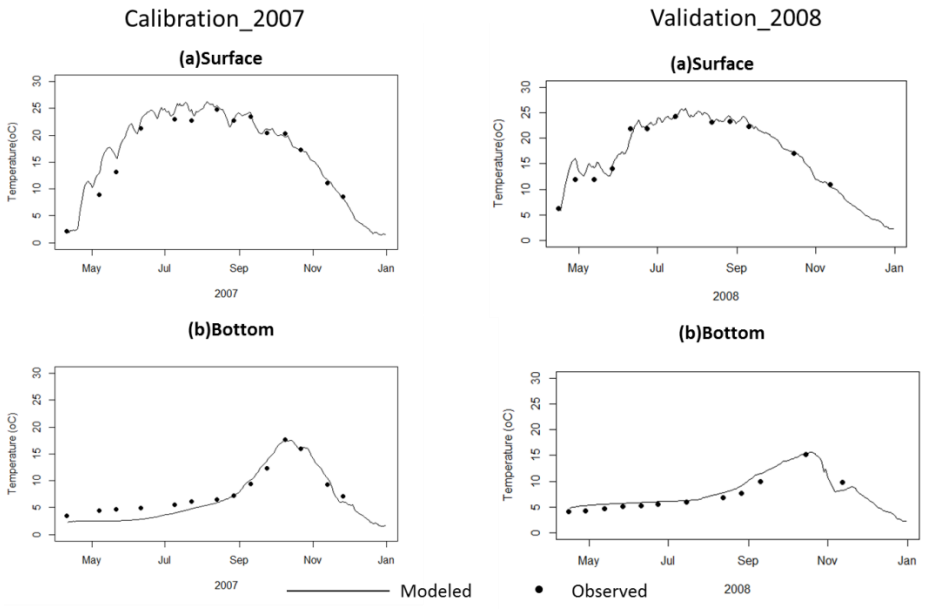

Figure 4.27. GLM simulated temperature for the surface water layer (a) and the bottom water layer (b) in Cannonsville Reservoir.

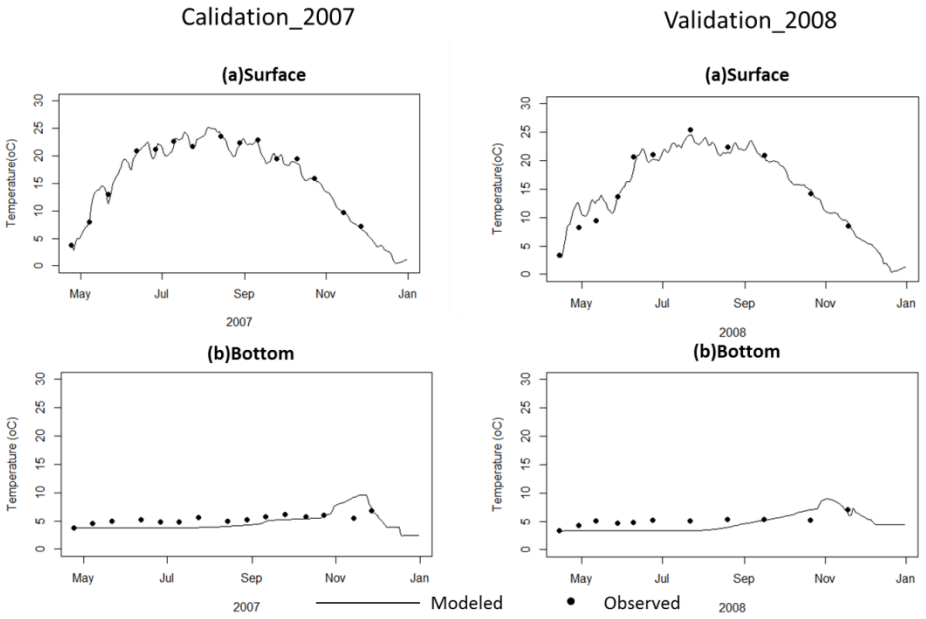

Figure 4.28. GLM simulated temperature for the surface water layer (a) and the bottom water layer (b) in Neversink Reservoir.

Table 4.9. The average root mean square error (RMSE) in predicted water column temperatures (°C).

	Cannonsville	Neversink
Calibration_2007	1.77	1.84
Validation_2008	1.95	2.56

For Cannonsville Reservoir, observed water column temperatures at site 4 were used for model calibration and validation. The one dimensional (1D) GLM model has a good model performance for predicting water column temperatures with the observed data at all sites in NYC reservoirs. During the calibration period (2007), the GLM simulated temperature profiles not only matched the field data at Site 4 well in Cannonsville Reservoir (Figure 4.29) but also matched well the observed data at all sites of Cannonsville Reservoir (Figure 4.30). During the validation period of 2008, the predicted temperature profiles matched the observed temperature profiles at all sites of Cannonsville Reservoir (Figure 4.31). GLM model predictions for Neversink for the calibration year (2007) are shown in Figure 4.32 and Figure 4.33, and validation results depicted in Figure 4.34. For Neversink Reservoir, observations for Site 1 were the basis for model calibration and validation. The observed temperature profiles in Cannonsville (Figure 4.30 and Figure 4.31) and Neversink (Figure 4.33 and Figure 4.34) indicate that there is little horizontal variation in water temperature from site to site. This indicates that, at least with respect to simulation of temperature, the one dimensional assumption is valid. The features of thermal stratification in both reservoirs were reproduced well in summer. This modeling feature is very important for simulating algal blooms and other water quality features. In the epilimnion, the interannual variation (2007 relative to 2008) of temperature was simulated well, which indicates that the GLM model has the ability of predicting the surface heat transfer and wind mixing. However, in the metalimnion and hypolimnion, the simulated temperatures on some specific dates were modestly lower than observations. Although some simulated thermocline depths did not always match the observed depths accurately, the simulated thermocline depth increased from summer to fall, which matched the observed pattern. These results are generally similar to that obtained the previous application of a one dimensional hydrothermal model to Cannonsville (Owens, 1998). Overall, the GLM model succeeded in tracking the seasonal changes of temperature in these two reservoirs.

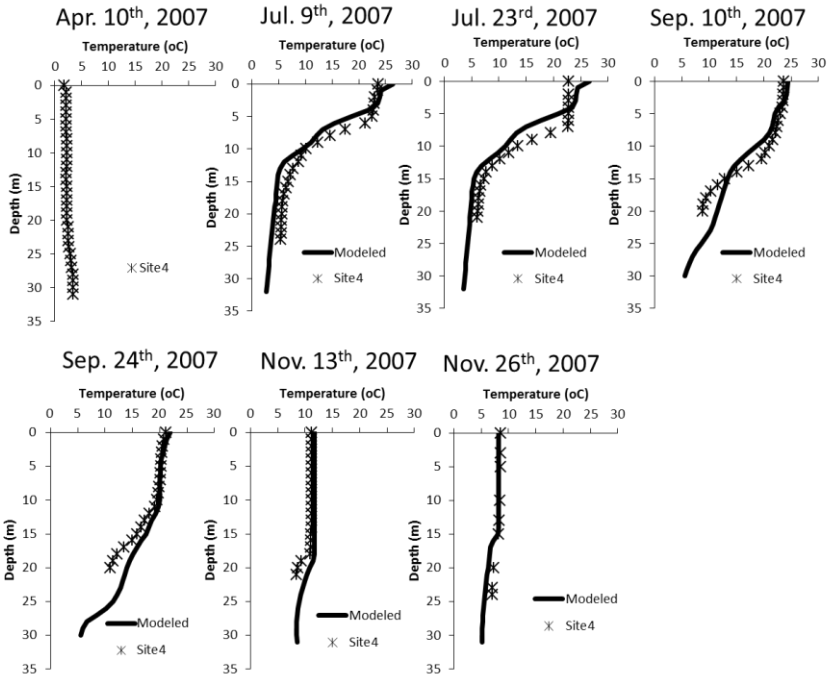

Figure 4.29. Simulated temperature profiles and field data at Site 4 in Cannonsville Reservoir in 2007.

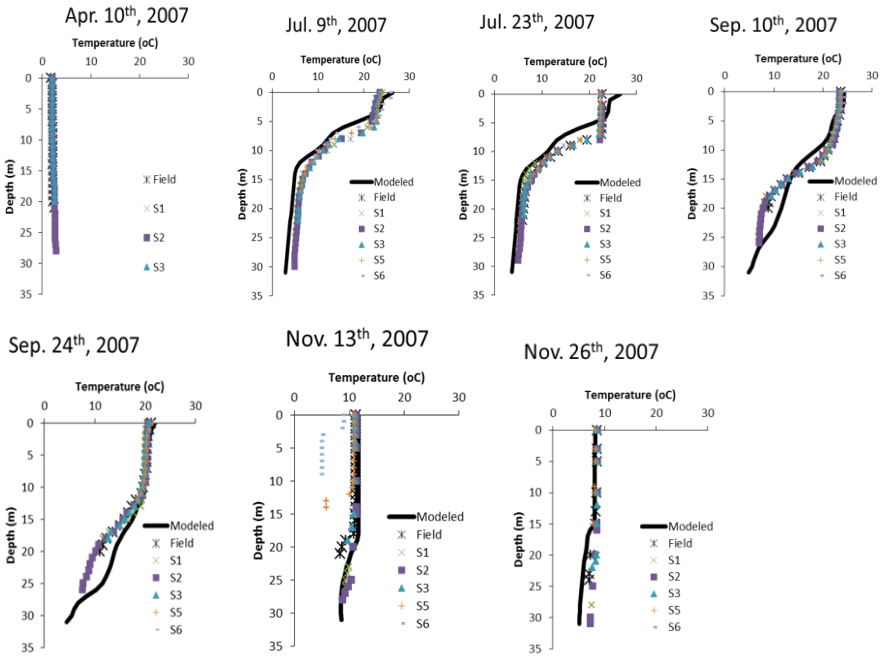

Figure 4.30. Simulated temperature profiles and field data at all sites of Cannonsville Reservoir in 2007.

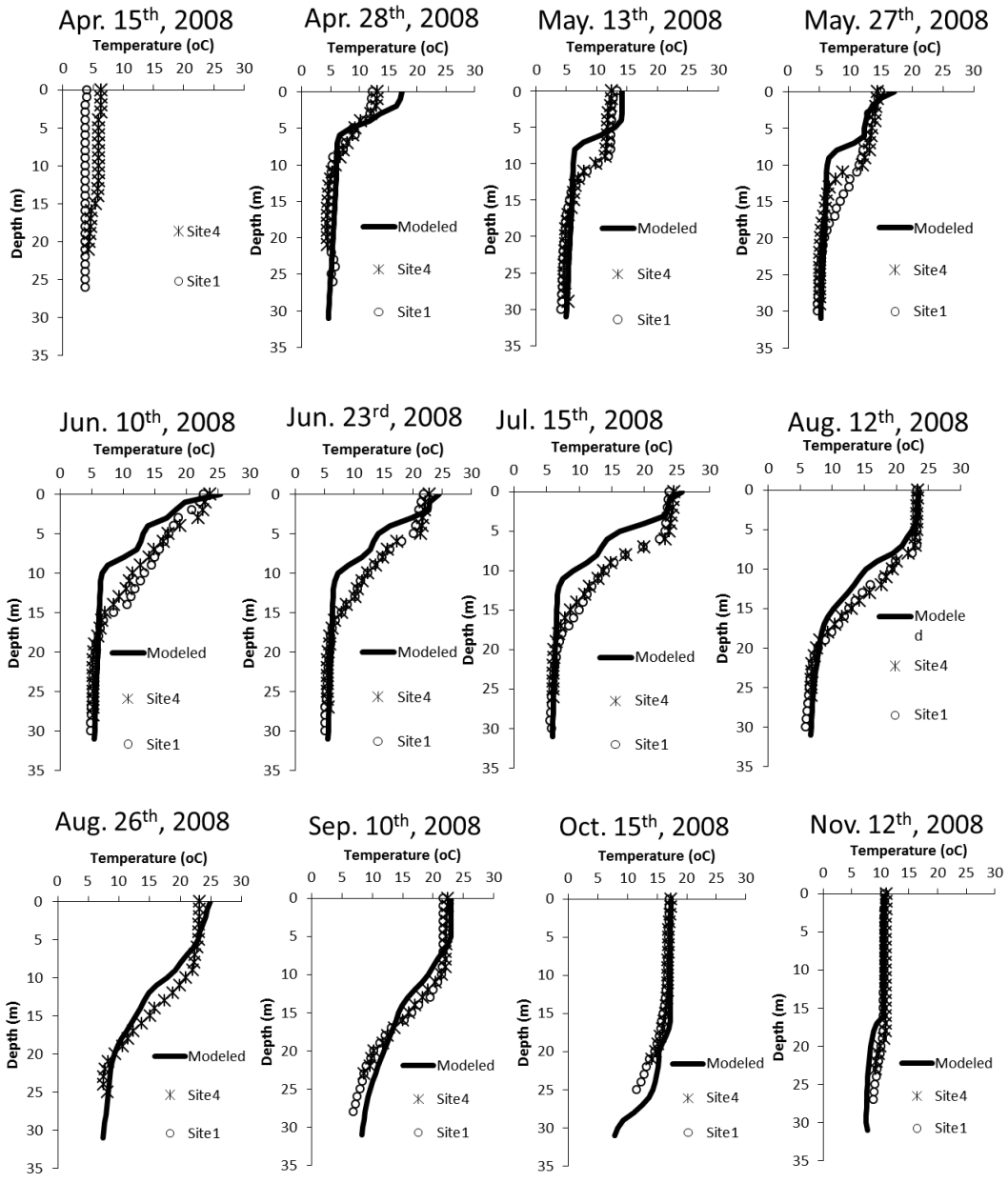

Figure 4.31. Simulated temperature profiles and field data at all sites of Cannonsville Reservoir in 2008.

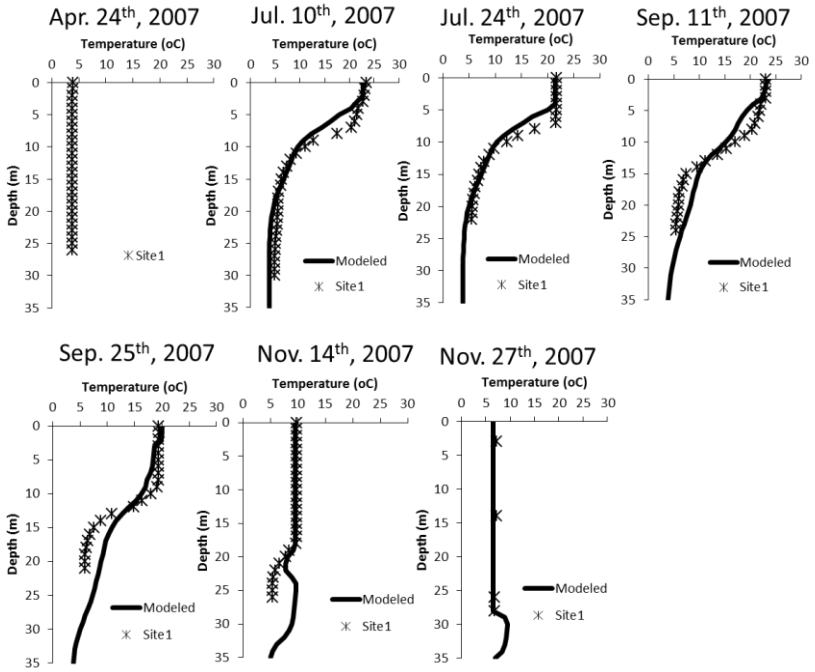

Figure 4.32. Simulated temperature profiles and field data at Site 1 in Neversink Reservoir in 2007.

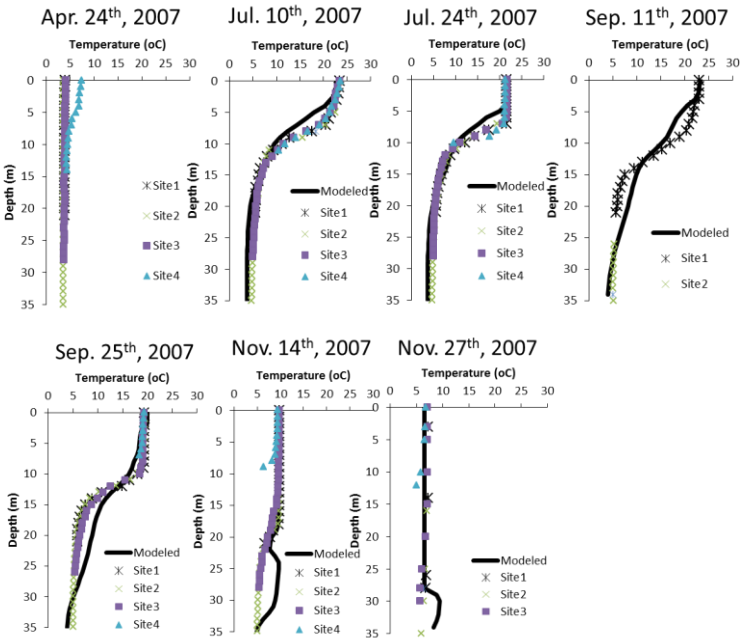

Figure 4.33. Simulated temperature profiles and field data at all sites of Neversink Reservoir in 2007.

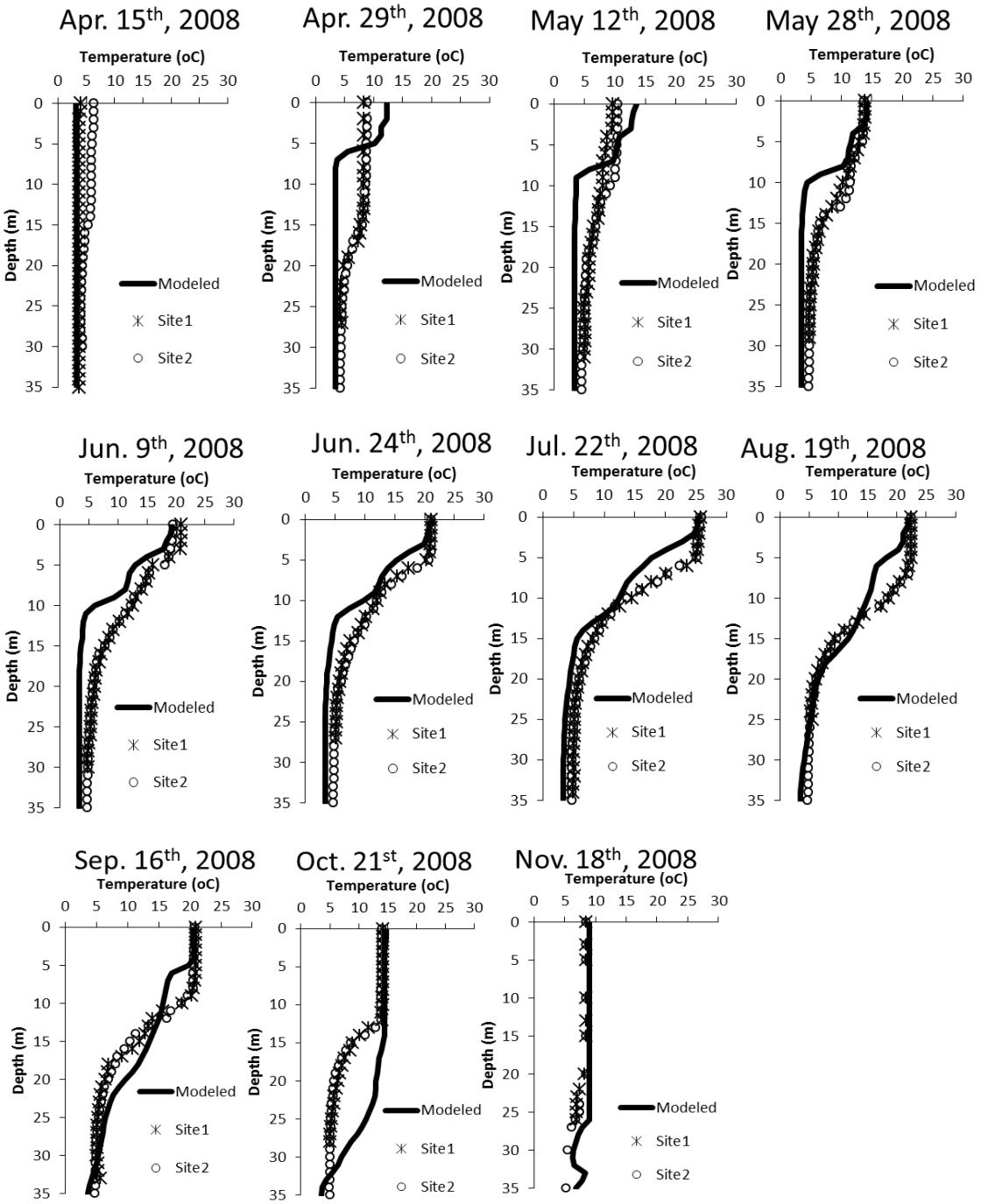

Figure 4.34. Simulated temperature profiles and field data at all sites of Neversink for 2008.

DEP observations of the temperature of the drinking water withdrawal were also compared with model predictions. This comparison not only tests the ability of the model to simulate water column temperature, but also tests the simulation of selective withdrawal

algorithms in the model. Although there was under prediction of withdrawal temperatures in the spring and early summer, the simulated trend of withdrawal temperatures was generally consistent with the observation in Cannonsville Reservoir (Figure 4.35). The blank area in the withdrawal temperature in Figure 4.35 indicates that there was no withdrawal. There was a consistently large difference between simulated and observed withdrawal temperatures in Neversink Reservoir (Figure 4.36). Additional calibration of selective withdrawal model coefficients (Hipsey et al., 2014) will be pursued for Neversink Reservoir in the future.

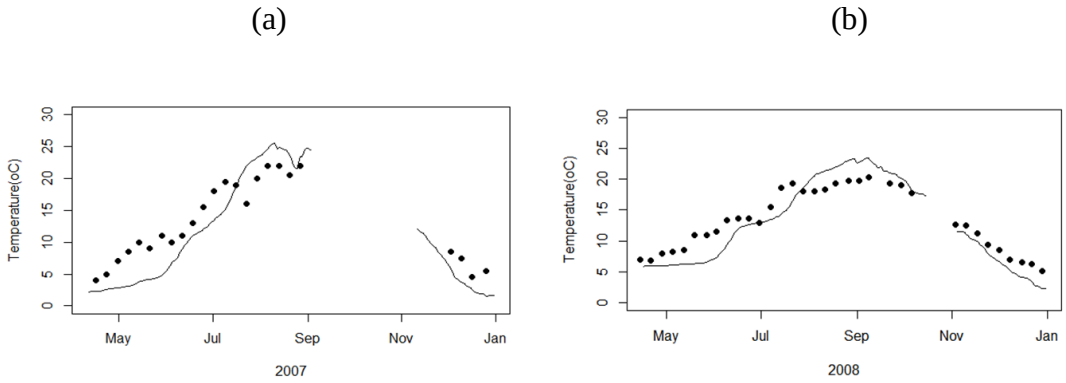

Figure 4.35. Simulated withdrawal temperatures (lines) and observed withdrawal temperatures (circles) of Cannonsville Reservoir: (a) 2007, and (b) 2008.

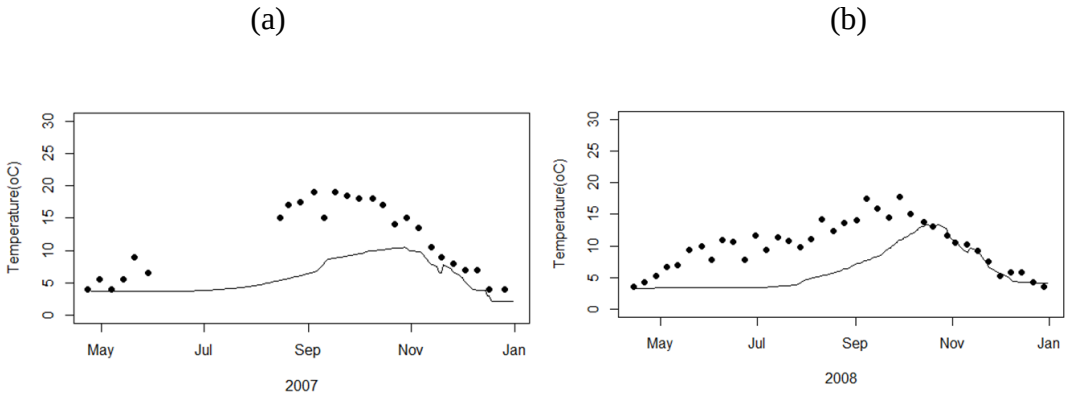

Figure 4.36. Simulated withdrawal temperatures (lines) and observed withdrawal temperatures (circles) of Neversink Reservoir: (a) 2007, and (b) 2008..

4.3. Development and Testing of a Probabilistic Turbidity Model for Rondout Reservoir

4.3.1. Background

NYCDEP now routinely uses the Operations Support Tool (OST) software (Hazen and Sawyer 2013) to help guide reservoir operating decisions involving both the quantity and quality of water. An important water quality parameter of concern for the City's water supply is turbidity. To address this, OST employs a two-dimensional (longitudinal-vertical) multiple size-class turbidity model (Gelda and Effler 2007, Gelda et al. 2009, 2012, 2013) based on the mass transport framework of CE-QUAL-W2 (W2; Cole and Wells 2013). For managing water quantity, OST includes the entire Delaware River Basin, the Catskill subsystem, and the Croton subsystem, though water quality (turbidity) models that have been integrated into OST are for Schoharie, Ashokan, and Kensico reservoirs only.

In the current version of OST, models for Schoharie and Ashokan reservoirs provide input of turbidity from the Catskill Basin to the Kensico Reservoir model, while input of turbidity from the Delaware Basin (mostly Rondout Reservoir water) is specified at historical median values. Here we develop a tool to forecast more realistic simulations of turbidity in Rondout Reservoir withdrawal which can then be specified as input to Kensico Reservoir turbidity model in OST thus making the forecasts of turbidity in the Kensico Reservoir withdrawal more accurate.

The proposed modeling tool is based on a separate turbidity model for Rondout Reservoir, which was developed and validated earlier (Gelda et al. 2013). With the added capability of using short-term ensemble forecasts of hydrological inputs, turbidity, and climatology as the model drivers, it can generate probabilistic forecasts of turbidity. The tool is expected to help guide operations of Rondout Reservoir during storm events in the watershed as well as provide realistic estimates of turbidity inputs for the Kensico Reservoir model in OST.

4.3.2. Approach

The central feature of the overall probabilistic modeling framework is the deterministic hydrodynamic-water quality model, W2 (Figure 4.37). It is capable of simulating transport within the reservoir, features of the thermal stratification regime, temperature in the withdrawal, patterns of turbidity within the reservoir, and in the withdrawal. The model drivers are meteorological conditions, inflows, inflow-temperatures, and inflow-turbidity from Rondout Creek, Chestnut Creek, and Cannonsville, Pepacton, and Neversink tunnels (Figure 4.38).

With the best forecasts of the model drivers, W2 can generate a single best forecast of turbidity. However, such forecast has limited management value because there is no probability associated with it. Further, the forecasts of model drivers have natural variability and uncertainty, which is not represented in the model if only best estimates are used. The probability approach presented here incorporates variability and uncertainty in the model inputs, including meteorological, hydrological, and water quality data (Figure 4.37). The model output generated from this approach is analyzed in a probabilistic format, allowing managers to make risk-based operations decisions. The details of this approach are discussed next.

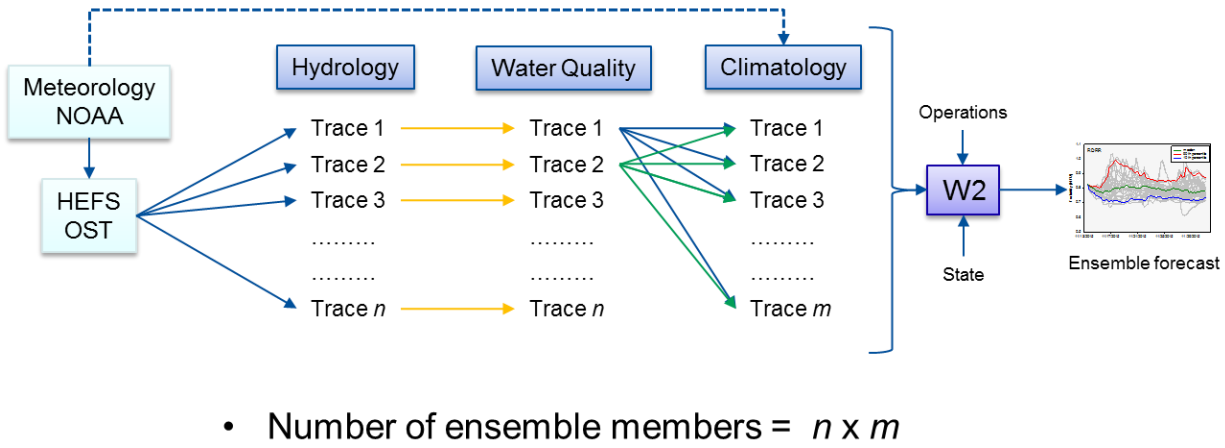

Figure 4.37. Conceptual framework of a probabilistic turbidity model for Rondout Reservoir. (NOAA: National Oceanic and Atmospheric Administration, HEFS: Hydrologic Ensemble Forecast System, OST: Operations Support Tool)

Definitions: Multiple time series of forecast are known collectively as an ensemble of forecast and an individual time series in an ensemble is referred to as an ensemble member. The values in a time series (or an ensemble member) when used in a model as an input can be called a trace. Linked input traces of meteorology, hydrology, and water quality together with the corresponding model output trace will form a complete model simulation trace. Such multiple simulation traces form the basis of ensemble reservoir water quality forecasts which are then used to construct probabilistic predictions.

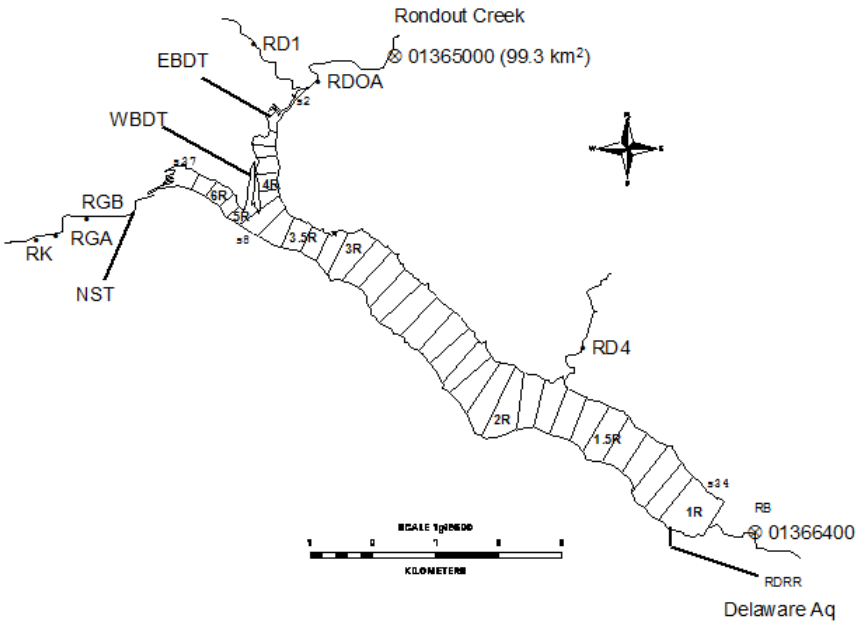

Figure 4.38. CE-QUAL-W2 model segmentation of Rondout Reservoir, including monitoring location on the tributaries, and in the reservoir. Inputs from the upstream Cannonsville, Pepacton, and Neversink reservoirs are indicated by WBDT, EDT, and NST, respectively.

Method: Ensemble forecasts of atmospheric conditions (e.g., temperature, precipitation) by National Oceanic and Atmospheric Administration (NOAA) are used by National Weather Service's (NWS) hydrologic models to generate hydrologic ensemble forecasts. These forecasts are accessed and post-processed by OST. The post-processing step corrects any statistical bias in the forecasts, formats data according to the input requirements of OST, and develops flow inputs for the locations in the model (Figure 4.37).

The modeling tool developed here, obtains from OST, traces (n = 47) of total inflow to Rondout Reservoir and divides into inflow from Rondout Creek, Chestnut Creek, and ungaged area (Figure 4.38), as required by W2 model. Corresponding to each of these hydrologic traces, a time series trace of turbidity is estimated from the empirical relationships developed between flow and turbidity (UFI 2013).

Site-specific short-term (e.g., days–weeks) forecasts of hourly meteorological data (air temperature, dew point temperature, wind speed and direction, and solar radiation) corresponding to the hydrologic traces are not available presently. Therefore, historical data available for the 1987-2012 (m = 25) interval were used. To combine the variability present in the hydrological data with the variability present in the meteorological data, m W2 model runs were made for each hydrological and water quality trace input, for a total of $m \times n$ (25 × 47 =

1125) runs (Figure 4.37). Additional inputs required by W2 model are initial state (i.e., temperature, water surface elevation and turbidity) of the reservoir and reservoir operations (inflows from the three upstream reservoirs, and withdrawal). The following section describes an example application of the approach and compares the predicted turbidities in the withdrawal, in a probabilistic context, with the actual observations.

4.3.3. Model Specifications for an Example Application

The model was applied to forecast turbidity in the withdrawal from Rondout Reservoir during a period of 11/13/2015–12/1/2015 (18 days). All hydrodynamic and water quality model parameters were adopted from the previously validated model (Gelda et al. 2013).

Future boundary conditions: Hydrologic ensemble forecast included 47 traces of total inflow, which was processed into three separate inflows from Rondout Creek, Chestnut Creek, and ungaged area represented in the model as distributed along the shoreline, according to the respective watershed areas. Turbidity associated with each hydrologic trace and source input was estimated according to the empirical relationships developed by UFI (2013). The contribution to the total turbidity from the three size classes of particles was estimated as specified by UFI (2013). Meteorology was obtained from the historical database developed for the reservoir site for 1987–2012 (25 year-long individual traces). Inflow temperatures were also obtained from the historical observations for the same interval. A trace of inflow temperature corresponded to the same time trace of meteorology.

Reservoir Operations: Inputs from the three upstream reservoirs – Cannonsville, Pepacton, and Neversink reservoirs – were specified as listed in Table 4.10. Neversink Tunnel was not in operations during the study period. Withdrawal and downstream release from Rondout Reservoir were set at 700 MGD, and 10 MGD, respectively. The elevation of the intake in use was 784 feet.

Initial conditions: The observed water surface elevation at the beginning of the forecast period was 836 feet. Initial values of the temperature and turbidity in the reservoir were obtained by linearly interpolating observations, from 3 sites and 3–4 depths at each site, made during a routine field survey on 11/10/2015 (Table 4.11).

Table 4.10. Specifications of operations of upstream reservoirs for the forecast interval of 11/13/2015–12/1/2015.

Source	Flow[+]	Temperature[*]	Turbidity[*]
Pepacton	500 MGD	historical median daily; daily values	historical 10th percentile daily; daily values
Cannonsville	200 MGD	historical median daily; daily values	historical median daily; daily values
Neversink	0	-	-

[+]option for choosing any time series will be added; specified flows were approximately equal to the actual operations and were projected to continue for the forecast period.
[*]option for choosing historical 5th, 10th, 25th, 75th, 90th, 95th percentile values or any time series is available.

Table 4.11. Observed temperature and turbidity depth profiles at sites 1, 2, and 3 in Rondout Reservoir on 11/10/2015.

Site	Depth (m)	Temperature (°C)	Turbidity (NTU)
1	3	12.7	0.8
1	20	12.1	0.85
1	36	8.8	0.85
1	47	7.5	1.6
2	3	12.5	0.7
2	17	12.4	0.6
2	32	11.3	1.5
3	3	12.3	0.9
3	14	12.3	0.6
3	25	11.1	1.4

4.3.4. Results and Discussion

Substantial variability was forecasted in the Rondout Creek inflow for the study period by Hydrologic Ensemble Forecast Service (HEFS) as depicted in Figure 4.39 by the 47 individual traces of inflow time series. The variability in the flow existed both from day to day and amongst the traces, however, the median forecast was nearly steady at about 1.25 $m^3 s^{-1}$ for

the duration of the study. Observations, which became available after the study, generally tracked the 90th percentile of the ensemble (Figure 4.39).

The full combined variability in the model output arising from the variability in the model drivers (hydrology, meteorology, and water quality, i.e., turbidity) is evaluated here for the predictions of turbidity in the withdrawal, a key point of water quality concern (Figure 4.40). Out of 1175 individual traces (47 hydrology traces × 25 meteorology traces) of predictions, only 100 are shown in Figure 4.40, however, the median, 10th and 90th percentiles depicted are obtained from all 1175 traces.

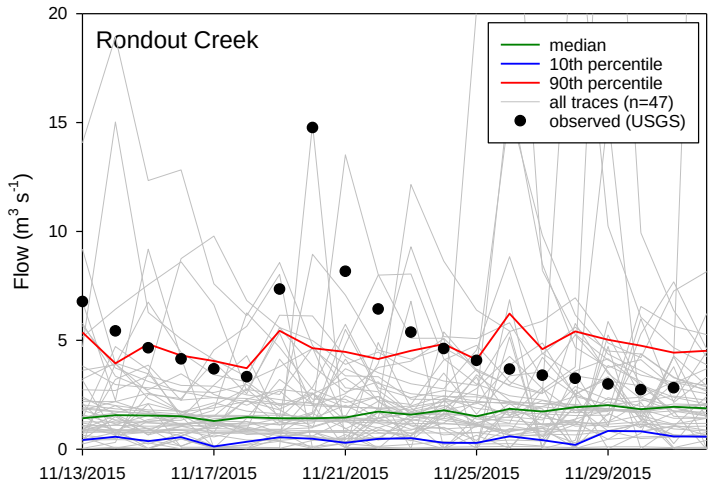

Figure 4.39. Ensemble forecast of Rondout Creek inflow for 11/13/2015–12/1/2015. Forty seven individual traces, median, 10th and 90th percentile traces are shown along with the observations from USGS.

The median forecast of turbidity indicated a modest downward trend during the study period, from ~ 0.85 NTU on 11/13/2015 to ~ 0.65 NTU at the end of the period on 12/1/2015 (Figure 4.40). Some of the individual traces predicted turbidity > 1.5 NTU after 11/26/2015 due to a couple of inflow traces that included a forecast of high runoff, and correspondingly high turbidity, on that day. Two such inflow traces combined with 25 meteorological traces resulted in 50 traces of anomalous withdrawal turbidity, which did not affect the median forecast (Figure 4.40).

The observations of turbidity for the same time interval provided the opportunity to validate the model forecasts (Figure 4.41). The modest decreasing trend in the turbidity as observed was well represented by the median forecast, and the intra-day variability in the

observations was approximately within the bounds of 10th and 90th percentile predictions (Figure 4.41). Additional applications of the model are planned in the current year to further validate the model for a wide range of hydrological and meteorological conditions.

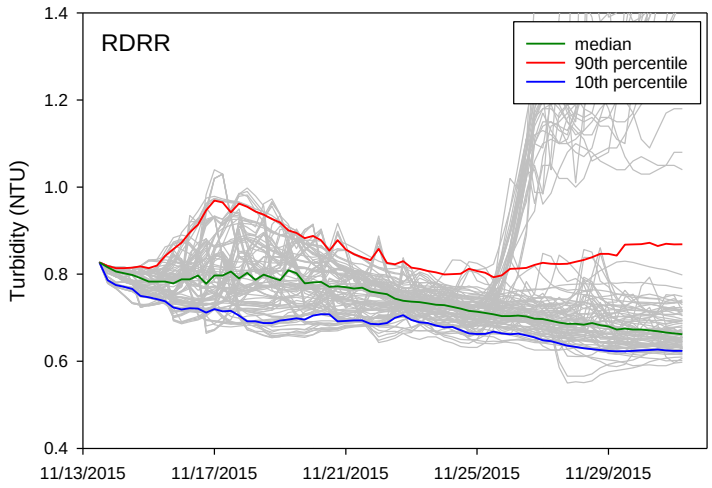

Figure 4.40. Ensemble forecast of turbidity in the withdrawal from Rondout Reservoir (RDRR) for 11/13/2015–12/1/2015. One Hundred of the 1175 individual traces, median, 10th and 90th percentile traces are shown.

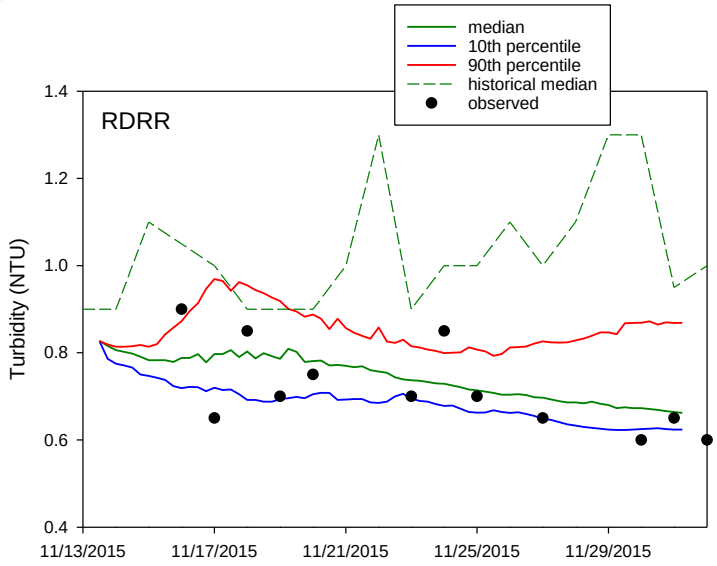

Figure 4.41. Predictions of turbidity in the withdrawal from Rondout Reservoir for 11/13/2015–12/1/2015 interval. Predicted median, 10th and 90th percentiles values are compared with historical median values and actual observations.

Probabilistic analysis: Uncertainty in the model predictions is evaluated by estimating the probabilities of exceedances of certain turbidity levels. For example, as shown in Figure 4.42, in 85% of the traces, turbidity never exceeded 1 NTU, which can be interpreted as that the probability of exceedance of 1 NTU is only 15%. Four other turbidity levels analyzed for the probability of exceedance were 0.5, 0.75, 2, and 2.5 NTU, which indicated that the probabilities of exceeding 0.5 and 0.75 NTU were 100% while it was < 1% for exceeding 2 and 2.5 NTU (Figure 4.42).

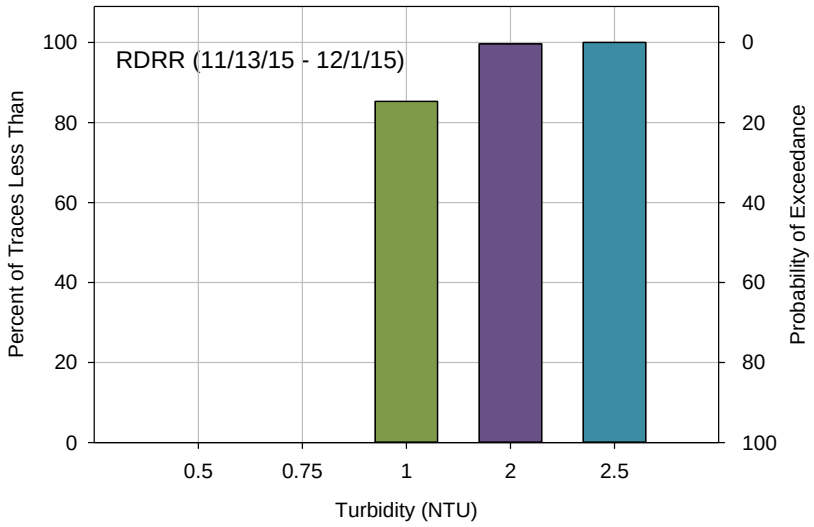

Figure 4.42. Predictions of turbidity in the withdrawal from Rondout Reservoir for 11/13/2015–12/1/2015 interval. Percentages of simulation traces that predict turbidity less than the specified levels (0.5, 0.75, 1, 2, and 2.5 NTU) and probability of exceedance (= 100 − percent of traces less than) are shown.

In addition to the probability of exceedance, the other important feature of the analysis is to compute the duration or severity of exceedance. In other words, in the simulation traces with exceedances, what is the average number of days when the turbidity is exceeded by a specified value? This is illustrated in Figure 4.43 for the same levels of turbidity as chosen for the probability calculation. For example, when turbidity exceeded 1 NTU, it exceeded on 4 days on average (out of 18 days of forecast period; 22%; Figure 4.43). Such analyses would enable managers to make risk-based decisions and adjust water supply operations accordingly as compared to deterministic forecasts which provide no information on uncertainty.

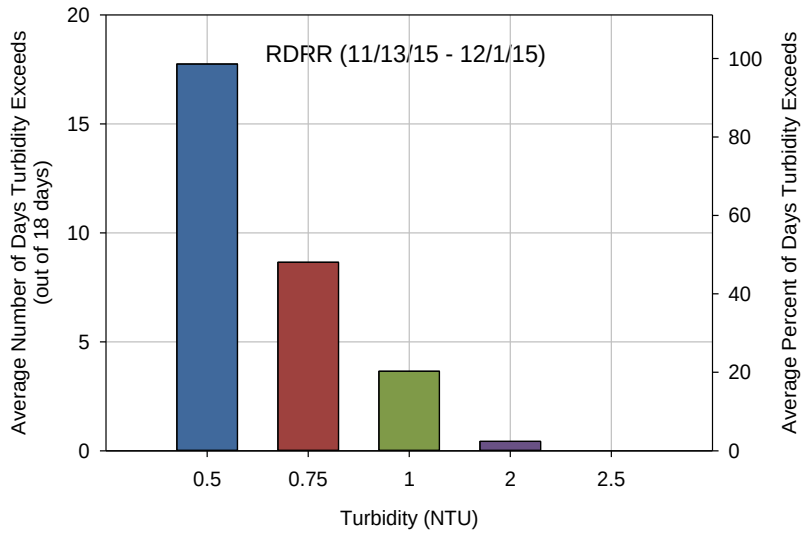

Figure 4.43. Predictions of turbidity in the withdrawal from Rondout Reservoir for 11/13/2015–12/1/2015 interval. Average number and percentages of the days the turbidity exceeds the specified levels (0.5, 0.75, 1, 2, and 2.5 NTU).

Sources of uncertainty: The relative importance of variability in the model drivers (hydrology versus meteorology) was examined by conducting simulation runs where variability in only one driver was considered while the other being held constant. The variability in the output was quantified in terms of standard deviation of withdrawal turbidity ($\sigma_{Tn,w}$) for the two cases of: (1) variable hydrology (47 traces) but constant meteorology (1 trace), and (2) variable meteorology (25 traces) but constant hydrology (1 trace). Trace 1 was chosen as the constant trace for both the cases from the respective groups of meteorological and hydrological traces. The overall magnitude of $\sigma_{Tn,w}$ was found to be similar for both of these cases implying that it was equally important to consider the variability in both the hydrological and meteorological drivers (Figure 4.44). Generally rising magnitude of $\sigma_{Tn,w}$ for Case 1 is due to the greater uncertainty associated with the hydrologic forecasts farther in the future. Uneven magnitude of $\sigma_{Tn,w}$ for Case 2 may just be a reflection of the variability in the historical meteorological conditions. Additional simulation tests need to be conducted to fully explain the nature of variability in this metric of evaluation.

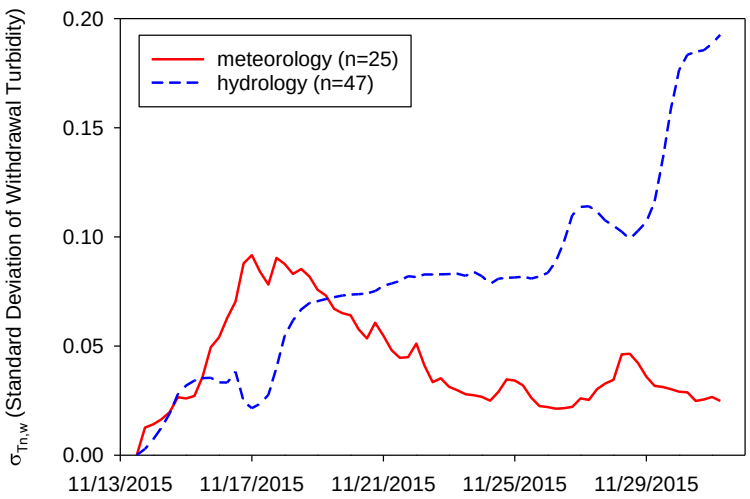

Figure 4.44. Time series of standard deviation of withdrawal turbidity computed from multiple traces of predictions due to variations in meteorology and hydrology.

Sensitivity of combinations of hydrology and meteorology: In the example discussed here, a complete factorial design of input variables (i.e., *n* hydrology traces × *m* meteorology traces, representing full interaction of input variables) was adopted. For $n = 47$ and $m = 25$, a total of 1175 simulation runs were conducted making it a computationally intensive method. In order to reduce the run time requirement, alternative partial factorial sampling was evaluated. The partial sampling included 25 groups (or, experiments) of 100 randomly selected combinations of hydrological and meteorological traces. The results of these simulation experiments are represented by the median turbidity in the withdrawal (Figure 4.45). In each of these simulations, the median turbidity was almost identical to the median turbidity obtained from the full 1175 simulations. This finding suggests that if management decisions are to be based on the forecasts of only median values, then a partial combination of input variables may be adequate.

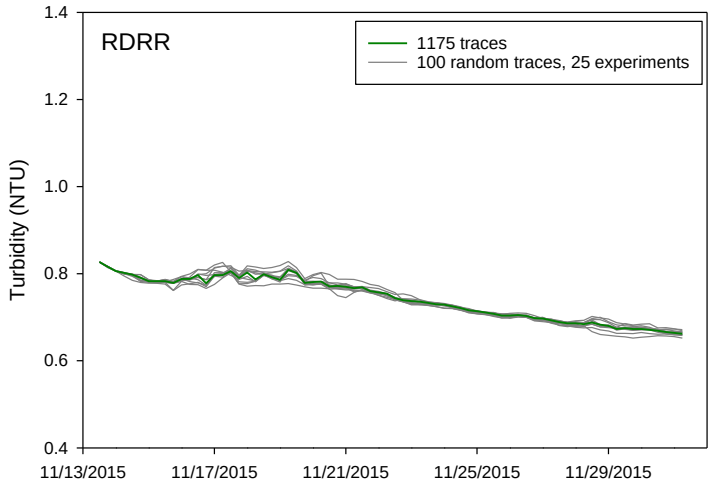

Figure 4.45. Predictions of median turbidity in the withdrawal from Rondout Reservoir for 11/13/2015–12/1/2015 interval. Median values as computed from 1175 traces are compared with values from 100 randomly selected traces in 25 of such sampling experiments.

4.3.5. Future Work

Future work related to the forecasting and modeling of uncertainty will likely involve the following tasks: (i) evaluation and validation of the hydrologic forecasts, (ii) acquisition and use of near-term site-specific forecasts of meteorological conditions, (iii) exploration of approaches to address uncertainty in turbidity loading from Rondout Creek, (iv) conducting additional tests of the approach discussed here and validate the turbidity model for a wide range of hydrological and meteorological conditions, (v) improving predictive skill of the turbidity model (recalibration, if necessary), and (vi) preparing a plan for issuing turbidity forecast reports routinely.

4.4. Simulation of the Impact of Drawdown of Cannonsville Reservoir on Turbidity in Rondout Reservoir

On July 9, 2015, a turbid discharge was discovered during a geotechnical investigation at the Cannonsville Dam. Out of an abundance of caution, DEP began to lower the elevation of Cannonsville Reservoir. Drinking water diversion (withdrawal) to Rondout Reservoir, and releases to the river downstream of the dam, were maximized.

The Operations Support Tool (OST), DEP's reservoir system operations model, was used to forecast reservoir operations during the planned drawdown of Cannonsville. Observations up to July 29 and forecasts of future conditions made on that date are the basis for the analysis described here. The drawdown of Cannonsville was forecast to continue until Sept. 23, when the reservoir water surface would approach the elevation of the lowest of 3 drinking water intakes (Figure 4.46).

While predictive turbidity models have been developed and validated for Schoharie, Ashokan, Rondout, and Kensico Reservoirs, DEP does not have a reliable, validated turbidity model for Cannonsville. As a result, historical turbidity observations were used in order to estimate the turbidity of the Cannonsville withdrawal to Rondout in response to drawdown. Simply looking at historical water surface elevations in Cannonsville, Figure 4.47 shows cumulative probability distributions for water surface elevation, considering 3 sets of water surface elevation observations:

1. All historical data 1966-2015
2. All data during period of reservoir water quality monitoring, 1988-2015
3. All data from periods when withdrawal or tap turbidity was measured

It is clear from Figure 4.47 that, while the reservoir has been drawn down to a water surface elevation of nearly 1050 feet, very little turbidity data is available for Cannonsville when it has been drawn down roughly to the elevation of intake 2 (1092 feet), which the July 29 OST forecast said would occur on Sept. 2. An additional 45 feet of drawdown was forecast to occur after Sept. 2, conditions for which there are no observations of turbidity.

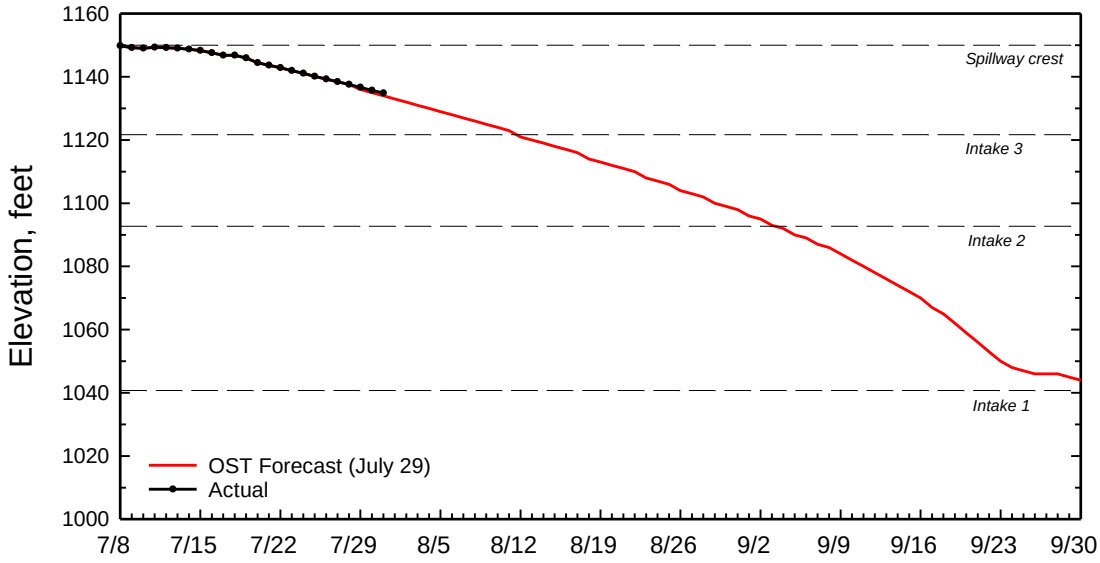

Figure 4.46. Cannonsville water surface elevation, observations and OST forecast, July through September, 2015.

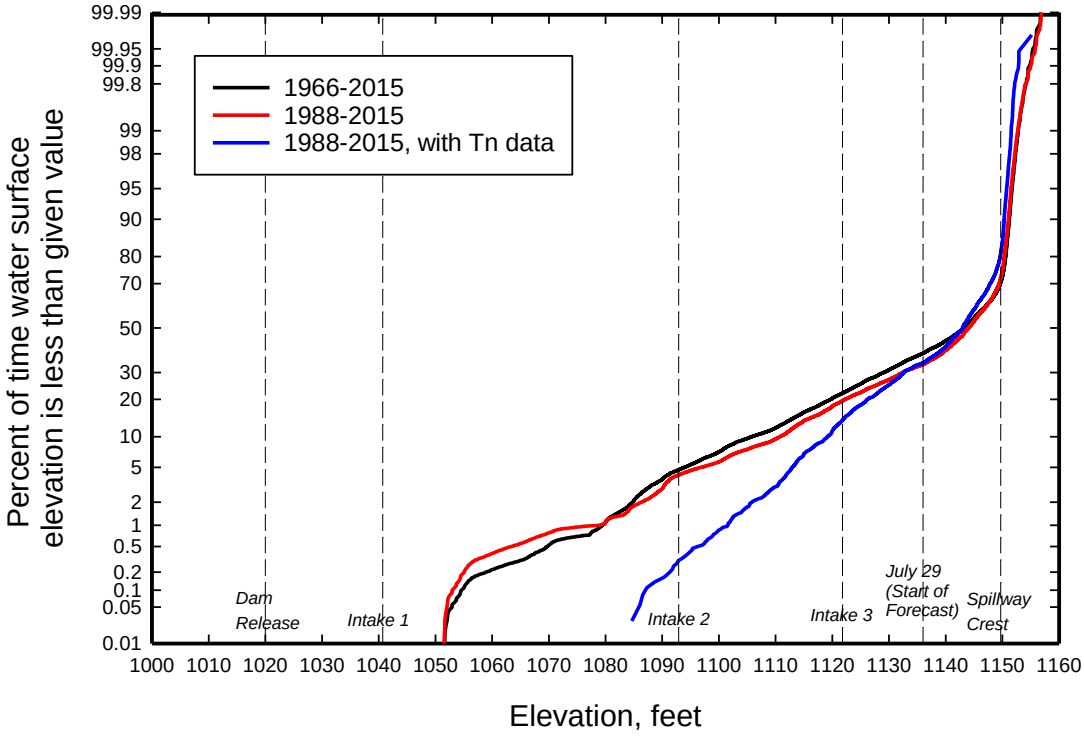

Figure 4.47. Frequency of occurrence of Cannonsville water surface elevation.

All Cannonsville withdrawal and tap turbidity data (from 1988 to present) was assembled to attempt to identify a relationship between withdrawal turbidity and reservoir drawdown. The

paired turbidity-reservoir elevation data was divided into 12 groups based on reservoir elevation, and cumulative probability statistics were computed for each group. The results are shown in Figure 4.48. For the example shown on Figure 4.48, for days when the Cannonsville water surface elevation was between 1127.5 and 1132.5 (plotted as 1130.0), 95% of the observations were less than 5.7 NTU, based on 545 observations of turbidity when the water surface elevation was in this range. The curves for 50, 90, 95 and 99th percentiles all show that turbidity generally increases with decreasing elevation. The occurrence of runoff events, which certainly has a greater influence on turbidity than reservoir elevation, contributes to the scatter in this figure. The apparent increase in turbidity when the reservoir elevation is around the elevation of Intake 3 is curious but may simply be due to the occurrence of runoff events when the reservoir elevation happened to be in this range. Note that the number of observations used to compute these statistics decreases as the water surface elevation drops; below a water surface elevation of 1100 feet, prediction of turbidity from the data alone becomes uncertain.

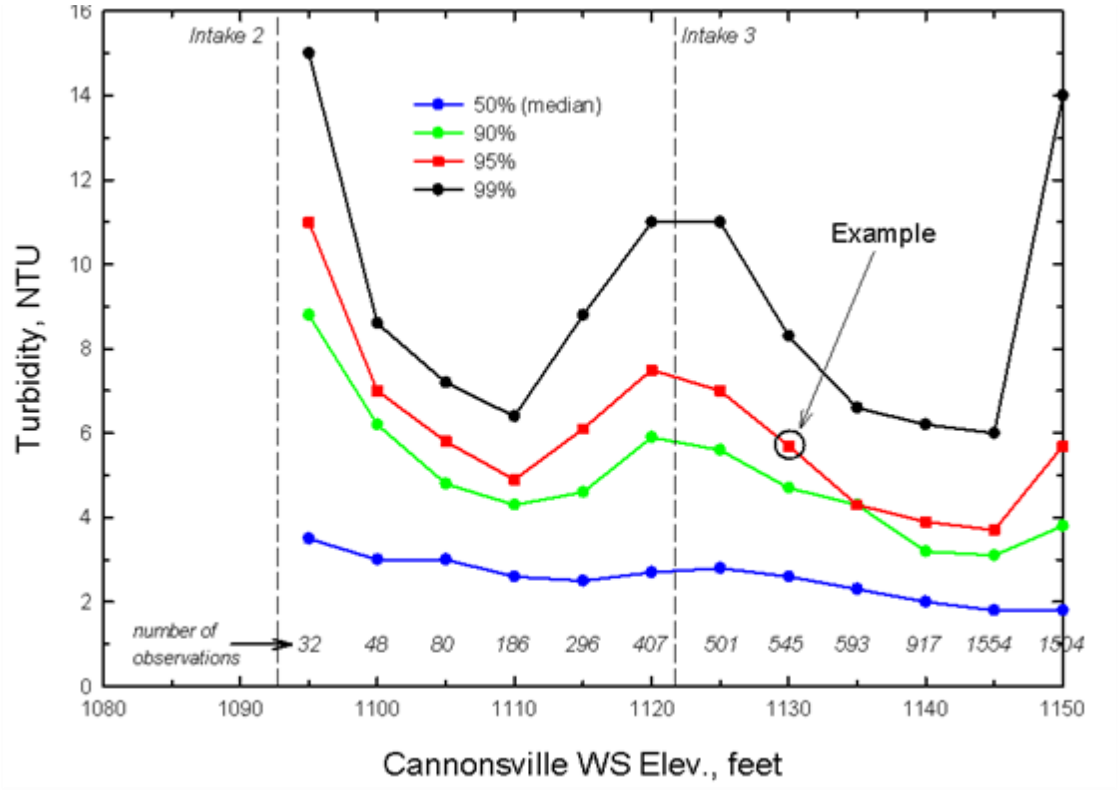

Figure 4.48. Statistics of Cannonsville withdrawal turbidity as a function of reservoir drawdown.

Figure 4.49 shows observations of Cannonsville withdrawal turbidity since early July, 2015. From July 8 to 29, there is an apparent modest increasing trend in turbidity that may be

related to the increasing drawdown. A turbidity of 3.0 NTU was observed in the withdrawal on July 29, when the reservoir elevation was 1136 feet. Using this turbidity as a starting point, the following predictive equation was used:

$$Tn_W = 3.0 + S\,(1136 - WSE) \tag{4.7}$$

where Tn_W is withdrawal turbidity (NTU), *WSE* is reservoir elevation (feet), and *S* is an empirical coefficient which determines the effect of *WSE* on Tn_W. Using least-squares regression a value of *S* was determined from the 95 and 99% statistics shown in Figure 4.48. The results are

95th percentile:

$$Tn_W = 3.0 + 0.15\,(1136 - WSE) \tag{4.8}$$

99th percentile:

$$Tn_W = 3.0 + 0.23\,(1136 - WSE) \tag{4.9}$$

These two alternative relationships were used to forecast the Cannonsville withdrawal turbidity for August and September of 2015, based on the OST forecast for *WSE* for this period shown in Figure 4.46. The resulting turbidity forecasts are shown in Figure 4.49. When Cannonsville withdrawal is greatly reduced on Sept. 23, the 95th and 99th percentile forecasts of withdrawal turbidity are 16.2 and 23.2 NTU, respectively. The red line in Figure 4.49 shows the turbidity for which 99% of the observations are less, based on the OST forecast reservoir elevation. Since there is no data for the elevations that are forecast to occur after Sept. 2, Equations (4.8) and (4.9) are simply extended. The underlying turbidity data represents periods when turbidity was high due to runoff events, and dry periods when the turbidity was lower. The use of 95 and 99th percentiles for the entire 2-month period effectively assumes that wet weather, that is the primary cause of unusually high turbidity, occurs throughout this period, a very conservative assumption.

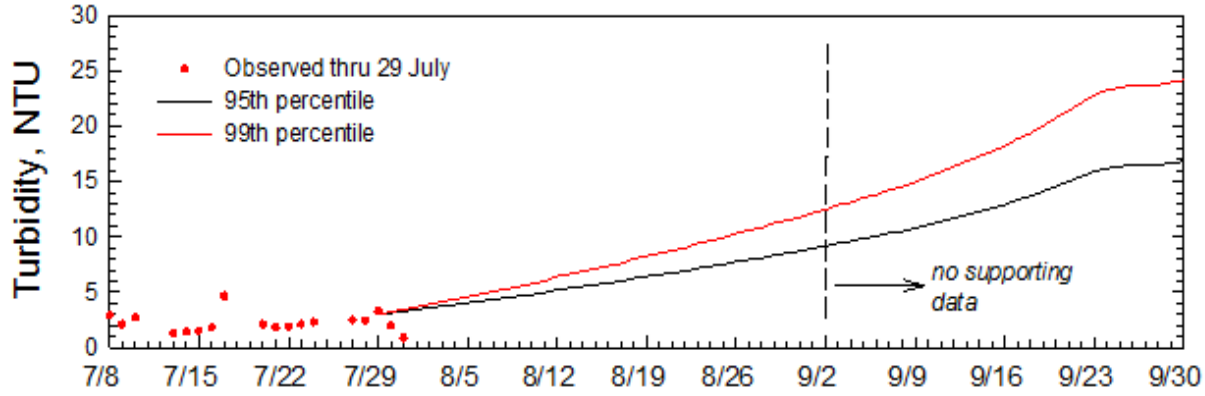

Figure 4.49. Forecast of Cannonsville withdrawal turbidity for the entire drawdown period, August and September, 2015, and measurements in July 2015.

The July 29 OST forecast of withdrawals from Cannonsville, Pepacton, and Neversink into Rondout are shown in Figure 4.50. The observed Rondout and Chestnut Creek hydrographs for August and September of 2012 were used in the simulations presented here. The Rondout Creek hydrograph for this period of 2012 is shown in Figure 4.50; this year was selected because a runoff event occurred on Sept. 19, 2012. As a result, the simulations shown here not only including the impact of elevated turbidity in the large inflow from Cannonsville (Figure 4.50), but also included a runoff event from the Rondout Reservoir watershed occurring during the later stages of the Cannonsville drawdown.

Observations of turbidity in the Pepacton and Neversink withdrawal flows into Rondout in July, 2015 were generally around 1 NTU (Figure 4.51). For forecasting, two conditions were considered:

1. Pepacton and Neversink turbidity constant at 1.0 and 0.9 NTU (median historical August-September values)
2. Pepacton and Neversink turbidity constant at 2.8 and 2.3 NTU, 95th percentile values for August-September based on historical data. Turbidity at these levels is due to runoff events; this effectively assumes that a series of runoff events occur over the entire drawdown period.

These Pepacton and Neversink turbidities are shown in Figure 4.51.

Temperatures of the Pepacton and Neversink inflow to Rondout Reservoir were taken as average values for a particular date, based on historical data. The temperature of Rondout and Chestnut Creeks were taken from 2012 observations (consistent with the assumed creek flow). The temperature of the Cannonsville inflow would certainly be affected by drawdown and its

likely effect on thermal stratification in the reservoir. The one-dimensional hydrothermal model of Cannonsville (Owens, 1998b), was used to forecast the temperature of the Cannonsville withdrawal, given the OST forecasts for Cannonsville inflow, withdrawal, release, and drawdown. The inflow temperatures shown in Figure 4.52 were used in the model predictions for Rondout Reservoir.

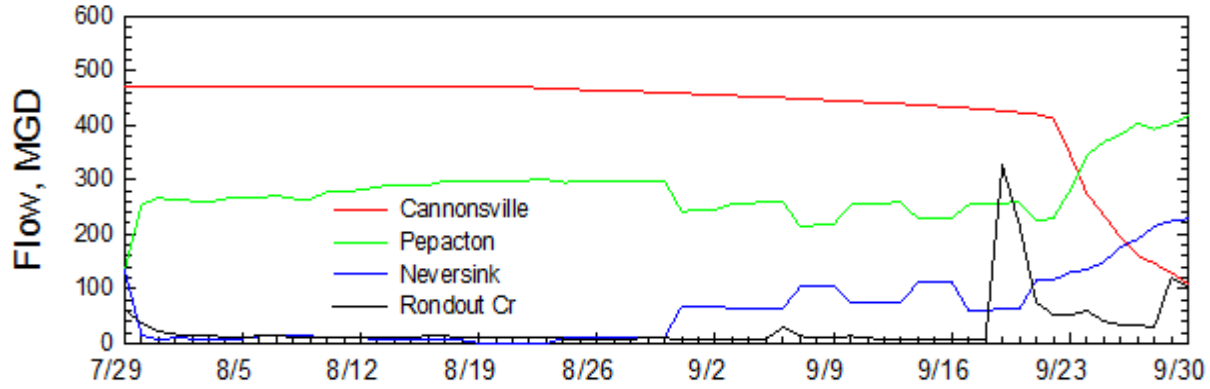

Figure 4.50. Forecasts of inflows to Rondout from upstream reservoirs for the August-September drawdown period, and the Rondout Creek hydrograph for August-September 2012.

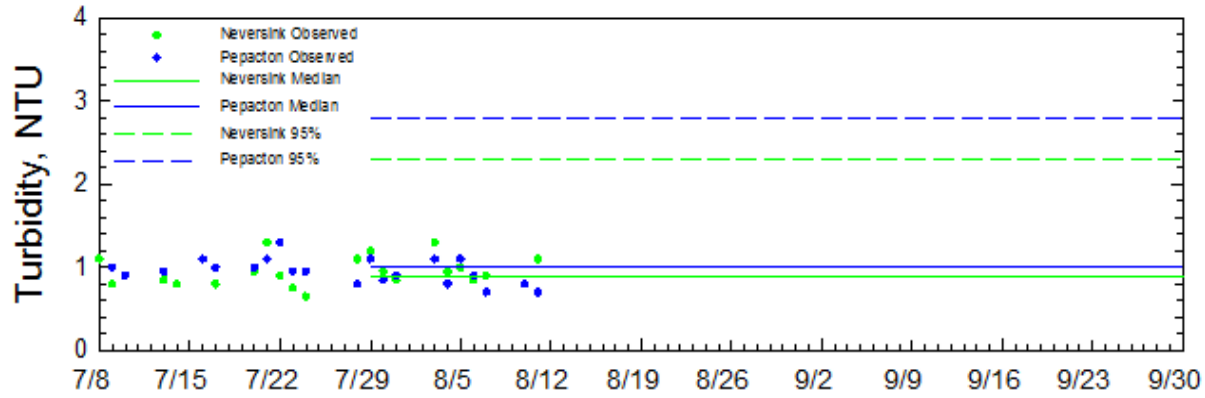

Figure 4.51. Observed and assumed turbidity in the Pepacton and Neversink inflows to Rondout for August-September, 2015.

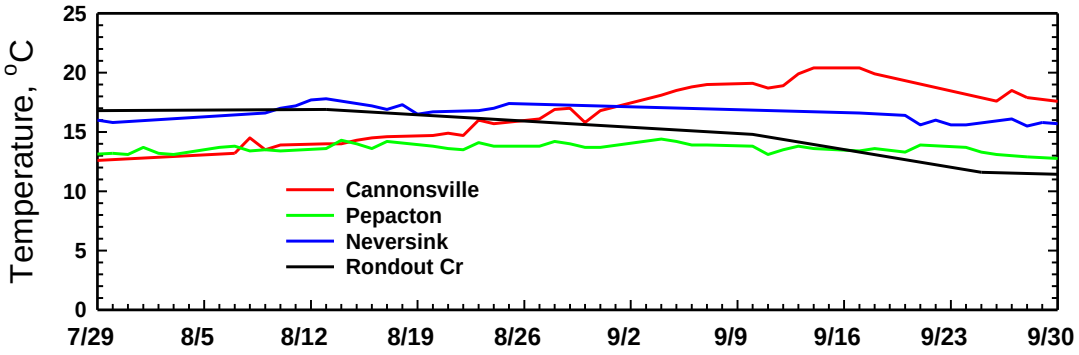

Figure 4.52. Temperatures of the inflows to Rondout for August-September 2015 period used in the model forecast. Cannonsville temperature determined from 1D hydrothermal model based on OST forecast of inflow and outflow. Pepacton and Neversink temperatures are average historical values, while Rondout Creek temperature is the observed time series for 2012.

Weather conditions (solar radiation, air temperature and humidity, wind) observed at Rondout in Aug.-Sept. 2012 were used in the forecasts for Rondout Reservoir. The initial condition for temperature and turbidity in the water column of Rondout was based on observed profiles from July 29, 2015, when turbidity ~0.2 NTU at the surface to ~0.7 NTU near the bottom. Drinking water withdrawal from Rondout was set to values from the July 29 OST forecast.

The Rondout W2 turbidity model was then used to predict temperature and turbidity in the water column and withdrawal of Rondout Reservoir for the period July 29 to September 30, 2015. Two separate predictions were made:

Case 1: Conservative forecast:

- Cannonsville withdrawal turbidity given by black (95th percentile) curve in Figure 4.49
- Pepacton and Neversink withdrawal turbidity at 1.0 and 0.9 NTU, respectively (historical median, solid curves median in Figure 4.51).

Case 2: Ultra-conservative forecast:

- Cannonsville withdrawal turbidity given by red (99th percentile) curve in Figure 4.49
- Pepacton and Neversink withdrawal turbidity at 2.8 and 2.3 NTU, respectively (historical 95th percentile, dash curves in Figure 4.51).

Predicted turbidity in the withdrawal for Rondout for these two cases is shown in Figure 4.53. Peak turbidities for the two cases are 1.79 and 2.70 NTU, both occurring on Sept. 27, 3 days after the withdrawal from Cannonsville was to be reduced due to drawdown approaching

the elevation of Intake 1 (1040 feet). These results show that Rondout Reservoir has the ability to withstand a 2-month period of significant turbid inflow. This is largely due to two factors:

1. For these conditions, the hydraulic residence time of Rondout is 63 days, assuming plug flow through the entire reservoir volume. Given its relatively warm temperature, the time of travel of the turbid Cannonsville inflow to the Rondout Dam is likely less. Nonetheless, it takes some time to displace the low turbidity (~0.3 NTU) water that resided in the reservoir on July 29.
2. Settling of particles contributing to turbidity within the reservoir, especially for the Cannonsville withdrawal, which was found in earlier studies by UFI to contain a relatively large fraction of fast-settling particles.

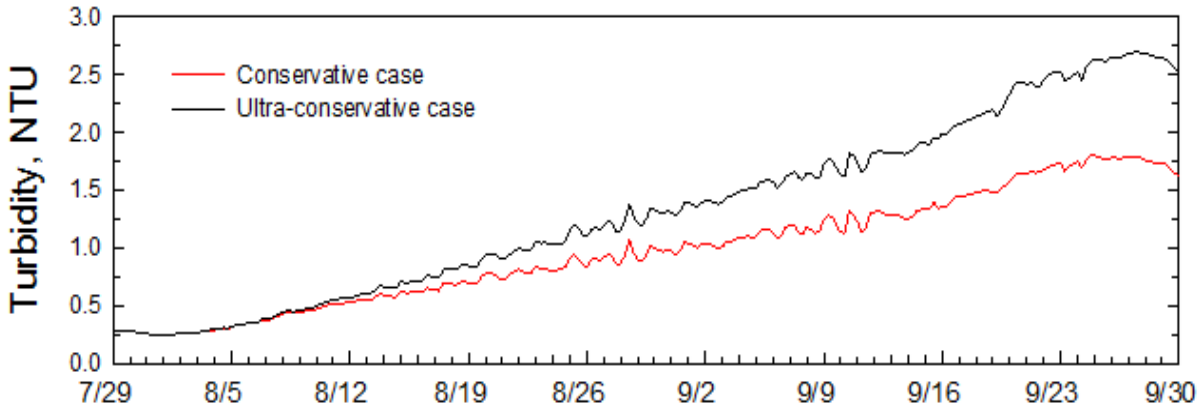

Figure 4.53. Predicted turbidity in the withdrawal from Rondout Reservoir during the period of drawdown of Cannonsville Reservoir.

On July 31, repair work at the Cannonsville Dam eliminated the turbid discharge, and the rapid drawdown of Cannonsville was halted. The actual water surface elevation of Cannonsville through August and September is shown in Figure 4.54. Even so, this episode demonstrates the utility of monitoring and modeling programs in forecasting and evaluating the potential future impacts of unusual or unforeseen events, and in planning appropriate responses.

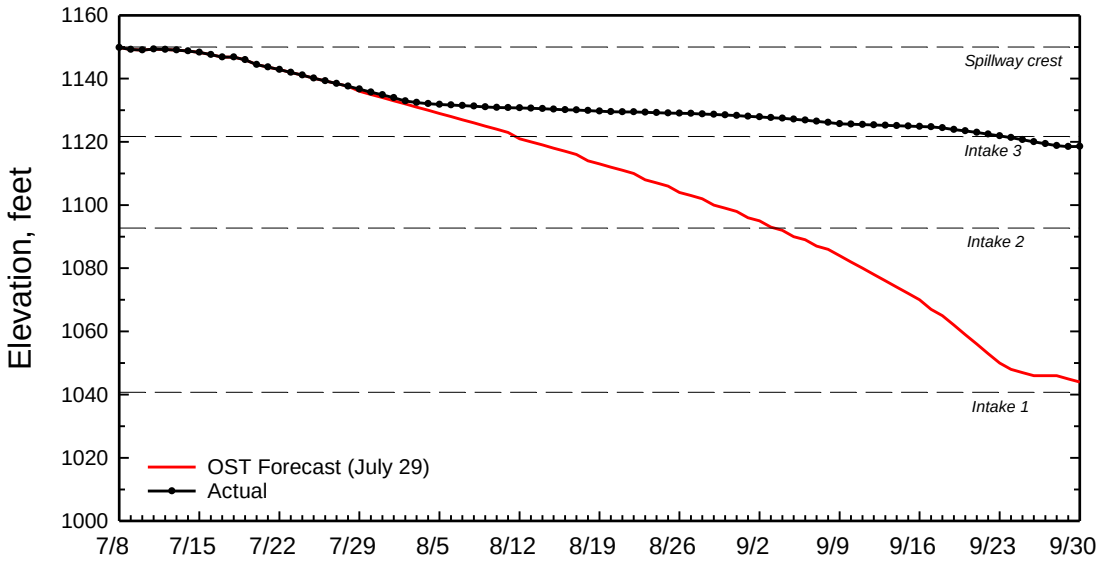

Figure 4.54. Actual drawdown of Cannonsville Reservoir, and July 29 OST forecast, for period July 8 through September 30, 2015.

4.5. Ecohydrologic Modeling

4.5.1. Introduction

Forests play a key role in regulating water quality in streams, and forest disturbances and climate change can affect the water quality through major changes in hydrologic function and ecosystem. Therefore, improving the understanding how these changes impact water quality is critical in managing water quality for forested watersheds. However, the use of models to predict water quality following forest disturbance and climate change is a challenge given the complex interactions among climate, hydrology, and biogeochemistry.

To accurately predict the impact of these disturbances on the water quality, models should be able to represent the current state of physical processes and incorporate the feedback processes (e.g. vegetation responses) to changing environmental conditions. In this study, an ecohydrologic model, Regional Hydrologic-Ecologic Simulation System (RHESSys) (Tague and Band, 2004) is used to study the impact of climate change and forest disturbance on ecohydrologic processes, including flow, evapotranspiration, nitrogen fluxes, and dissolved organic carbon fluxes. Previous applications of RHESSys showed the capacity to represent coupled hydrologic and vegetation fluxes, and ecohydrologic responses to climate change and vegetation change (Band et al., 1996; Baron et al., 1998; Hwang et al., 2012; Zierl et al., 2007).

The study sites are located in the Neversink River basin, the least developed New York City water supply watershed. Due to climate change and introduced insects and diseases, the forest and stream have experienced changes in hydrologic processes, the quality of soil and stream waters, and the forest species. Due to recent hemlock decline caused by the hemlock woolly adelgid, decreased winter transpiration and degraded riparian habit is expected (Brantley et al., 2013). Forest harvesting in Shelter Creek watersheds increases the streamflow, nitrogen, and dissolved carbon concentrations. As well, recent climate impact studies in Catskill Mountain watersheds predicted an increase in winter streamflow, and decrease in summer flow using watershed models (SWAT and GWLF-VSA) and future climate scenarios based on General Circulation Models (GCM) (Anandhi et al., 2011; Matonse et al., 2011; Zion et al., 2011). The Catskill Mountains have high levels of nitrogen depositions, and this deposition modifies the biogeochemistry of soils, and increases the acidification in streams (Lawrence et al., 2000). Therefore, accurately quantifying hydrologic change and biogeochemistry in soils and streams and vegetation change in our study sites is essential step for preparing for the guideline to mitigate these changes, and maintain high quality water in streams.

To conduct this study, the framework shown in Figure 4.55 is used to test the impact of climate change and forest disturbance on ecohydrologic processes using RHESSys. Various remote sensing data including Landsat, MODIS and LIDAR are used to initialize the model state of vegetation, and validate the model prediction of forest recovery after forest harvest, and forest

responses to climate variability. Observed streamflow, nitrogen fluxes, and dissolved carbon (DOC) fluxes measured at the outlet of each watershed are used to calibrate and validate the watershed responses of ecohydrologic processes to climate variability and forest disturbance at multiple scales. The impacts of forest disturbance vary with scale; for example, the impacts may decrease with watershed size, and increase with the extent of disturbance and forest harvesting. However, the impact of climate change may occur over large areas (Blöschl et al., 2007). Application of this framework is described at three different scales: a headwater catchment, a medium size catchment and a large river basin. The combined effects of forest disturbance and climate change on ecohydrologic processes is investigated. This study is presently under development, and preliminary results of model calibrations and remote sensing data analysis are presented.

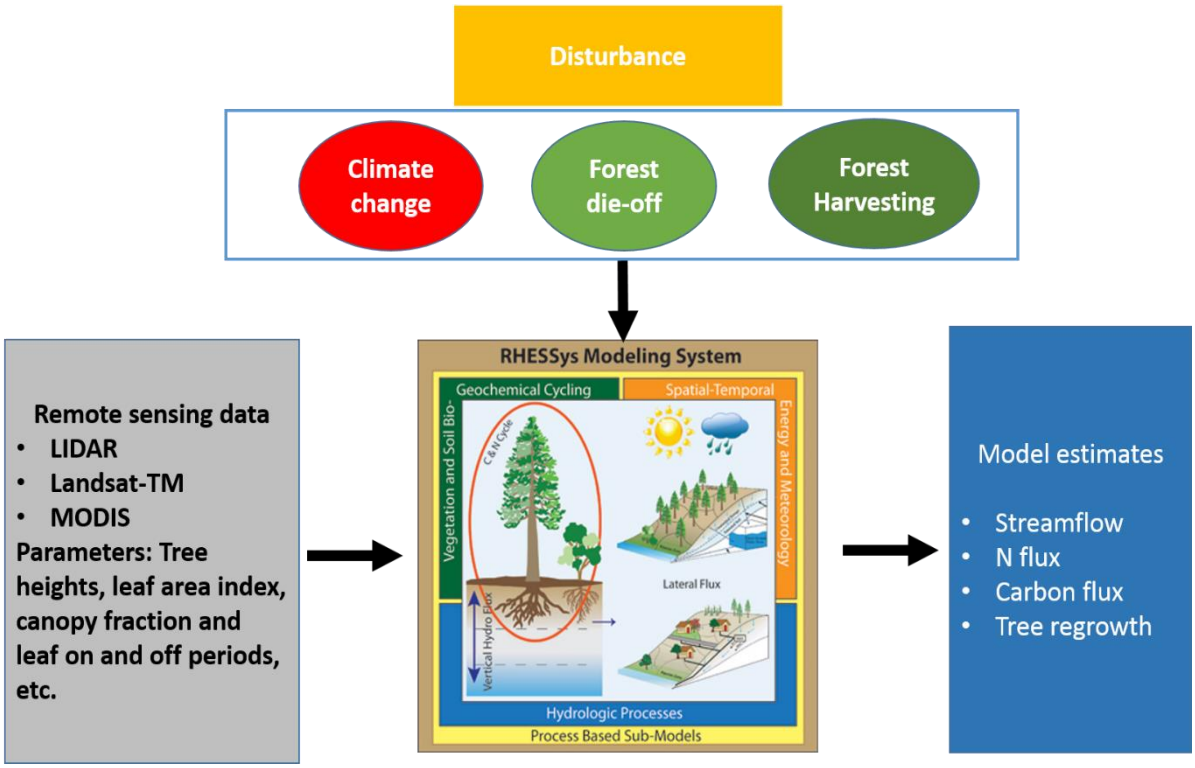

Figure 4.55. The framework for studying the impact of disturbance on ecohydrologic processes using RHESSys.

4.5.2. Study sites

The study sites are three watersheds of varying size located in Catskill Mountain region: Shelter Creek watershed, Biscuit Brook watershed, and Neversink watershed. Table 4.12 summarizes each watershed, and Figure 4.56 shows the geographic extent and boundary of each watershed. The Neversink watershed is the largest watershed (245.6 km^2), and it includes the Shelter Creek (1.6km^2) and Biscuit Brook (9.2 km^2) watersheds. The two smaller watersheds drain into the Neversink reservoir. The major landcover type is forest for all watersheds, and mixed northern hardwood forest is the dominant forest type, consisting of American beech, red maple, sugar maple and yellow birch (Harpold et al., 2010). Balsam fir is found above 1000 m elevation, and hemlock is found at the ridge and near streams.

The major soil type is Inceptisols, and its depths range from 0.5 - 1 m. Soils have coarse texture, and are well drained. Major surface geologic type is sandstone (60%). Underlying bedrock type is sedimentary rock, and the bedrock has high percentages of fractures. Bedrock mineralogy is spatially uniform. The till depth is shallow (<1 m), and in the valley bottoms, the coarse sand and gravel is formed by the glacial outwash and recent alluvium deposits. The average precipitation (based on Slide Mountain climate station, located in the summit of Neversink basin) is 1570mm, and mean air temperature is 5.2℃. The proportion in snow of the total precipitation ranges from 20 to 35% (Harpold et al., 2010). Shelter Creek watershed experienced forest harvesting in the winters of 1995-96 and 1996-97. Figure 4.57 and Table 4.13 show the area of forest harvesting and the different harvesting history for each watershed. NS25 is 'light selective harvest' watershed, and 7% basal area decreases after the harvests. SC20 is 'heavy selective harvest' watershed, and have 8% decrease basal area after the harvest. DC57 is 'clear cut harvest' watershed, and have the 80% decrease in the basal area. C25 is used as a control watershed. A detailed description of the forest harvesting history is available (McHale et al., 2008). The collected data, including stream-water and soil chemistry at the Shelter Creek before and after the harvests will be used to test the impact of forest harvesting on ecohydrologic processes using RHESSys.

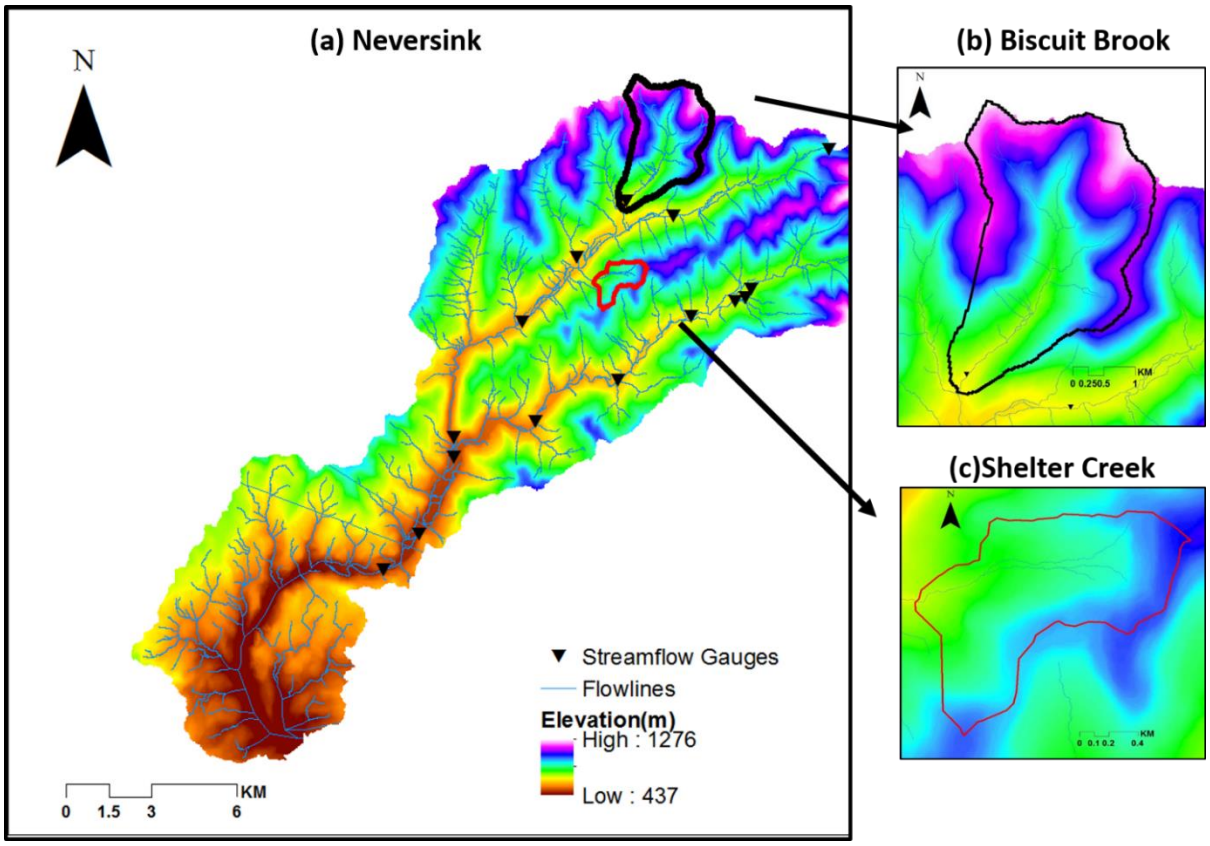

Figure 4.56. The study sites: (a) Neversink, (b) Biscuit Brook, and (c) Shelter Creek.

Table 4.12. Watershed descriptions

Watershed	Size (km^2)	Elevation (m)	Major soil type	Major land cover
Neversink	245.6	437-1276	Inceptisols	Mixed hardwood forest
Biscuit Brook	9.2	618-1124	Inceptisols	Mixed hardwood forest
Shelter Creek	1.6	652-921	Inceptisols	Mixed hardwood forest

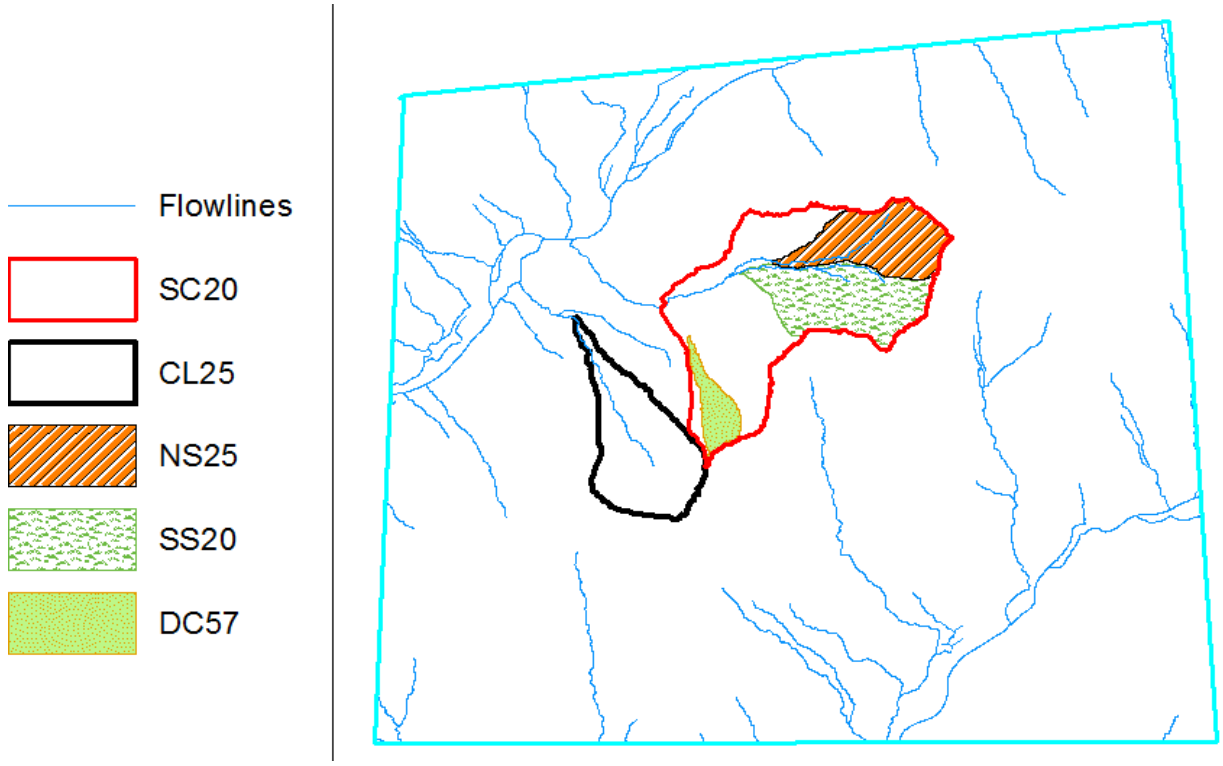

Figure 4.57. The Shelter Creek watershed with different forest harvest regimes.

Table 4.13. Shelter Creek watersheds with different forest harvest regimes

Watershed	Size (km^2)	Harvesting Period	Intensity
CL25	0.52	NAN	Control (0%)
NS25	0.34	Winter, 1995-96	Light harvest (2% decrease in basal area)
SS20	0.43	Fall, 1996	Heavy harvest (8% decrease of basal area)
DC57	0.1	Winter, 1996-97	Clear Cut (97% cut, 90% decrease of basal area)

4.5.3. RHESSys model

The RHESSys model was applied to the two small watersheds, Shelter Creek and Biscuit Brook In future study, the RHESSys model will also be applied to the overall Neversink watershed. RHESSys requires various input data; climate inputs (e.g. daily precipitation and daily minimum and maximum temperature data), topography (i.e. Digital Elevation Model), soil and vegetation data. For climate input data, this study used meteorological data from the Slide

Mountain climate station, located about 6km and 9km from Shelter Creek and Biscuit Brook, respectively. Other climate variables (e.g. solar radiation, saturation vapor pressure, and relative humidity) are computed using a climate interpolation model (MT-CLIM, Running et al., 1987). NYCDEP produced 1m Digital Elevation Model (DEM) using LIDAR point data. This study used resampled 10m DEM to generate the topographic parameters (elevation, slope, aspect, flow drainage maps, watershed boundary maps, etc.). Soils parameters are estimated based on Soil Survey Geographic (SSURGO, USDA Natural Resources Conservation Service) and existing RHESSys parameter library (available at https:www.github.com/RHESSys/ParamDB). NYC DEP landcover data were used to define the different vegetation functional types, and associate vegetation parameters for each vegetation type was based on the RHESSys parameter library. Current model setups assume a spatially uniform value of 4 for Leaf Area Index (LAI) for the two watersheds.

4.5.4. Estimates of vegetation indices using Landsat TM imagery

In the RHESSys model, LAI is a key biophysical parameter for modeling the spatial distribution of vegetation productivity, evapotranspiration and surface energy balance. The field measurement of LAI using LAI-2000 Plant Canopy Analyzer (PCA, Li-Cor, Lincoln, NE, USA) over the large area is difficult, especially for mountain areas. To overcome this difficulty, LAI over large areas is estimated using the relationship between field-measured LAI and remote sensed derived vegetation indices.

In this study, a Landsat-TM image (06/21/1991) was used to derive several vegetation indices: simple ratio (SR), normalized difference vegetation index (NDVI), enhanced vegetation index (EVI), infrared simple ratio (ISR). Images analysis has been conducted using GRASS GIS imagery tools (*i,landsat.toar* and *i.landsat.acca). i.landsat.toar* calculates the surface reflectance, and *i.landsat.acca* calculates the extent of cloud, and removes the cloud. Figure 4.58 shows the calculated vegetation indices for the Shelter Creek watershed. All vegetation indices show similar pattern of vegetation coverage at the coarse scale, but have different variability at the fine-scale.

Additionally, LAI values are estimated using the two empirical calibrated equation developed in other studies (Hwang, unpublished data and Fernandes et al., 2003) because the measured LAI data are not available in our sites. Using the two empirical calculations, data show similar pattern of vegetation but the range of LAI varies. The LAI values using the equation of Hwang are higher than the LAI value of Fernades et al., (2003). Uncertainty of LAI estimates leads to error in estimating evapotranspiration, net primary productivity and streamflow, etc. In order to improve the estimate of LAI, the field measurement of LAI will be necessary. Recent studies (Ganguly et al., 2012, 2008) show the potential of using radiative

transfer theory of canopy spectral invariant to estimate the LAI at the Landsat TM scale (30 m). Using LIDAR data, LIDAR data (Richardson et al., 2009), we can generate finer resolution (<30 m) LAI values over large areas.

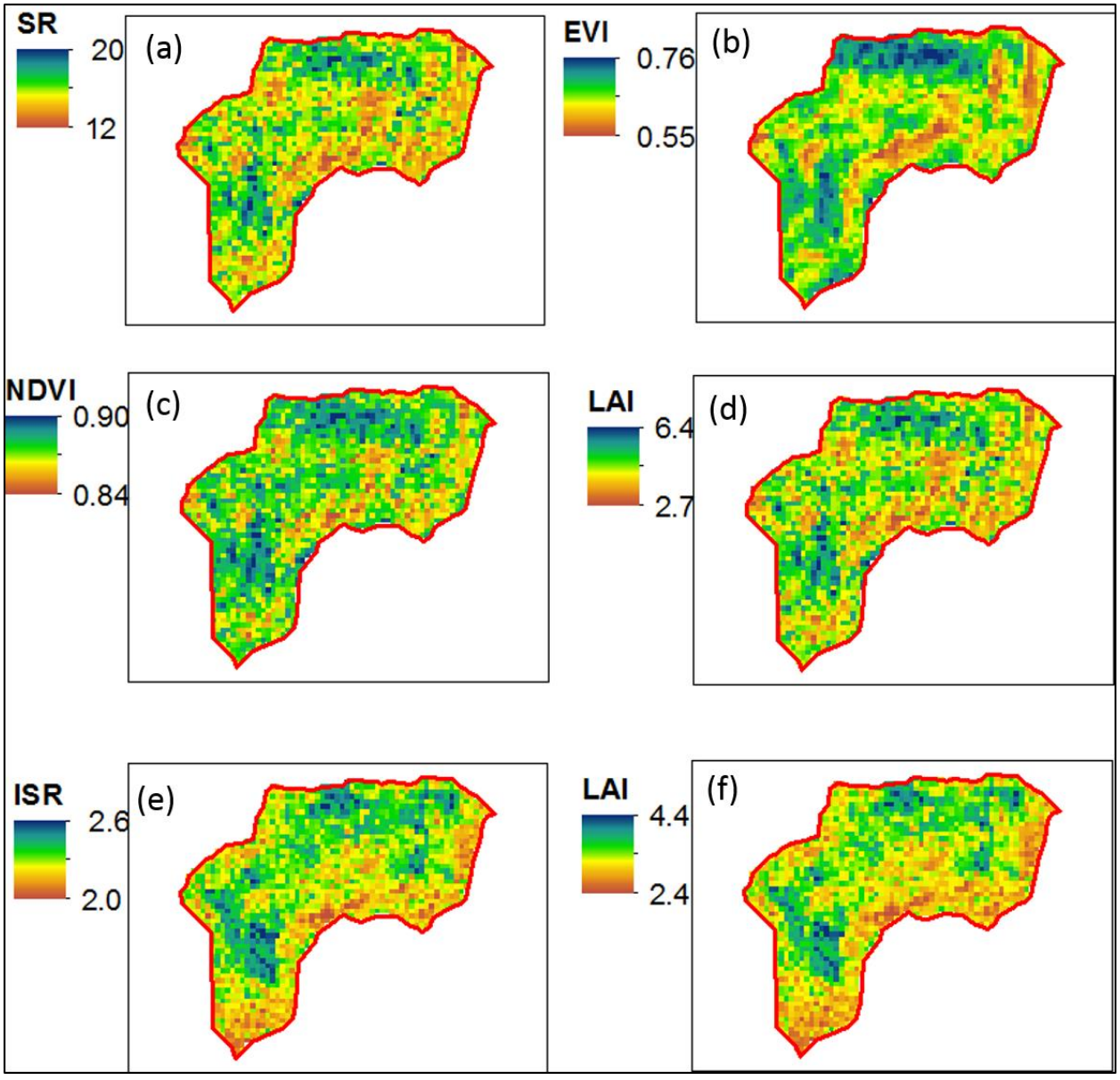

Figure 4.58. Derived vegetation indices using Landsat-TM: (a) SR, (b) EVI, (c) NDVI, (d) LAI using the calibrated equation (Hwang, unpublished data), (e) ISR, and (f) LAI using the calibrated equation (Fernandes et al., 2003).

4.5.5. RHESSys calibration

The RHESSys model requires various data to calibrate model parameters and validate model predictions. In this study, the model calibration is limited to streamflow, but in the future study, additional data sets, such as nitrate and dissolved organic carbon (DOC) fluxes will be included to evaluate the model performance. To quantify the predictive uncertainty of model estimates, Generalized Likelihood Uncertainty Estimation (GLUE) approach (Beven and Freer, 2001) will also be used.

The calibration was conducted by adjusting the soil parameters to match the predicted streamflow with measured streamflow, and the calibrated soil parameters are saturated hydraulic conductivity (Ksat), decay of Ksat with depth (m), the fraction of infiltrated soil water that directly drains to deep soil parameter (gw1), linear coefficient of deep groundwater storage (gw2), air entry pressure (ae) and pore size index (psi). Streamflow data from 2 USGS gages (01434092 and 01434025) were used to compare with the predicted streamflows for Shelter Creek and Biscuit Brook respectively. The first two years of climate data were used to initialize soil and groundwater storage for the two watersheds. Measured streamflow data in the period 1992-1994 for Shelter Creek are used for calibrating soil parameters because forest harvesting was conducted in the period 1995-97. For Biscuit Brook, data in the period 1996- 2000 were used for the calibration.

To quantify the model accuracy of streamflow prediction, several measures of model accuracy were used as given in Equations (4.10) through (4.13). R_{eff} (Nash and Sutcliffe, 1970) tends to emphasize the peak flow, and R_{logeff} emphasizes the low flows, and percentage of error (*PerErr*) focus on the total volume of flow. By combining the three accuracies, errors in the different aspects of flow predictions is quantified:

$$R_{eff} = 1 - \frac{\sum_i (Q_{obs,i} - Q_{sim,i})^2}{\sum_i (Q_{sim,i} - \bar{Q}_{obs,i})^2} \tag{4.10}$$

$$R_{logeff} = 1 - \frac{\sum_i (\log(Q_{obs,i}) - \log(Q_{sim,i}))^2}{\sum_i (\log(Q_{sim,i}) - \log(\bar{Q}_{obs}))^2} \tag{4.11}$$

$$PerErr = \frac{(\bar{Q}_{sim} - \bar{Q}_{obs})}{\bar{Q}_{obs}} \times 100 \tag{4.12}$$

$$Accuracy = R_{eff} \times R_{logeff} \times \left(1 - \left|\frac{PerErr}{100}\right|\right) \tag{4.13}$$

where $Q_{obs,i}$ is the observed streamflow and $Q_{sim,i}$ is the simulated flow at any given time step (i), and $\overline{Q_{obs}}$ and $\overline{Q_{sim}}$ are the average of daily streamflow.

Figure 4.59 shows the preliminary calibration results for Shelter Creek and Biscuit Brook. For Shelter Creek, the model underestimated the peak flow, and failed to reproduce some small peaks. However, the model successfully captured the observed flow recession. The flow accuracy measures using Equations (4.10) through (4.13) reflect this pattern; R_{eff} had lower value (0.46) than R_{logeff} (0.65) (Table 4.14). For Biscuit Brook, the model had lower flow accuracy compared with those for Shelter Creek. The model also underestimated peak flow, and showed better prediction of low flows (R_{logeff}=0.54) that those of high flows (R_{eff} =036). For the two watersheds, the high error in peak flow may be related to the uncertainty of precipitation input data and snow prediction. Tang et al. 2014 showed that using the data from 10 Cooperative Observer Program stations (COOP) has better streamflow prediction for Biscuit Brook; R_{eff} values range from 0.58 to 0.61. The uncertainty of soil depth data may be a potential source for error in the peak flow prediction. Compared with Shelter Creek, Biscuit Brook had higher percentage error in flow. The assumption that LAI is spatially uniform may also contribute to this error.

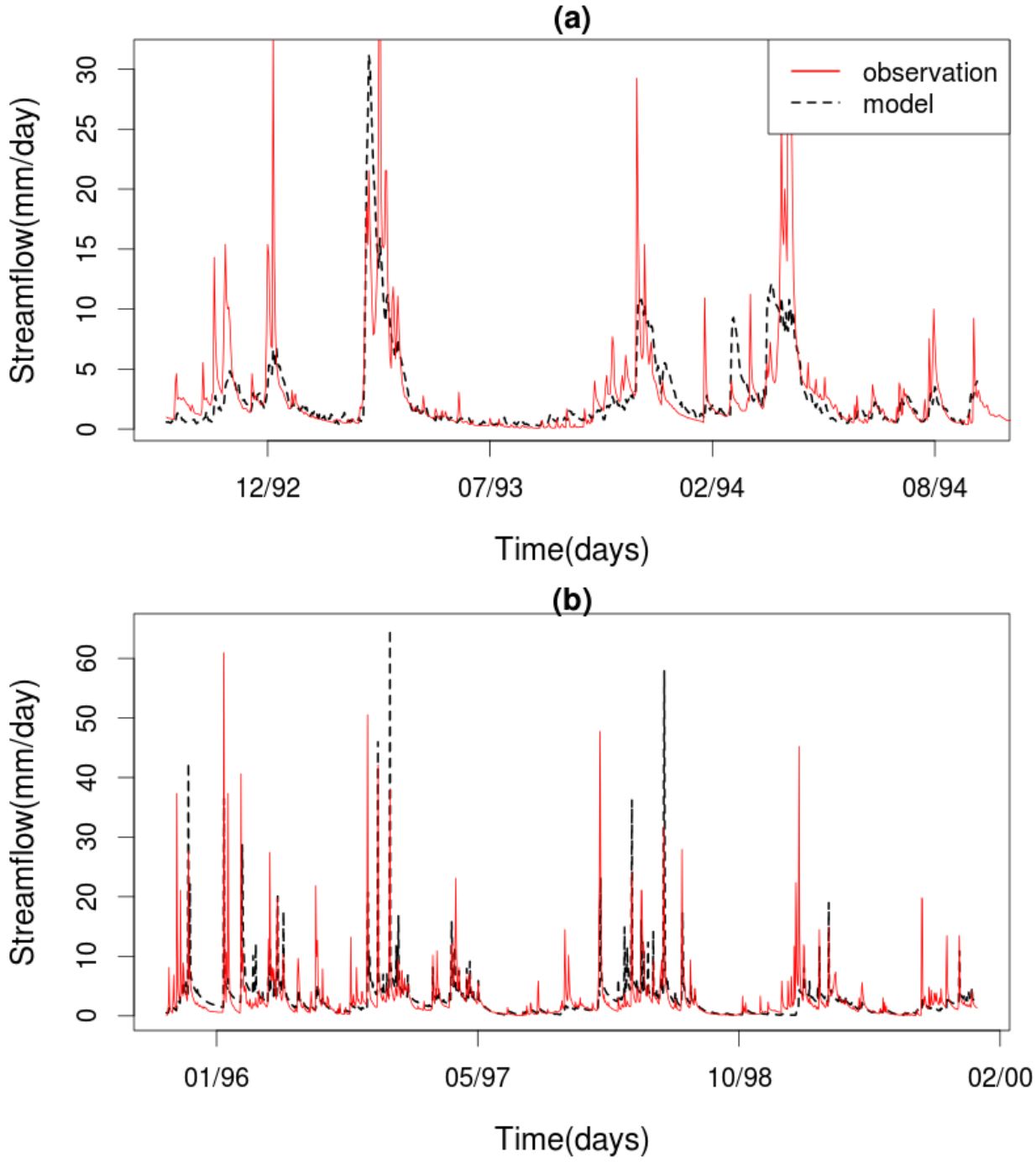

Figure 4.59. Streamflow calibration for Shelter Creek and Biscuit Brook watershed: (a) Shelter Creek watershed, and (b) Biscuit Brook watershed

Table 4.14. Accuracy of Streamflow predictions for the Shelter Creek Watershed and the Biscuit Brook watershed

Watershed	R_{eff}	R_{logeff}	*PerErr*	*Accuracy*
Shelter Creek	0.46	0.65	-11.9	0.26
Biscuit Brook	0.36	0.54	-5.6	0.19

4.5.6. Conclusions and future plans

This study shows the initial results of streamflow predictions using RHESSys, and the estimates of vegetation indices (SR, NDVI, ISR and LAI) using Landsat TM imagery. Simulated streamflow results suggest a necessity for improving climate inputs, soil parameters and vegetation parameters. In future work, various remote sensing data (Landsat-TM, LIDAR and MODIS) will be included to improve the vegetation parameters (LAI, vegetation species, and phenology parameters of deciduous forests). In addition, the current model used the daily precipitation and air temperature data from the Slide Mountain climate station that is far from Shelter Creek and Biscuit Creek. Using these data results in higher uncertainty in the climate input for RHESSys modeling. Future work will improve the climate input data by combining the available climate station data with PRISM data. Current model calibration is limited to measured streamflow data. Soil and stream biogeochemistry data (nitrate and DOC) will be included in future model calibration. The predictability of forest recovery in the Shelter Creek watershed after the forest harvesting will be tested. Forest recovery data can be estimated using the vegetation indices (NDVI, LAI, etc.) derived from Landsat imagery data. The predicted LAI using the calibrated model will be compared with the estimated forest recovery data. It is expected that using these additional data will improve model parameterizations and predictions. The improved model will be used to test the impact of climate change and forest disturbance on flow, ET, and nitrate and DOC fluxes.

5. Data Analysis to Support Modeling

5.1. West of Hudson Reservoir Water Budgets, 2000-2015

In order to form a basis for data analysis and water quality modeling of the West of Hudson (WOH) reservoirs for the entire period of water quality monitoring, DEP has been working to compute water budgets for all of the WOH reservoirs. Here we describe the general procedure used to compute these water budgets, and the results for Delaware system reservoirs (Cannonsville, Pepacton, Neversink, and Rondout) for the period 2000 through 2015 are presented.

A water volume conservation equation for a reservoir may be expressed as

$$\frac{dV}{dt} = Q_{IG} + Q_{IU} + Q_G - Q_O + A_S(P - E) \tag{5.1}$$

where V is the reservoir volume (storage), t is time, Q_{IG} is the gaged surface inflow, Q_{IU} is the ungaged surface inflow, Q_O is the total outflow (sum of drinking water withdrawal, spill, and dam releases), A_S is the surface area of the reservoir, and P and E are the precipitation directly onto and evaporation from the surface of the reservoir.

All of the reservoirs have at least one gaged tributary, with discharge measurements available from USGS. A list of USGS stream gages in the WOH watersheds are shown in Table 5.1; note that this table does not list gages that are upstream of other gages in a particular watershed. For Ashokan and Neversink, one USGS gage determines the gaged reservoir inflow; there are two gages for Cannonsville and Rondout, three for Schoharie, and four for Pepacton. The ungaged watershed areas as a percentage of the total watershed area is in the range of 22 to 38 percent for WOH, with the exception being Schoharie, where only 6% of the watershed is ungaged.

Table 5.1. U.S. Geological Survey (USGS) stream gaging and reservoir elevation stations in the West of Hudson reservoirs. Stream gaging stations that are upstream of other stations are not included. USGS gage remarks refer to accuracy of stream gaging observations.

Reservoir and USGS Gage	Drainage Area mile^2	Average Flow MGD	USGS Gage Remarks	% of area ungaged
Ashokan Reservoir (A_S= 7800 acres)				
Esopus Creek at Coldbrook	192		Good	
Ashokan Reservoir	256	-		25.0
Esopus Creek near Lomontville	279		Fair	
Cannonsville Reservoir (A_S= 5260 acres)				
W.Branch Delaware R. at Walton	332	394	Good	
Trout Creek at Trout Cr.	20.2	24	Fair	
Cannonsville Reservoir	454	-		22.4
W. Branch Delaware R. at Stilesville	456	407	Fair	
Neversink Reservoir (A_S= 1430 acres)				
Neversink River at Claryville	66.6	127	Fair	
Neversink Reservoir	92.5	-		28.0
Neversink River at Neversink	92.6	44	Good	
Pepacton Reservoir (A_S= 4940 acres)				
E. Branch Delaware R. at Margaretville	163	205	Good	
Mill Brook	25.2	37	Fair	
Tremper Kill	33.2	39	Fair	
Platte Kill	34.9	45	Good	
Pepacton Reservoir	372	-		31.1
E. Branch Delaware R. at Downsville	372	156	Good	
Rondout Reservoir (A_S= 2060 acres)				
Rondout Creek near Lowes Corners	38.3	67	Fair	
Chestnut Creek at Grahamsville	20.9		Fair	
Rondout Reservoir	95.4	-		37.9
Rondout Creek at Rosendale	383		Good	
Schoharie Reservoir (A_S= 1140 acres)				
Schoharie Creek at Prattsville	237	366	Fair	
Manor Kill at W. Conesville	32.4	35	Fair	
Bear Kill near Prattsville	25.7	30	Fair	
Schoharie Reservoir	315	-		6.3
Schoharie Creek at Gilboa	316	304	Fair	

Similarly, Q_O is the total reservoir outflow, which is the sum of drinking water withdrawal, release of water through the base of the dam to the stream channel downstream, and spill. The precipitation term P is the rate of precipitation (depth/time) falling directly onto the water surface of the reservoir, while E is a similar term representing evaporation from the reservoir water surface.

The magnitude of the precipitation and evaporation terms can be estimated using Cannonsville Reservoir (surface area A_S=5260 acres) as an example. Using annual average precipitation and evaporation rates of 45 and 30 inches per year yields the following estimates for corresponding terms in Equation (5.1): $P\,A_S \approx 17$ MGD, $E\,A_S \approx 12$ MGD, and net $(P - E)\,A_S \approx 7$ MGD, which is about 2% of the average annual gaged inflow at Cannonsville (418 MGD; Table 5.1). Given the accuracy of the streamflow gaging measurements for gages classified as fair or good (Table 5.2), the magnitude of the precipitation/evaporation term is smaller than errors likely to be present in Q_{IG}. Regarding the net groundwater inflow/outflow term Q_G, there is little basis for estimating this term individually for any of the WOH basins, and it is assumed to be negligibly small relative to Q_{IG} and Q_O. As a result, the precipitation, evaporation, and groundwater terms in Equation (5.1) are neglected, so that their value is effectively lumped into the calculation of Q_{IU}. The resulting water balance equation used here is then

$$\frac{dV}{dt} = Q_{IG} + Q_{IU} - Q_O \tag{5.2}$$

This equation was applied to Cannonsville Reservoir by Owens (1998) in order to determine the ungaged inflow Q_{IU} from observations of Q_{IG}, Q_O, and reservoir water surface elevation for 1995, and is used here.

Table 5.2 Descriptors of accuracy of USGS streamflow measurements (included in USGS documents in "Remarks" section).

USGS Gage Description	Accuracy
Excellent	95% if data within 5% of true value
Good	95% if data within 10% of true value
Fair	95% if data within 15% of true value
Poor	Less than Fair

This calculation procedure is based on daily average observations of Q_{IG} and Q_O, and daily observations of the reservoir water surface elevation. From bathymetric curves or tables, values of the reservoir storage volume V are determined from water surface elevation, or vice versa. The subscript i associated with V, Q_{IG}, Q_{IU}, and Q_O represents the value on day i. Using daily values of the reservoir storage volume, there are three simple alternative ways to approximate the time derivative in Equations (5.1) and (5.2). These are:

Forward difference:

$$\left(\frac{dV}{dt}\right)_i \approx \frac{V_{i+1} - V_i}{\Delta t} \tag{5.3}$$

Centered difference:

$$\left(\frac{dV}{dt}\right)_i \approx \frac{V_{i+1} - V_{i-1}}{2\,\Delta t} \tag{5.4}$$

Backward difference:

$$\left(\frac{dV}{dt}\right)_i \approx \frac{V_i - V_{i-1}}{\Delta t} \tag{5.5}$$

where the time interval Δt is the time interval of calculations, which here is 1 day. Water volume calculations were performed for each of these 3 alternative approximations. With these alternative approximations for dV/dt, the following Equation (5.2) is used to solve for daily values of the ungaged inflow Q_{IU}.

$$(Q_{IU})_i = \left(\frac{dV}{dt}\right)_i - (Q_{IG})_i + (Q_O)_i \tag{5.6}$$

Application of Equation (5.6) to a dataset of observations intermittently leads to the result that $(Q_{IU})_i$ is negative. This occurs due to errors in the quantities on the right side of Equation (5.6). Since we are describing this quantity as an ungaged inflow, a negative value is not realistic. As a result, a modified version of Equation (5.6) is used. An error term is introduced into the water balance, where errors occur due to the constraint that $(Q_{IU})_i \geq 0$. The following procedure is used:

if $\left[\left(\frac{dV}{dt}\right)_i - (Q_{IG})_i + (Q_O)_i + E_{i-1}\right] \geq 0$ then:

$$(Q_{UI})_i = \left[\left(\frac{dV}{dt}\right)_i - (Q_{IG})_i + (Q_O)_i + E_{i-1}\right], \text{ and}$$

$$E_i = 0$$

---

else if $\left[\left(\frac{dV}{dt}\right)_i - (Q_{IG})_i + (Q_O)_i + E_{i-1}\right] < 0$ then: (5.7)

$$(Q_{UI})_i = 0 \text{ , and}$$

$$E_i = \left[\left(\frac{dV}{dt}\right)_i - (Q_{IG})_i + (Q_O)_i + E_{i-1}\right]$$

This computational procedure begins with the initial error E_0=0. When applied, this procedure may lead to the result that $(Q_{UI})_i = 0$ and the error is non-zero for a single isolated day. In other cases, $(Q_{UI})_i$ may be set to zero for a number of consecutive days, and the error in the water balance that results will accumulate over that period. For all cases for which the procedure was applied here, (Cannonsville, Neversink, Pepacton, and Rondout for 2000 through 2015), a water balance with nonzero error persists for no more than a week or two, and the impact of the accumulated error on the water surface elevation is small.

An example of the application of this procedure is shown in Figure 5.1, where components of the water budget equations are shown for the period of February 20 through March 20, 2000 at Cannonsville. For the period Feb. 20 through 27, nonzero values of the ungaged inflow (blue line) are computed and the error is zero. On Feb. 28, a negative value of ungaged inflow is computed from the basic water balance; this ungaged inflow is set to zero and a nonzero error is computed. Zero values of ungaged inflow, and nonzero error continues until March 11, when a balance without error is established.

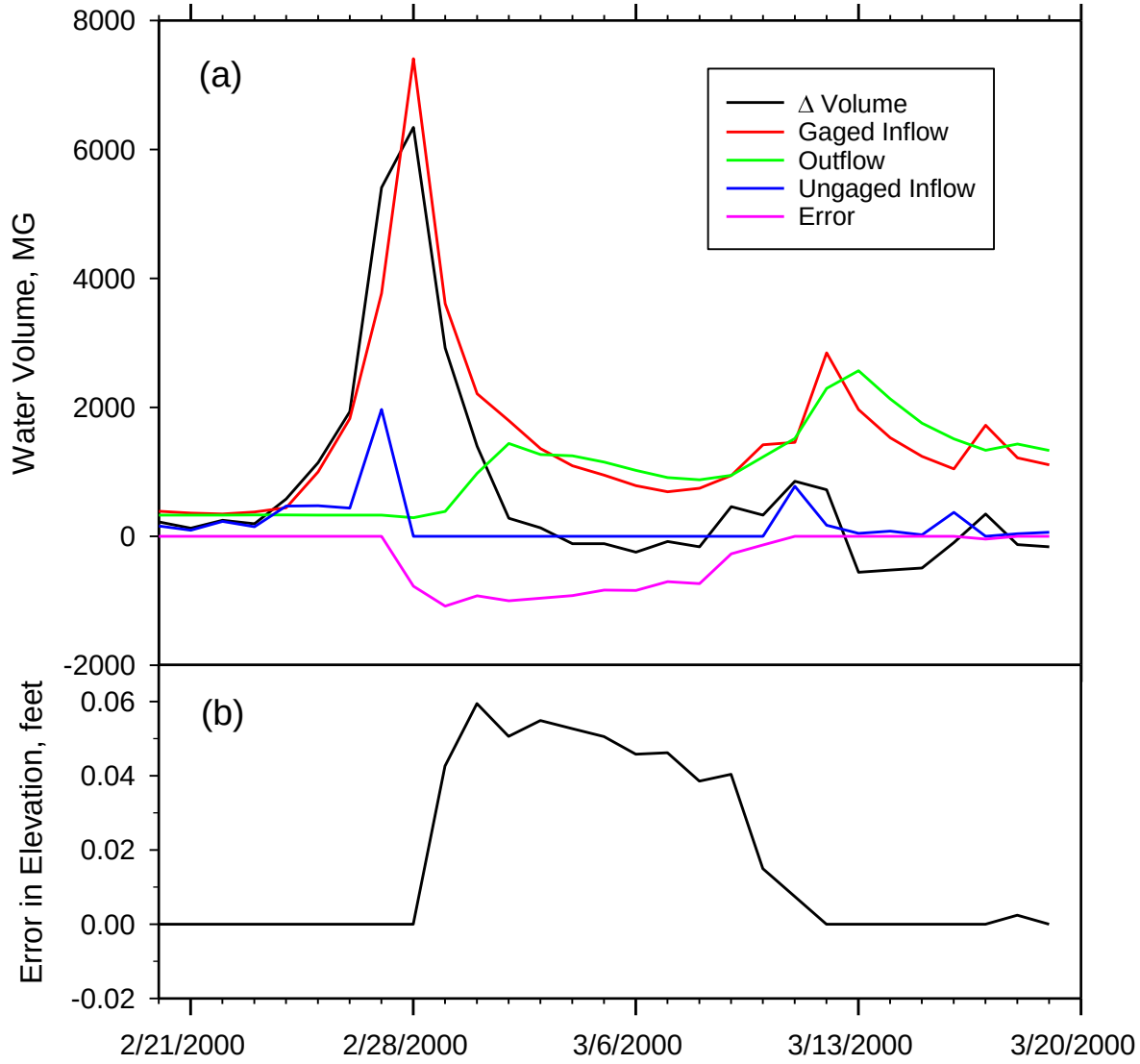

Figure 5.1. Example of water budget calculation for Cannonsville for Feb. 21 to March 20, 2000: (a) components of the budget calculation, and (b) resulting error in water surface elevation.

To investigate the effect of errors, the computed time series of ungaged inflow is then used together with the observed time series of gaged inflow and total outflow in a prediction of storage volume, using the following predictive form of the water budget equation:

$$V_{i+1} = V_i + \Delta t\left[\left(Q_{IG}\right)_i + \left(Q_{IU}\right)_i - \left(Q_O\right)_i\right] \quad (5.8)$$

During periods when there is no error in the balance ($E_i = 0$), the volume computed from Equation (5.8), and the associated water surface elevation exactly match observations; the use of the water balance equation to compute the ungaged inflow ensures this result. However, when nonzero errors exist, the volume from Equation (5.8), and the associated water surface elevation, are greater than the observations. The maximum value of the error in water surface elevation and summarized below.

Regarding the three alternatives for approximating the dV/dt term in the water balance equation (Equations (5.3) through (5.5), the forward difference approximation gave the smallest errors, only slightly smaller than the centered difference approximation, while the backward difference approximation produced substantially larger errors. As a result, the forward difference approximation (5.3) was used in all water budget calculations presented here.

The application of this procedure to Cannonsville for the 16-year period of 2000 through 2015 is summarized in Table 5.3. On average, the annual computed ungaged volume was 15.5% of the total (gaged and ungaged) volume. There were periods during each of the 16 years where the errors in the water balance were introduced as described above. However, the resulting maximum error in predicted water surface elevation during any individual year was generally less than 0.1 feet, with a maximum for the 16-year period of 0.13 feet. The time series of observed gage inflow (sum of West Branch Delaware River and Trout Creek) and computed ungaged inflow for 2015, and the error in computed reservoir water surface elevation determined from application of Equation (5.8), are shown in Figure 5.2.

Similar tabular summaries of the application of this water balance procedure for 2000-2015, and predictions and water surface elevation errors for 2015, are presented for Neversink (Table 5.4 and Figure 5.3), Pepacton (Table 5.5 and Figure 5.4), and Rondout Reservoirs (Table 5.6 and Figure 5.5). Note that the total gaged inflow at Rondout is the sum of USGS discharge measurements for Rondout and Chestnut Creeks, and DEP observations of aqueduct flows from Cannonsville, Neversink, and Pepacton.

The ungaged watershed area as a percentage of the total (gaged plus ungaged) watershed area for each of the 4 reservoir watersheds is shown in Table 5.7 together with the ungaged reservoir inflow as a percentage of the total (gaged plus ungaged) inflow for 2000-2015. In all cases, the ungaged percentage of total inflow is less than the ungaged percentage of total watershed area. This leads to the conclusion that in terms of streamflow generated per unit watershed area, ungaged areas generate less streamflow that the gaged portions of the watershed.

Table 5.3. Annual water balance calculations for Cannonsville Reservoir, 2000 through 2015. Change in storage over the year and total annual inflow and outflow volumes are in billion gallons (BG).

Year	Change in Storage	Gaged Inflow	Outflow	Ungaged Inflow	Ungaged % of Total Inflow	Max. Error Water Surf. Elev., feet
2000	27	195	198	31.1	13.8	0.07
2001	-87	94	202	21.1	18.4	0.06
2002	75	159	117	33.6	17.5	0.03
2003	15	245	264	32.3	11.7	0.08
2004	-1	190	224	32.6	14.6	0.05
2005	-9	180	235	46.4	20.6	0.02
2006	4	243	305	65.2	21.3	0.08
2007	2	202	233	32.6	13.9	0.08
2008	2	216	250	35.7	14.2	0.09
2009	-9	178	221	34.2	16.2	0.07
2010	-1	192	219	26.0	11.9	0.13
2011	4	300	340	43.9	12.8	0.13
2012	-9	127	158	22.3	15.0	0.02
2013	5	178	196	22.7	11.4	0.08
2014	-24	145	206	36.4	20.1	0.02
2015	16	136	151	30.8	18.5	0.01
2000-15	4	2972	3515	547	15.5	0.13

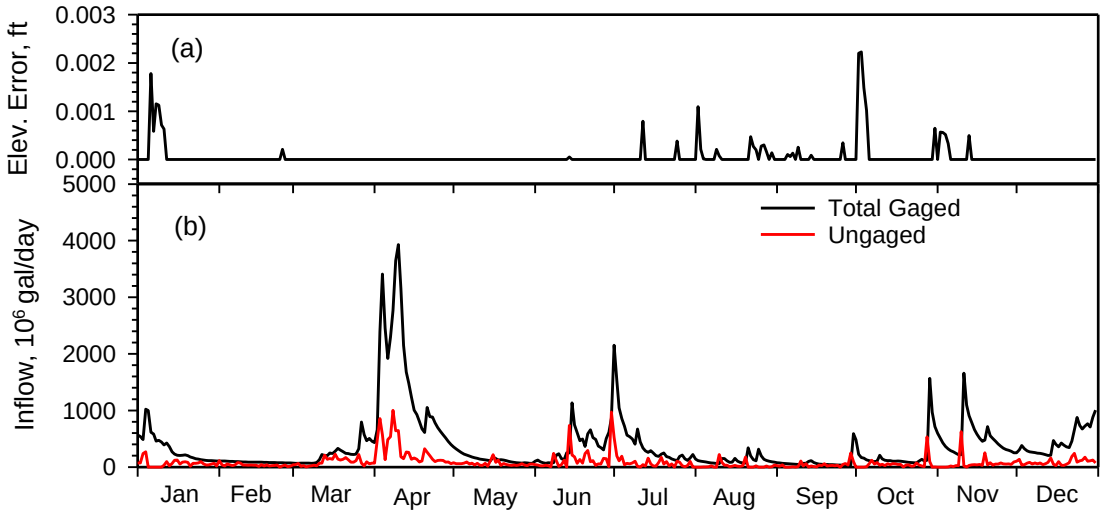

Figure 5.2. Cannonsville water budget results, 2015: (a) error in predicted water surface elevation, and (b) gaged and ungaged inflows.

Table 5.4. Annual water balance calculations for Neversink Reservoir, 2000 through 2015. Change in storage over the year and total annual inflow and outflow volumes in billion gallons (BG).

Year	Change in Storage	Gaged Inflow	Outflow	Ungaged Inflow	Ungaged % of Total Inflow	Max. Error Water Surf. Elev. meter
2000	14	56	54	12.1	17.7	0.007
2001	-17	33	57	6.7	17.2	0.017
2002	15	41	35	8.1	16.4	0.013
2003	7	74	86	20.1	21.5	0.011
2004	-3	59	78	17.0	22.4	0.031
2005	1	60	77	19.0	24.1	0.024
2006	0	62	77	13.9	18.2	0.016
2007	-4	50	64	10.9	17.9	0.015
2008	5	63	71	13.5	17.7	0.015
2009	-3	57	73	12.6	18.0	0.009
2010	-1	57	68	9.8	14.7	0.051
2011	5	82	105	28.9	26.1	0.018
2012	-1	48	65	16.5	25.6	0.006
2013	-1	43	58	13.2	23.4	0.010
2014	-4	50	62	7.4	12.9	0.011
2015	4	45	48	6.9	13.1	0.009
2000-15	17	880	1079	216	19.7	0.051

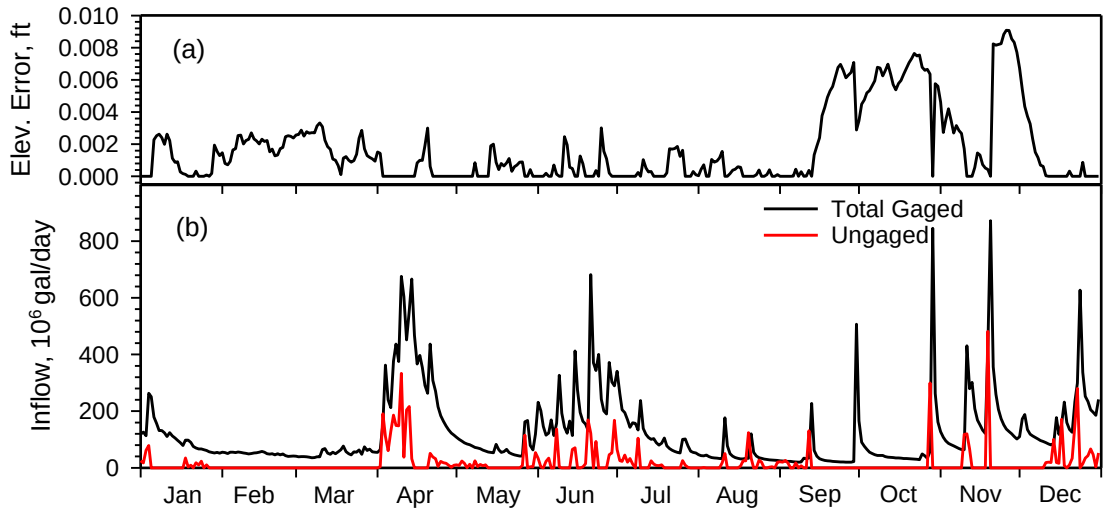

Figure 5.3. Neversink water budget results, 2015: (a) error in predicted water surface elevation, and (b) gaged and ungaged inflows.

Table 5.5. Annual water balance calculations for Pepacton Reservoir, 2000 through 2015. Change in storage over the year and total annual inflow and outflow volumes in billion gallons (BG).

Year	Change in Storage	Gaged Inflow	Outflow	Ungaged Inflow	Ungaged % of Total Inflow	Max. Error Water Surf. Elev. meter
2000	16	157	177	35.6	18.5	0.005
2001	-65	85	172	20.9	19.7	0.014
2002	61	126	96	31.1	19.8	0.012
2003	25	219	243	50.3	18.7	0.002
2004	0	162	183	30.0	15.6	0.055
2005	-14	160	203	19.2	10.7	0.036
2006	4	195	240	48.6	19.9	0.014
2007	-3	172	216	41.4	19.4	0.002
2008	12	183	209	37.6	17.0	0.005
2009	-10	131	183	41.9	24.2	0.001
2010	-4	166	205	35.8	17.7	0.007
2011	13	245	285	52.4	17.6	0.006
2012	-26	108	167	32.6	23.2	0.002
2013	6	135	161	32.2	19.2	0.003
2014	-19	132	184	33.6	20.3	0.003
2015	11	106	117	21.1	16.6	0.003
2000-15	7	2483	3040	564	18.5	0.055

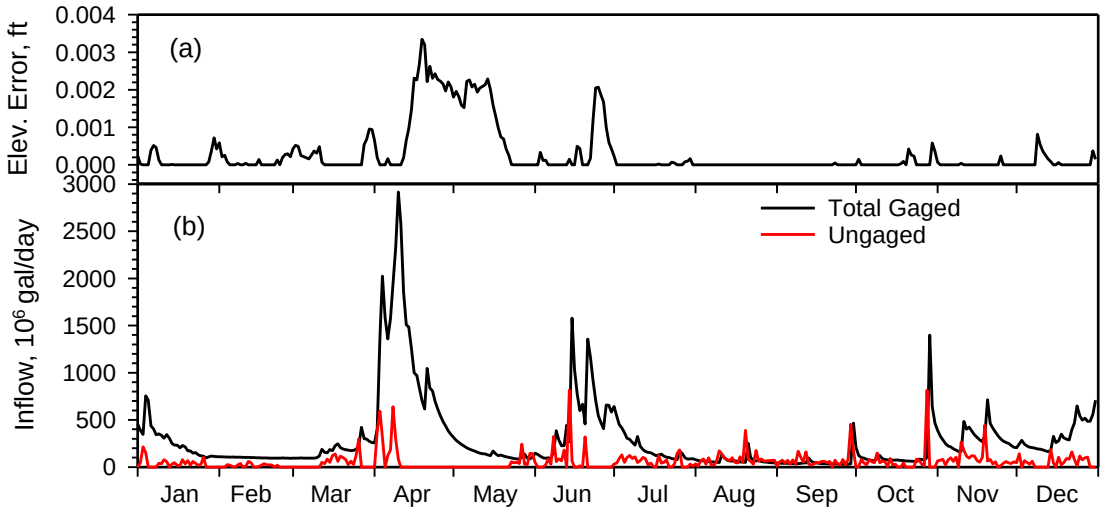

Figure 5.4. Pepacton water budget results, 2015: (a) error in predicted water surface elevation, and (b) gaged and ungaged inflows.

Table 5.6. Annual water balance calculations for Rondout Reservoir, 2000 through 2015. Change in storage over the year and total annual inflow and outflow volumes in billion gallons (BG).

Year	Change in Storage	Gaged Inflow	Outflow	Ungaged Inflow	Ungaged % of Total Inflow	Max. Error Water Surf. Elev. meter
2000	-1	256	283	26.1	9.2	0.008
2001	1	261	271	11.3	4.2	0.018
2002	1	210	226	16.9	7.5	0.019
2003	1	215	238	23.9	10.0	0.011
2004	1	239	260	22.3	8.5	0.003
2005	-1	240	262	21.5	8.2	0.018
2006	0	192	212	18.9	8.9	0.039
2007	-2	241	258	14.9	5.8	0.019
2008	1	197	217	20.8	9.6	0.009
2009	0	219	234	15.2	6.5	0.027
2010	1	248	262	14.8	5.6	0.015
2011	0	261	289	28.7	9.9	0.009
2012	-1	261	277	14.7	5.3	0.011
2013	1	255	268	13.6	5.1	0.014
2014	-1	226	239	11.4	4.8	0.032
2015	1	210	221	12.0	5.4	0.010
2000-15	1	3731	4016	287	7.1	0.039

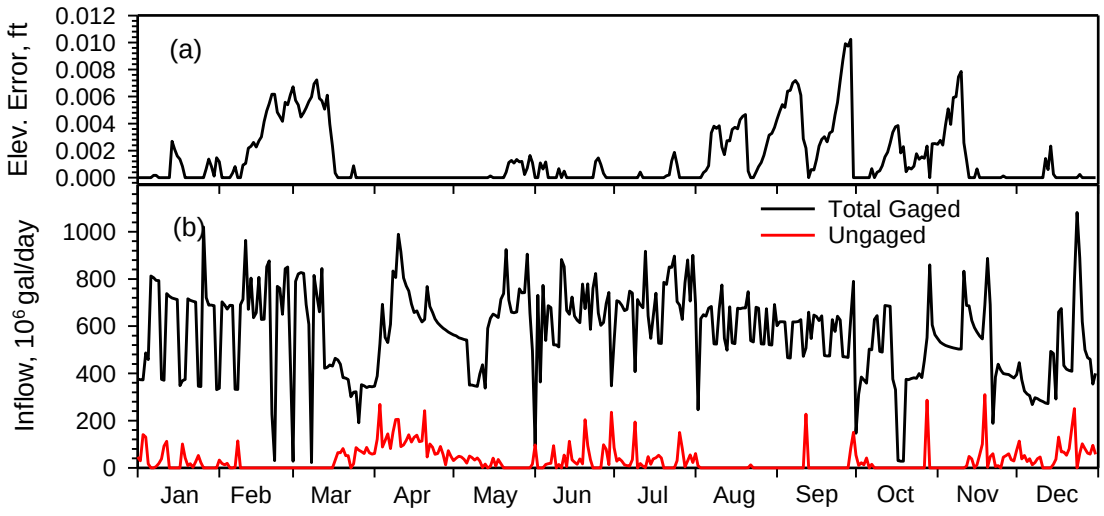

Figure 5.5. Rondout water budget results, 2015: (a) error in predicted water surface elevation, and (b) gaged and ungaged inflows.

Table 5.7. Comparison of computed ungaged inflow as a percentage of total (gaged plus ungaged) inflow for the 16-year period, and the ungaged watershed area as a percentage of the total (gaged plus ungaged) watershed area.

Reservoir	Ungaged % of Total Inflow	Ungaged % of Total Watershed Area
Cannonsville	15.5	22.4
Neversink	19.7	28.0
Pepacton	18.5	31.1
Rondout	7.1	37.9

5.2. Hydraulic Residence Time in West of Hudson Reservoirs

The hydraulic residence time in a reservoir is defined as the time period that a parcel of water resides within the reservoir basin, beginning at inflow from a tributary stream until leaving the basin through either drinking water withdrawal, dam release, or spill. The hydraulic residence time is generally expected to be a function of the shape and bathymetry of the reservoir basin, rates of inflow to and outflow from the reservoir, weather conditions, and thermal stratification and mixing within the reservoir.

Even under steady inflow and outflow conditions and invariant weather, the residence time experienced by individual parcels of water is variable due to turbulent transport and mixing within the reservoir basin, and the variety in pathways by which a parcel can move through the reservoir. These effects can be observed in a tracer experiment, where a quantity of a conservative tracer (such as rhodamine dye) is released quickly into a reservoir inflow. If the concentration of tracer is then measured over time in a reservoir outflow, such as drinking water withdrawal, a curve generally like that shown in Figure 5.6 would be observed. This curve generally indicates that some parcels of water are transported relatively quickly to the outflow point, while other parcels travel more slowly. The hydraulic residence time identified from this experiment would be equal to the elapsed time after release required for one-half of the tracer mass to arrive at the outflow. For the NYC reservoirs that have multiple tributaries and generally three different types and locations of outflow, the residence time varies for each pair of inflow and outflow.

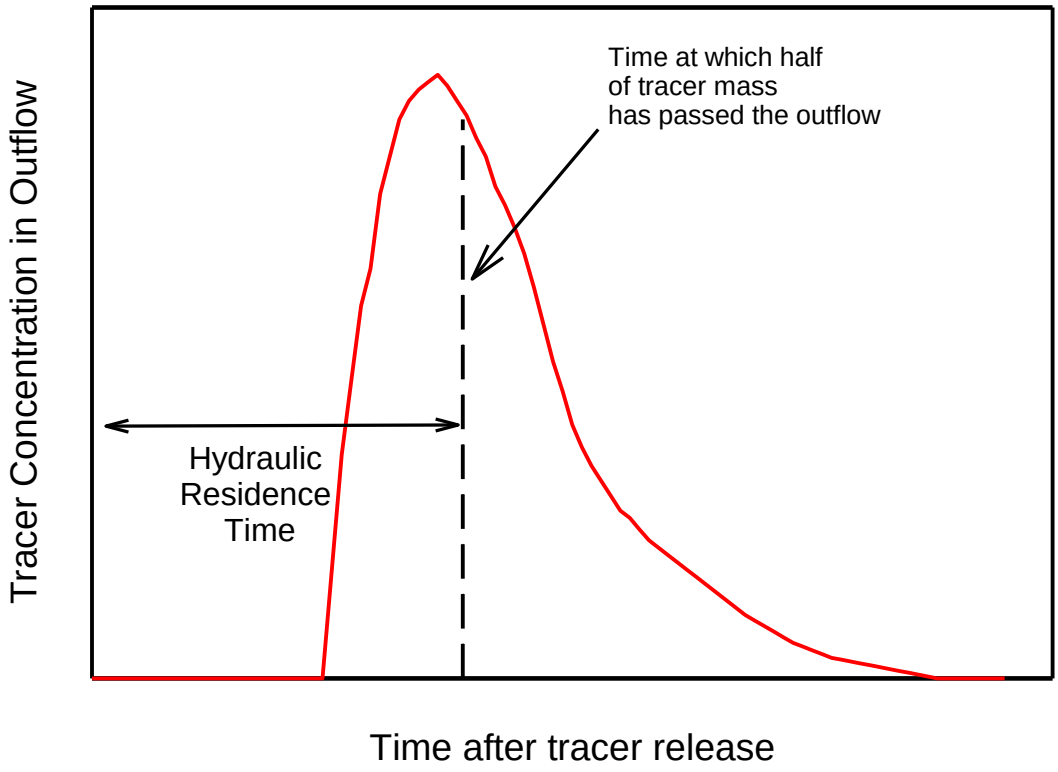

Figure 5.6. Typical or expected observation of dye tracer concentration in a reservoir outflow in response to a quick release of tracer in a reservoir inflow.

Conducting such a dye tracer experiment is the only way to physically measure hydraulic residence time. However, mathematical model simulations can be made to replicate this field experiment. Model application to determine residence time is much more economical and flexible, in that a range of environmental conditions (inflow and outflow rates, weather, reservoir stratification) can be considered. However, the model must be validated under a range of such conditions to ensure that predictions are a good representation of field conditions.

In the absence of such simulations, the residence time for a reservoir can be estimated by assuming that the reservoir is completely mixed, and that plug flow occurs from reservoir inflow to the outflow. Completely mixed conditions exist in the reservoirs only during spring and fall turnover, when thermal stratification is absent. Plug flow assumes that individual parcels of water entering the reservoir move from inflow to outflow like the individual cars that make up a railroad train moving down the tracks; the parcels remain in the order at which they entered as they move through the reservoir. The assumption of plug flow neglects dispersion in the reservoir.

Under these assumptions, the reservoir residence time is equal to equal to V / Q_O, where V is the reservoir volume and Q_O is the total rate of reservoir outflow. Of course, these quantities

vary with time. In order to reduce the variability in the quantities, 1-year moving averages of V and Q_O were computed from records of daily records of these quantities. For example, a 1-year average of V for March 25, 2015 was computed by averaging daily values of V for March 26, 2014 through March 25, 2015.

Values of the 1-year moving average reservoir storage for the Catskill and Delaware system reservoirs are shown in Figure 5.7 and Figure 5.8. Periods of significant reservoir drawdown for both systems occurred in 1980-1981, 1985, and 2001-2002. Similarly, the 1-year moving average values of reservoir outflow are shown in Figure 5.9 and Figure 5.10. Periods of significant low flow are generally consistent with the noted drawdown periods. Unusually high outflows occur when the spill is large, as occurred in the wet periods in 1976, 2006-2007, and 2011. The residence time, this being the quotient of volume and outflow, for the Catskill and Delaware reservoirs is shown in Figure 5.11 and Figure 5.12. Statistics for the hydraulic residence time for each reservoir over the entire 40 year record are given in Table 5.8. Despite the relatively small variability in volume and particularly inflow, Rondout Reservoir displays a coefficient of variation (ratio of standard deviation to the mean) that is similar to the other reservoirs.

Table 5.8. Statistics for hydraulic residence time for Catskill and Delaware system reservoirs, 1966 through 2015. Mean and standard deviation in days.

Reservoir	Mean	Standard Deviation	Coeff. of Variation
Schoharie	39	8.5	0.22
Ashokan West	78	16	0.21
Ashokan East	123	26	0.21
Cannonsville	143	25	0.18
Neversink	162	29	0.18
Pepacton	250	40	0.16
Rondout	61	10	0.17

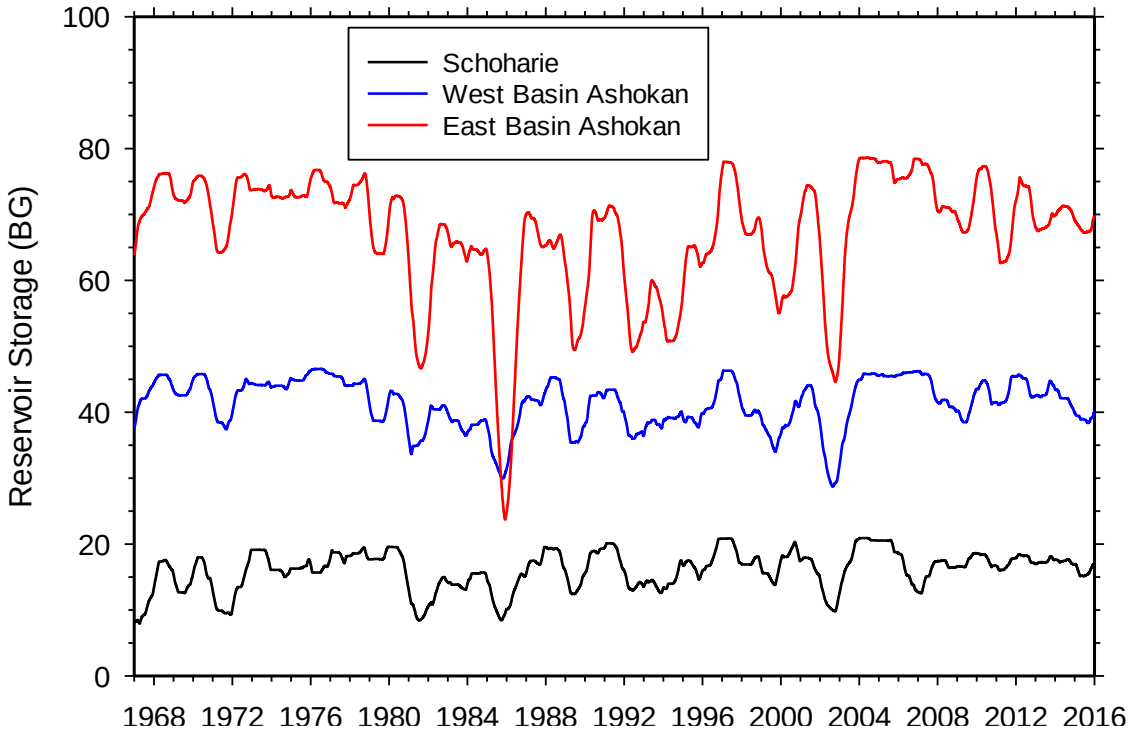

Figure 5.7. Storage in Catskill System Reservoirs, 1966 through 2015.

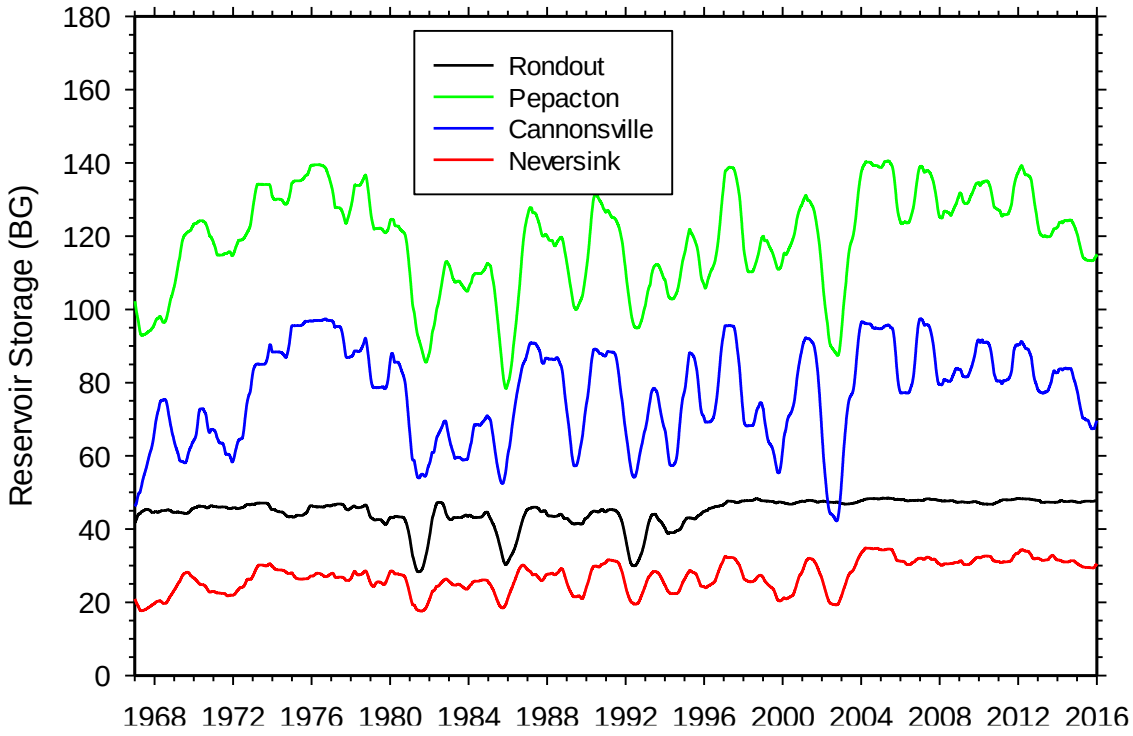

Figure 5.8. Storage in Delaware System Reservoirs, 1966 through 2015.

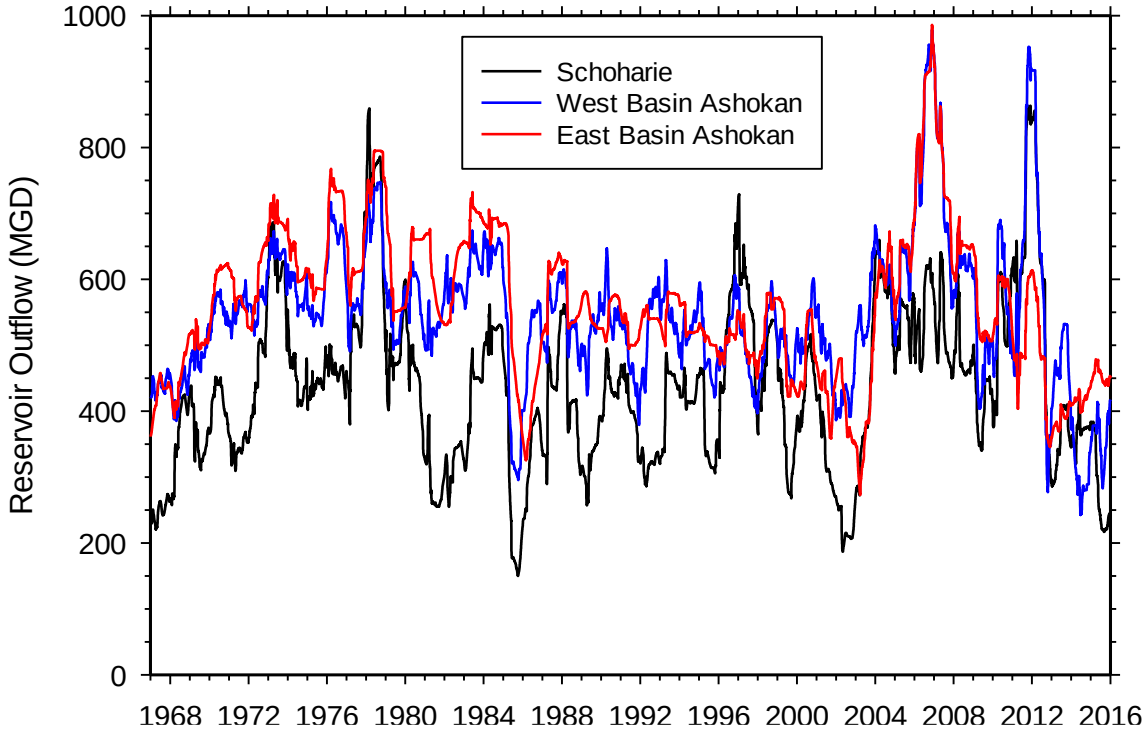

Figure 5.9. Reservoir outflow for Catskill system reservoirs, 1966 through 2015.

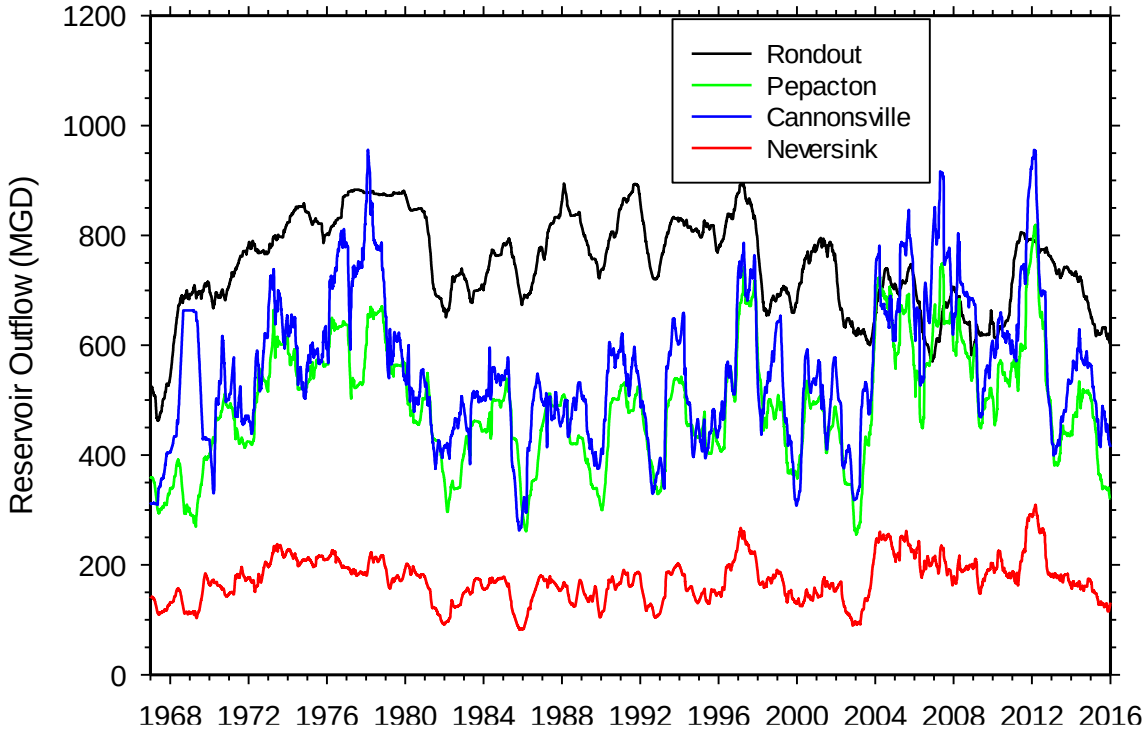

Figure 5.10. Reservoir outflow for Delaware system reservoirs, 1966 through 2015.

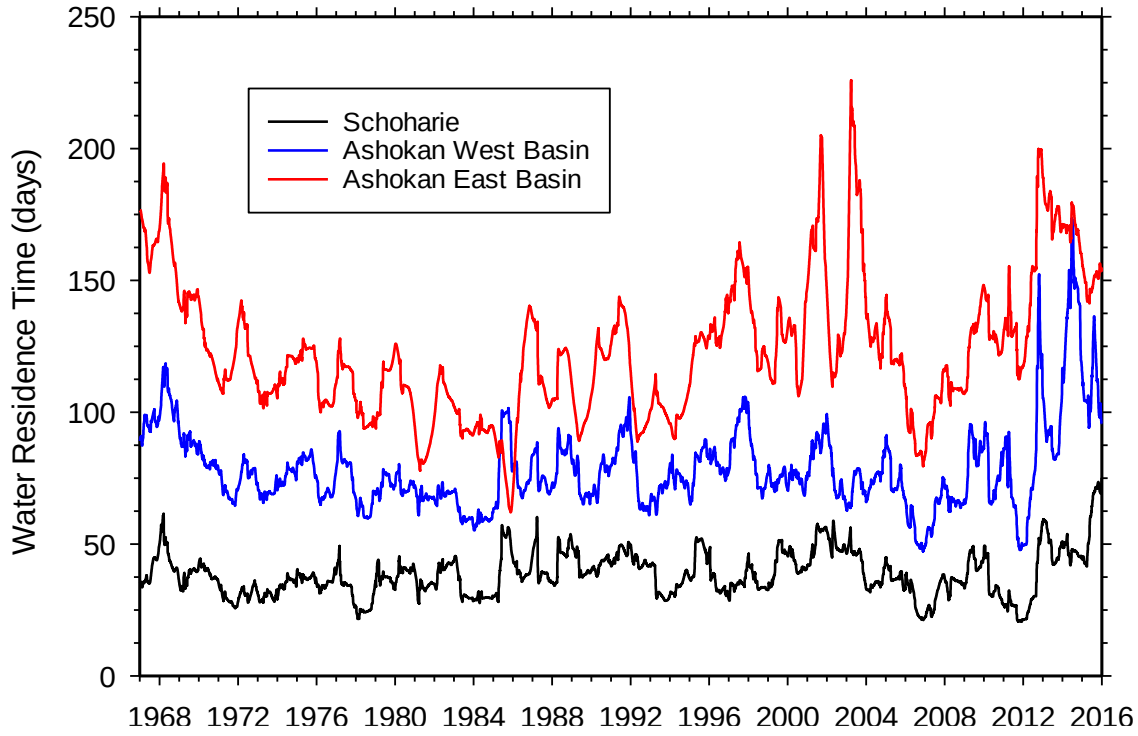

Figure 5.11. Hydraulic residence time for Catskill System Reservoirs, 1966 through 2015.

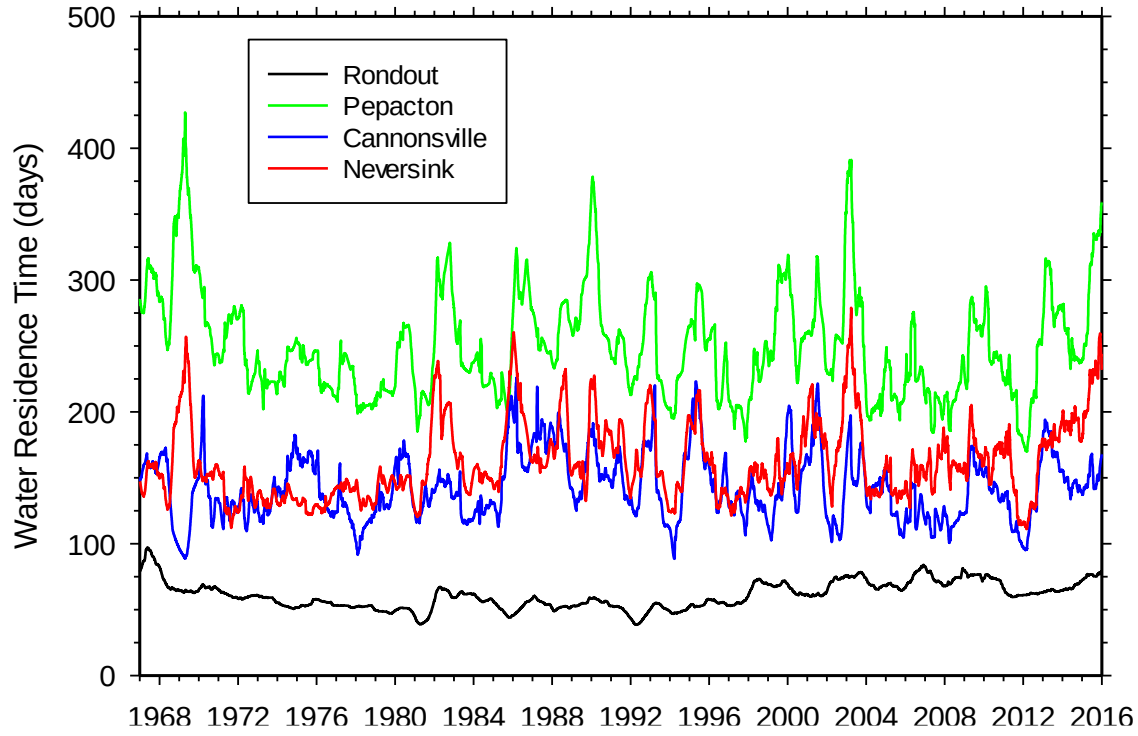

Figure 5.12. Hydraulic residence time for Delaware system reservoirs, 1966-2015.

6. Model Data Acquisition and Organization

6.1. GIS Data Development for Modeling

6.1.1. Water Quality Monitoring Sites

In 2015, the Water Quality Modeling Section's GIS data library was updated with additions to water quality monitoring sites and biomonitoring sites. These locations were georeferenced from site descriptions provided by data samplers as part of the DEP's LIMS database entry. DEP snow monitoring and snow pillow locations data were updated with revised information provided by DEP's Operations Directorate.

6.1.2. Support for modeling projects

GIS support was provided to Water Quality Modeling Section staff, CUNY Postdoctoral researchers, as well as other DEP staff in the Division of Water Quality Science and Research. This support included the production and revision of maps included in the 2015 FAD Summary and Assessment Report, the 2015 update to the Watershed Water Quality Monitoring Plan, and conference presentations and posters.

Table 6.1 lists the types of GIS data used by the Water Quality Modeling Section. While GIS data is used in virtually all DEP reservoir and watershed models, a particular area of use in 2015 was the support of application of two terrestrial (watershed) models: RHESSys and SWAT. RHESSys applications include information derived from LiDAR data collected by DEP. The LiDAR data, along with remote sensing images, are being compiled and analyzed for the Neversink watershed to identify the spatial variation of canopy height and leaf area index (LAI) that is used by RHESSys.

DEP's Operations Directorate has been involved in application of the Army Corps of Engineers HEC-RAS (River Analysis System) model to address questions related to cold water releases from Cannonsville Reservoir to the downstream West Branch Delaware River. The HEC-RAS model has been applied to this river channel to simulate the effect of channel morphology changes on downstream river temperatures. To generate a geometric description of the river channel for use in this model, input data were generated using HEC-GeoRAS using available stream networks, elevation and cross section data. This work will continue to 2016 to inform planning decisions.

Table 6.1. Inventory of GIS data used in water quality modeling.

Data Type	Data Source	Data Description	Dates	Modeling Needs
LiDAR	DEP	Tree height, canopy fraction and LAI	2009	RHESSys Model Input
DEM (1 meter)	DEP	Watershed delineation, topographic parameters	2009	Watershed delineation
Land Use/ Land Cover	DEP	Spatial extent of types of land use and land cover	2009	SWAT Model Input
SSURGO2 Soil Survey	USDA	Soil Characteristics, Percent Clay, Ksat, Ksattop, Available Water Content, Depth to Water Table,	2012	SWAT Model Input
Aerial Imagery	USGS	Landsat TM multispectral imagery	1990-current	Leaf area index (LAI) values and tree phenology
	NASA	MODIS multispectral imagery	2002-current	LAI, and tree phenology
Forest Stands	DEP, USFS	Forest spatial extent	2009	RHESSys Model Input
Vegetation	Cary Institute of Ecosystem Studies	Spatial extent of 11 vegetation species	1986-1993	RHESSys Model Input

6.2. Ongoing Modeling/GIS Projects

6.2.1. Reservoir Bathymetry Surveys

Accurate, current bathymetry data are required for modeling water quantity and quality of NYC reservoirs. Last surveyed in the late 1990's, the 6 WOH reservoirs are being re-surveyed by the USGS through an Intergovernmental Agreement signed in 2013. The USGS will produce GIS surface models of the reservoir bottoms, 2-foot elevation contours and an updated elevation-area-capacity table for each reservoir. Work continued in 2015 on the processing of data collected for the 6 WOH reservoirs. All fieldwork had been completed, and select draft data were delivered to DEP in 2014. The USGS contractors have been processing all reservoir data in parallel in order to deliver a complete set of draft data for review in early 2016.

To further improve reservoir data and provide additional information to the Modeling Section, DEP is reviewing a proposed scope of work to conduct new bathymetric surveys for the 13 EOH reservoirs and 3 controlled lakes. The draft scope of work was submitted by the USGS, and will provide the same level of detail as the data being created for WOH. If approved, the project will provide all data deliverables, including surface models, 2-foot elevation contours and elevation-area-capacity tables to DEP no later than 2020.

6.2.2. Modeling Database Design

Historically, data used by the Water Quality Modeling Section are primarily stored and classified by individual staff members to suit the needs of the specific models. An effort is currently underway to centralize and standardize the storage of datasets to improve data interoperability between all staff and associated researchers. Multiple software programs are being evaluated to determine an optimal solution that will allow all modelers to access datasets. The resulting database will include the capability to properly document the data, including the data source, collection date, and identification of data used in models.

This effort will improve data access and reduce duplication of effort in the central compilation of data with customized queries to provide appropriately formatted data files for each staff member. An additional goal of the project is to create a warehouse to store and document the data used to calibrate each model, and the results of model runs, including all key datasets and parameters used. Maintaining these data will ultimately detail the lineage of the models, and can aide in the interpretation of results. In some cases, data may be appropriately stored in a relational database structure internally, but in others, such as time-series monitoring data owned by other agencies, they will only be accessed as needed. A data curation solution will be designed to support the variety of data access and management requirements as described by the modeling group.

6.3. Time Series Data Development

An inventory of the necessary raw time series data for watershed and reservoir model input and calibration is presented in Table 6.2 and Table 6.3, respectively. The time series data includes meteorology, streamflow, water quality, and point source loads for watershed models. For reservoir models the data includes meteorology, streamflow, stream, reservoir and key point water quality and reservoir operations. Data sets are updated as new data become available. Lag times between the current date and the dataset end dates are the result of QA/QC processes at the data source and/or procurement timelines driving the acquisition of any purchased data.

In this reporting period, existing meteorological datasets being supplemented with climate data from the PRISM climate model. PRISM data are calculated with 4 km^2 resolution grid cells, with variables including precipitation, min/max temperature and dew point. Data are

available from 1981-present, and were downloaded directly from the PRISM website (http://prism.oregonstate.edu).

Table 6.2. Inventory of time-series data used for watershed modeling.

Data Type	Data Source	Data Description	Dates*	Modeling Needs
Meteorology	Northeast Regional Climate Center	Daily Precipitation and Max/Min Temperature	Pre 1960-2013	Model Input
	PRISM	Climate Data	2004	Model Input
Wastewater Treatment Plants	DEP	Monthly WWTP Nutrient Loads	1990-2009	Model Input
Streamflow	USGS	Daily and Instantaneous Streamflow	Period of record available online via USGS	Hydrology Calibration / Nutrient and Sediment Loads
Water Quality	DEP	Routine and Storm Stream Monitoring	Period of record avail. via LIMS	Nutrient and Sediment Loads for Water Quality Calibration
	NYSDEC**	Stream Monitoring at West Branch Delaware River	1992-2010 w/ recent years avail. via LIMS	Nutrient and Sediment Loads for Water Quality Calibration

*Dates represent total span for all data sets combined. Individual station records vary.
**Now part of the DEP Water Quality dataset.

Table 6.3. Inventory of time-series data used for reservoir modeling.

Data Type	Data Source	Data Description	Dates*	Modeling Needs
Meteorology	DEP	Air Temperature, Relative Humidity, Solar Radiation, PAR, Wind Speed, Wind Direction, and Precipitation	1994-June, 2010 Period of record avail. Operations	Model Input
Keypoint and Reservoir Operations	DEP	Tunnel Water Quality, Flow and Temperature; Reservoir Storage, Spill, Withdrawal, and Elevation	Period of record avail. via LIMS	Model Input
Streamflow	USGS	Daily and Instantaneous Streamflow	Period of record available online via USGS	Model Input
Stream Hydrology	DEP	Stream Water Quality, Flow and Temperature	Period of record avail. via LIMS	Model Input
Limnology	DEP	Reservoir Water Quality, and Temperature Profiles	Period of record avail. via LIMS	Model Input

*Dates represent total span for all data sets combined. Individual station records vary.

7. Modeling Program Collaboration

7.1. Water Research Foundation Project 4422 – Advanced Techniques for Monitoring Changes in NOM and Controlling DBPs Under Dynamic Weather Conditions

The goals of this project were to develop and test the effectiveness of on-line (in-situ) monitoring tools that can detect changes in the character and amount of natural organic matter (NOM), and associated disinfection byproducts under typical operating conditions, extreme weather events, and future climate condition scenarios. Most of the work involved the evaluation of advanced on-line instrumentation which utilizes ultraviolet (UV) absorbance and/or fluorescence spectral measurements to detect changes in the concentration and chemical character of NOM and associated formation potential for disinfection byproducts.

To achieve these goals, water samples were collected from various DEP reservoirs and analyzed for a number of parameters including DBP formation potential, ultraviolet-visible light absorbance using both laboratory and field instruments, and laboratory fluorescence measurements. Formation potential measurements included the regulated total trihalomethanes and haloacetic acid components as well as unregulated components including acetonitriles and haloketones. XAD fractionation and polarity rapid assessment method (PRAM) were used to separate and characterize NOM.

This work was completed in 2015, with the final report release in early 2016. This study confirms that ultraviolet-visible spectroscopy and fluorescence can be a useful surrogate for natural organic material and disinfection byproducts. Field instruments that can produce high-quality data with minimal maintenance are commercially available. Application of these instruments can provide additional information to utilities such as DEP with respect to formation potential, thus allowing operations to be modified in response. However, the results indicate that the optical measurements do not capture all of the potential variability in formation potential, and that further study is needed to identify appropriate surrogate measures for formation potential that cannot be measured with ultraviolet-visible light absorbance or fluorescence. In addition, reservoir-specific models may need to be developed in order to refine decision making about the optimal selection of individual water sources.

This project was completed by researchers from Hazen and Sawyer Engineers, and the Department of Civil and Environmental Engineering at the University of Massachusetts, with sponsorship by NYCDEP and WRF.

7.2. Water Research Foundation Project 4590 - Wildfire Impacts on Drinking Water Treatment Process Performance: Development of Evaluation Protocols and Management Practices

NYCDEP is one of six water utilities (the others being Denver Water, City of Westminster Colorado, San Francisco Public Utilities, Truckee Meadows Water Authority, and Metropolitan Water District of Southern California) participating in this WRF study, which is now in its second year. Given the anticipated effect of climate change on frequency and intensity of wildfires, this study is evaluating the effects of wildfires on forested watersheds, including water quantity and availability, and water quality. The project will develop a laboratory-based burn procedure to simulate the effects of wildfire on water quality and treatability.

A literature review will be conducted to document how wildfires have changed water quality, including particulates, nutrients, metals, and organic matter. The six participating utilities will supply historic data from their watersheds regarding the impact of fires. Samples will be collected to monitor the impact of previous wildfires, and the treatability of samples will be evaluated. Compilation of these results will allow the site-specific implications to be identified. The work is being conducted by researchers at the University of Colorado and Hazen & Sawyer Consulting Engineers, and the project will be complete at the end of 2016.

7.3. Water Utility Climate Alliance (WUCA)

New York City DEP is one of ten large water utilities in the United States that form the Water Utility Climate Alliance. This group was formed in order to identify, understand, assess the impact of climate change, and to plan and implement programs to meet climate challenges. WUCA members are involved in enhancing climate change research and improving water management decision-making to ensure that water utilities will be positioned to respond to climate change and protect our water supplies. Two white papers recently released by the Water Utility Climate Alliance feature case studies of water utilities addressing the threat of climate change, including DEP. These white papers advance understanding of how the relatively new enterprise of climate change assessment and adaptation is developing.

DEP is also one of four WUCA utilities (New York, Tampa Bay, Seattle, and Portland) participating in the Piloting Utility Modeling Applications (PUMA) project. In this program, the four PUMA utilities have formed partnerships with scientific institutions to explore how to integrate climate considerations into their specific programs for water quality and quantity management. PUMA has convened workshops where water utility representatives and

researchers meet to discuss and compare approaches for addressing the impact of climate change on water utilities. The four utilities pursued customized approaches based on specific utility needs and learned important lessons in conducting assessments that may be of interest to the wider adaptation community. In addition, these projects attempted to create a "climate services" environment in which utility managers worked collaboratively and iteratively with climate scientists to understand both utility concerns and the ability or limitations of today's climate science to respond to those concerns.

7.4. Global Lake Ecological Observatory Network (GLEON)

GLEON is a 10-year old organization that has been built around issues associated with the setup and deployment of robotic buoys for observing physical and water quality conditions in lakes and reservoirs, storage, processing, and analysis of the high-frequency data gathered by such buoys, and use of the data in modeling. DEP staff have attended recent annual GLEON meetings in Quebec and South Korea. DEP staff are also collaborating with other GLEON members in the intervals between meetings, including sharing of selected data. This participation has helped to ensure that DEP is getting the most out of its sizable investment in robotic monitoring in the reservoirs and tributary streams. DEP has made use of GLEON software tools in the analysis of robotic buoy data.

DEP is also applying the reservoir hydrothermal model GLM (General Lake Model) and associated Aquatic Ecodynamics (AED) water quality model. These models are "open source" software, and are thus open to use and revision by other researchers and professionals. These models are currently being applied to Cannonsville and Neversink Reservoirs by one of the CUNY postdoctoral researchers working in DEP's Water Quality Modeling Section.

Several collaborations have developed from DEP's participation in GLEON annual meetings, where scientists meet to develop ideas and tools to analyze data from an array of lake and reservoir sensors deployed around the globe to address local issues for individual aquatic ecosystems. Additionally, this network of collaborators works to document changes in lake and reservoir ecosystems that occur in response to different environmental conditions and stressors. This is done in part by sharing and interpreting high-frequency sensor data and other water quality and environmental data. DEP contributed data to four collaborative GLEON research projects in 2015.

1. **Temperature Sentinels in Northeastern North America (NENA): In-depth Study of Lake Thermal Responses and Teleconnections in Northeastern North America**

The primary intent of this study is to examine subsurface water temperature profiles from lakes and reservoirs across the northeastern region of North America to determine how water temperature responds to regional-scale climatic drivers and teleconnections. To accomplish this, the researchers will examine a set of lakes and reservoirs with long-term, high resolution temperature profile data and a larger set of NENA lakes and reservoirs with temperature profiles from a single annual profile. Historical water temperature data for Cannonsville, Pepacton, Neversink, and Rondout reservoirs at the deepest sites at the time of peak thermal stratification were formatted and shared with the project lead scientist, Dr. David Richardson, SUNY New Paltz for use in this GLEON-sponsored study.

2. **GLEON Fellowship SALT project:**

A study of increasing salinization of lakes and reservoirs was conducted as part of the GLEON Fellowship Program in 2015. The Fellowship Program trains cohorts of graduate students to explore the information contained in large data sets, work in diverse international teams, and communicate their findings to a broad range of audiences. DEP contributed data for a modeling analysis of global trends and drivers of lake and reservoir salinity to assess ecological impacts. Data included specific conductivity, chloride, sulfate, and sodium concentrations for the period of 1987 to 2014 for ten reservoirs, including Cannonsville, Pepacton, Neversink, Schoharie, Boyds Corners, Cross River, Croton Falls, Middle Branch, New Croton, and Kensico. The work was carried out in connection with the Cary Institute of Ecosystem Studies in Millbrook, New York. The lead investigator was Dr. Hilary Dugan, a post-doctoral scientist at the University of Wisconsin−Madison.

3. **Iron concentration trends around the globe**

This project is an analysis of how iron concentrations in freshwaters around the world have changed over the past 20 years. Data analysis is being performed by Caroline Björnerås, a doctoral candidate at Lund University, Sweden, under the supervision of Dr. Emma Kritzberg from Lund University and Dr. Gesa Weyhenmeyer, Uppsala University, Sweden. Data contributed by DEP in 2015 included iron, total organic carbon, dissolved organic carbon, water color, pH, sulfate, silica, dissolved oxygen, water temperature, and aluminum for two sites on New Croton Reservoir for the period of 1994-2009.

4. Effects of Climate Change on Spring-Winter Runoff and Lake Productivity

The Climate Sentinels working group in GLEON is looking at the effects of ongoing changes in the seasonality of winter – spring streamflow on lake productivity. The initial hypothesis is: Changes in the timing of spring runoff, with more runoff occurring in the winter and early spring, will lead to reduced productivity and phytoplankton biomass during the summer stratified period. The foundation for this expectation is based on our current understanding that nutrients delivered to a lake during colder, deeply mixed, and possibly ice covered conditions, could be less effective at stimulating phytoplankton growth. To test the hypothesis we are assembling data from a large variety of lakes that meet the following minimal requirements:

- In a geographic location where snow accumulation and melt significantly impact the seasonality of stream discharge.
- A lake or reservoir with data from 1990 or earlier and continuing to present. There should be multiple samples per year that cover at least the period of thermal stratification.
- Measurements of chlorophyll profiles during thermal stratification and/or measurements of hypolimnetic oxygen at the onset and just before the loss of thermal stratification.
- Stream discharge measurements of a major inflow to the lake starting in 1990 or earlier, or measurements from a nearby stream or river than can be used to provide an index of lake inflow.

Dr. Don Pierson, currently at Uppsala University, Sweden, is taking the lead with DEP data contributed to the project.

5. Signal Processing Working Group

The GLEON Signal Processing working group has gathered profiling buoy data from 12 different lakes and reservoirs to assess subsurface dissolved oxygen and chlorophyll fluorescence maxima across lake types. DEP has contributed 3 years (2009, 1010, and 2010) of robotic buoy data from the west basin of Ashokan Reservoir to this project. This project is being coordinated by Jennie Brentrup from Miami University of Ohio and Annie Scofield at Cornell University.

7.5. NYCDEP – City University of New York (CUNY) Modeling Program

Through the reporting period, DEP has maintained a contract with the Research Foundation of the City University of New York (RF-CUNY) that provides support for model and data development by providing postdoctoral scientists who work with DEP water quality modeling staff, and supporting research advisors. The work described in Sections 3.2, 4.1, 4.2, and 4.5 of this report has been completed largely by CUNY postdoctoral research staff, working together with their research advisors and staff of the Water Quality Modeling Section.

In August, 2014, a new 4-year contract was initiated between DEP and RF-CUNY. Under this contract, RF-CUNY has hired four fulltime postdoctoral researchers who work in DEP's Water Quality Modeling office in Kingston, NY. Each of the researchers has an associated research advisor who receive part-time support under this contract. The research that has been initiated by these researchers continues to be a significant and critical component of DEP's modeling work. The postdoctoral program provides support in the form of providing model development and application expertise, modeling software, and data sets and in three project areas: (1) Evaluation of the effects of climate change on watershed processes and reservoir water quality as a part of CCIMP; (2) evaluation of FAD programs and land use changes on watershed processes and stream and reservoir water quality; and (3) development of the modeling capability to simulate watershed loading of dissolved organic carbon (DOC), and reservoir and water supply concentrations of DOC and disinfection byproduct formation potential (DBPFP). At the end of 2015, all four postdoctoral positions were filled.

8. Modeling Program Scientific Papers and Presentations

8.1. Published Scientific Papers

Mukundan, R., D. C. Pierson, E. M. Schneiderman, and M. S. Zion, 2015. **Using detailed monitoring data to simulate spatial sediment loading in a watershed**. *Environmental Monitoring and Assessment*, DOI 10.1007/s10661-015-4751-8

Abstract: The use of watershed models as cost-effective tools to quantify the impact of conservation practices on water quality is often constrained by lack of data for model parameterization. This study uses short-term (3 years) detailed monitoring data to guide spatially distributed model parameterization and modeling analysis for suspended sediment in the Upper Esopus Creek Watershed (UECW) that is part of the New York City water supply. The calibrated Soil and Water Assessment Tool (SWAT) model simulated suspended sediment loading from tributary sub-basins and at the watershed outlet that were comparable to field measurements. Model simulations estimated that stream channels contributed the majority (85%) of stream sediment in the study watershed followed by upland erosion (11%) and point sources (4%), consistent with previous estimates and field observations. Long term (12 years) simulation of the calibrated model was used to apportion the average annual sediment yields from tributary sub-basins which ranged between 12 and 161 t km^{-2} $year^{-1}$. Model simulations were also used to understand the inter-annual variability and seasonality in suspended sediment loading in the study watershed. We demonstrate the wider applicability of short-term detailed monitoring for model parameterization and calibration, and long-term simulation of water quality using the SWAT model.

8.2. Conference Presentations

Association for the Sciences of Limnology and Oceanography (ASLO)
Aquatic Sciences Meeting
February 22-27, 2015, Granada Spain

Simulating the effects of climate change on phytoplankton in a New York City Water Supply Reservoir
Pierson, D. C., N. R. Samal, H. Markensten, and E. M. Owens

Abstract: The impacts of climate change on the phytoplankton in Cannonsville Reservoir, a part of the New York City water supply, is evaluated using a coupled watershed and reservoir modeling system, driven by downscaled climate scenarios derived from CMIP3 climate models. The Generalized Watershed Loading Function (GWLF) model simulates streamflow as well as dissolved and particulate nutrients, which become inputs to a one dimensional reservoir model which includes the PROTECH based phytoplankton functional group algorithms. Simulations predict that there will be a future 10-15% increase in total chlorophyll during the period of thermal stratification and that this increase will coincide with a reduction in the importance of diatoms and an increasing importance of cyanobacteria. Average summer cyanobacteria concentrations are simulated to increase by approximately 20% -70%. Model sensitivity analysis suggests that it is largely the effects of climate change on reservoir thermal structure as opposed to watershed loading that is responsible for the changes in phytoplankton. These results are evaluated relative to previous changes in phytoplankton associated with point and non-point source nutrient reductions.

Long term changes in ice seasons of twenty-one geographically distributed freshwater lakes: Modeling Simulations and Observations
N. R. Samal, K. D. Jöhnk, D. C. Pierson, M. Leppäranta, H. Yao, B. R. Hargreaves, T. Kratz, S. Sharma, A. Laas, D. Hamilton, R. Adrian, J. Rusak, D. Oezkundakci, C. Williamson, D. Vachon, B. Denfeld, G. Kirillin, K. Czajkowski and L. Camarero

Abstract: Long term trends and variability in the seasonality of lake ice dynamics are some of the clearest indicators of changes in climate conditions. The timing of ice formation, ice cover duration and ice loss in lakes and reservoirs will modulate the impact of regional weather conditions on lake thermal structure and mixing, and thus will ultimately influence phytoplankton succession and trophic status of a lake. Here a simple lake ice model that predicts lake ice timings and thickness has been applied to 21

freshwater lakes and reservoirs around the globe. The model is driven by measurements of air temperature and wind speed, as these are the most important factors influencing formation and breakup. The effects of snowfall and solar radiation on ice characteristics are not explicitly considered but can be parameterized. Even though the model does not make detailed calculations of the ice cover energy budget it reproduces long-term trends allowing for historical analysis of ice cover in these geographically distributed lakes. Work of this ongoing GLEON project will include simple snow cover estimates derived from precipitation and temperature data.

Gordon Research Conference and Seminar: Catchment Science
June 13-14, 2015
Andover, MA

Innovative Models for the Organic Carbon Budget of New York City (NYC) Reservoirs.

Li, Y., K.E. Moore, R.Van Dreason, P.C. Hanson.

Abstract: In order to investigate the role of climate change in the carbon cycling of aquatic systems, it is necessary to better understand organic carbon (OC) budgets at the catchment scale. However, present studies on OC budgets are incomplete and uncertain due to the complicated nature of cycling processes in lakes and reservoirs. This study used the Framework for Aquatic Biogeochemical Models (FABM) to theoretically explore the classic "Nutrient Phytoplankton Zooplankton Detritus" (NPZD) model for the carbon cycling processes. Two NYC reservoirs with different catchment characteristics were preliminarily examined to evaluate the role of allochthonous carbon and to approximate the OC budgets for these reservoirs. This work will provide an improved basis for water quality model structure, uncertainty analysis, and could ultimately lead to improved modeling tools to help manage and plan for a regional water supply that serves more than 9 million residents in NYC and upstate communities in a changing climate.

Gordon Research Conference and Seminar: Drinking Water Disinfection By-Products
August 8-14, 2015
South Hadley, MA.

Conceptual Model for Simulating Disinfection By-Products (DBPs) Precursors in New York City (NYC) Reservoirs

Li, Y., R. Van Dreason., D.A. Smith K.E. Moore, P.C. Hanson, and E.M. Owens

Abstract: With more stringent regulatory requirements for disinfection byproducts (DBPs) in drinking water by USEPA, it is important to better understand the origins of DBP precursors in water supply systems. Due to the complex chemical characteristics associated with DBP precursor origins, many DBP models are empirical and are unable to identify the relative importance of autochthonous and allochthonous sources of DBP precursors. This study used Cannonsville Reservoir, one of the NYC water supply reservoirs, to preliminarily investigate algal-produced precursors compared to terrestrial sources. Observed time series of nutrients (total phosphorus and nitrogen, TP and TN), algal abundance (based on chlorophyll concentration), and organic matter (dissolved and total organic carbon, DOC and TOC) during 1995-2014 illustrate long-term patterns of the water quality variables that are commonly related to DBP formation. Furthermore, the relationships between TN, OC, and DBP formation potential (DBPFP) were studied in 2007 and 2008 to develop a conceptual model for studying algal-produced DOC as a source of DBP precursors. This conceptual model will help in the development of mechanistic models to simulate and potentially predict DBP precursors, with the ultimate goal of understanding the potential changes in DBP precursors in the NYC water supply under climate change.

The Occurrence of Dissolved Organic Carbon in the Catskill Mountain Watersheds of the NYC Water Supply

R. Van Dreason, R. Mukundan

Abstract: An empirical model was recently developed by Mukundan and Van Dreason (2014) that indicated that organic carbon concentration was the most important factor explaining trihalomethane (THM) formation within the NYC distribution system. THMs and other Disinfection by-products (DBPs) occur in drinking water as a result of a reaction between organic matter naturally occurring in the water and the disinfectant (e.g. chlorine) added to control microbial contaminants. THMs and other DBPs are a major concern to water suppliers because of their suspected carcinogenic properties.

Because of its important role in regulating DBP formation, in this presentation we will describe the occurrence of DOC within the Catskill Mountain portion of NYC's water supply system. Regional and seasonal patterns will be compared using data collected from the Catskill reservoirs. We also examine the patterns in DOC concentrations over time, since increases in the reservoirs could have important ramifications on future DBP formation in the distribution system.

NYC Watershed Science and Technical Conference
September 9, 2015
West Point, New York

Performance Assessment of Stochastic Weather Generators for Precipitation over Catskill Mountain watersheds, New York, USA
Acharya, N., A. Frei, K.E. Moore, and J. Mayfield

Abstract: The New York City Department of Environmental Protection (DEP) has performed studies to assess the potential impacts of climate change on the availability of high quality water in this water supply system. To better address this, there is a need to develop future climate scenarios that can be used as inputs to the DEP's integrated suite of hydrological models. There are two familiar approaches used to incorporate climate change into vulnerability analyses viz., top-down and bottom-up approaches. Top-down approaches use scenarios from Global Climate Models (GCMs). Bottom-up approaches identify the climate vulnerabilities of a water supply system over a wide range of potential climate changes. Stochastic weather generators are often employed in bottom-up risk assessments to simulate potential shifts in both long-term (decadal) precipitation means and persistence as well as in extreme daily precipitation amounts. The main goal of the current work is to document the performance of two weather generators, the widely used generator WGEN, and the comparatively new and sophisticated WeaGETS, in simulating precipitation over the Catskill Mountain region. The performances of these two weather generators are compared in order to assess their capabilities of reproducing the observed statistical properties including the probability distributions, means and variances, and the frequencies and magnitudes of extreme events.

Trends of Chlorophyll and Phytoplankton for New York City's West of Hudson Reservoirs (1988-2014)
Ray Homolac, NYCDEP

Abstract: The New York City Department of Environmental Protection (DEP) performs limnology surveys on most of the water supply reservoirs and many water quality monitoring parameters are analyzed. The historical record of DEP data will be examined for long-term trends of chlorophyll a and total phytoplankton in the Catskill/Delaware System reservoirs. An overview of the time period 1988 through 2014 will be presented leading to a more in depth focus for 2004 through 2014.

Exploration and Evaluation of Long-Term Water Quality Data
Karen Moore, NYCDEP

Abstract: An important goal in watershed protection is to document changes in water quality and look for linkages to what is occurring on the landscape. We applied statistical methods including Weighted Regressions for Time, Discharge, and Season (WRTDS) to the major inflows of New York City water supply West-of-Hudson reservoirs to look at water quality changes and corresponding explanatory variables related to land management, climatic, and hydrologic conditions.

Development of a Watershed Timeline to Chronicle Historical Events for Potential Contribution to Changes in Water Quality
David Quentin, NYCDEP

Abstract: There are many natural events that can affect a watershed, and the quality of the water, that may require a change in the operation of a water supply. With this in mind, a New York City Watershed Event Timeline ("Timeline") was developed to ascertain "cause and effect" relationships by linking significant environmental events (e.g. droughts and hurricanes) within the New York City Department of Environmental Protection (DEP) watersheds to water quality variations. Moreover, the effects these events have on DEP operations and infrastructure (e.g., alum treatment, wastewater treatment plant operations, intensified monitoring) can be related for planning purposes. This timeline portrays information from 1985 to the present, and will continue to be a "living document" that can be updated as needed with more information, and new parameter headings that directly relate to other aspects of water supply operation.

Best Management Practices and their Impact on Turbidity in Stony Clove Creek
Jim Mayfield, Karen Moore, and Danyelle Davis, NYCDEP

Abstract: Stony Clover Creek has been identified as the predominant source for turbidity and suspended sediment in the Ashokan Reservoir basin. Four best management practices (BMPs) were designed and installed in an effort to reduce the sediment and turbidity. A water quality monitoring program and a channel morphology monitoring program has also been conducted on this reach. The data collected to date by DEP and USGS will be examined to quantify the effects of BMPs.

Overview of Hillview Reservoir Protozoan Data and Update on Related Research Studies – New York City Water Supply
Kerri Alderisio, NYCDEP

Abstract: As the pre-finished water reservoir for New York City's water supply, Hillview Reservoir is a critical component to the drinking water system. Protozoan sampling was conducted from 2006-2008, and again from 2011 to the present as a result of an administrative order related to covering the reservoir as described in the LT2. An overview of the data will be presented as well as up-to-date results related to any pathogen research associated with Hillview Reservoir.

***Giardia* Concentrations in New York City's West of Hudson Streams and Reservoirs: Catskill Watershed Case Study**
Christian Pace and Kerri Alderisio, NYCDEP

Abstract: Since 2002 the NYCDEP has taken over 2,800 protozoan samples from West-of-Hudson streams and reservoir outlet sites. This presentation will summarize this data and illustrate *Giardia* reductions as water travels down through the watersheds and from reservoir to reservoir. The presence of seasonal and long-term trends at some locations will be discussed and additional focus will be given to the Schoharie watershed where additional sites have been selected and sampled over the last few years.

Fifth International Workshop on Climate Informatics
September 24-25, 2015
National Center for Atmospheric Research, Boulder, CO

Analysis of Weather Generators: Extreme Events
Acharya, N., A. Frei, and E. M. Owens

Abstract: Stochastic weather generators (WGs) are often used to simulate synthetic weather time series based on observed statistical properties in a particular location. Most studies evaluate WG skill on average properties. Our objective is to assess how the WGs perform in simulating extremes, especially high precipitation amounts. We analyzed 13 different WGs using two parallel approaches: extreme event indices associated with large precipitation events; and recurrence intervals based on the Generalized Extreme Value (GEV) distribution.

Global Lake Ecological Observatory Network (GLEON) Meeting
October 12-16, 2015
Chuncheon, South Korea

Use of Robotic Monitoring and Modeling to Forecast the Downstream Impact of Rapid Drawdown of Cannonsville Reservoir
Owens, E.M., L.L. Janus, and A. Matonse

Abstract: Turbidity is of special concern in the 19 drinking water reservoirs that serve the nine million consumers in City of New York because of its potential to interfere with disinfection. In July 2015, a pressurized flow of turbid water from a bore hole occurred during a geotechnical investigation of a site immediately downstream of Cannonsville Reservoir. A possible source of the pressure and turbid water flow was the reservoir itself, which raised the question of whether or not the dam was undermined. While this source was judged to be very unlikely, rapid reservoir drawdown was initiated by maximizing both the transfer of drinking water to downstream Rondout Reservoir and the release to the river downstream of the dam. While increases in turbidity in Cannonsville are most closely linked to runoff events, turbidity also increases with drawdown. In the absence of a turbidity model for the upstream reservoir, an elevation-turbidity relationship was developed for Cannonsville using available historical data. Robotic monitoring of turbidity in the two reservoirs and the connecting aqueduct, together with a two-dimensional turbidity model of the downstream (Rondout) reservoir, were used to forecast the impact of the unprecedented drawdown of Cannonsville on turbidity in

Rondout, a terminal reservoir of the water supply. Robotic monitoring was used to provide near real time data on the storage, flow and turbidity conditions in the system, and to initialize the model to current conditions. Three weeks into the drawdown, the pressurized water source was determined to be an artesian aquifer, the bore hole was sealed, safety concerns were eliminated, and the drawdown was halted. Nonetheless, this episode provided meaningful lessons on the importance and role of monitoring and modeling in dealing with emergency events.

Dissolved Oxygen and Phytoplankton Seasonality in New York City (NYC) Reservoirs of Contrasting Trophic Status

Li, Y., P. C. Hanson, K. E. Moore, E. M. Owens, L. L. Janus, and R. VanDreason.

Abstract: An increase in human activities and associated increased nutrient loading have resulted in eutrophication and water quality degradation in lakes and reservoirs worldwide. This study considers two New York City water supply reservoirs (Cannonsville and Neversink) with differing trophic states to investigate dissolved oxygen (DO) and phytoplankton dynamics. Seasonal patterns of water temperature and DO profiles were examined, and the dominant phytoplankton species were identified for NYC reservoirs. Based on the phytoplankton identification, six functional groups were chosen to characterize the successional patterns of phytoplankton in Cannonsville Reservoir. Capturing the successional patterns and oxygen dynamics are important steps in the application of the LakeMetabolizer software, and in simulations using the GLM-FABM-AED models to predict primary production and carbon cycling. This work may ultimately help in planning management of reservoirs in a regional water supply that serves more than 9 million residents and upstate communities under changing climate conditions.

International Soil and Water Assessment Tool (SWAT) Conference
October 14-16, 2015
Purdue University, West Lafayette, IN

Reducing equifinality in semi-distributed models by using spatial wetness information and reducing complexity in the SWAT-Hillslope model

Hoang, L., E.M. Schneiderman, T.S. Steenhuis, S.M. Pradhanang, K.E. Moore, and E.M. Owens

Abstract: Estimating model parameters in simulation models can be problematic because of the non-linearity and interdependence of the parameter sets since changes of some parameters might be compensated by others. It is not uncommon when calibrating distributed hydrological models against discharge at the basin outlet to find multiple parameter vectors with reasonably good performance. This is known as equifinality which contributes to uncertainty of model predictions. Equifinality for semi-distributed hydrological models may be reduced by employing conceptually appropriate models, calibrating with both spatial and temporal observations, and by reducing complexity. We will apply our conceptual model to the Catskill Mountains (New York State) where subsurface connectivity determines the wetting pattern in the landscape. The model used is SWAT-Hillslope, a modified version of SWAT that incorporates topographic characteristics in Hydrological Response Unit (HRU) definition and introduces a perched water table with the ability to route interflow from "dryer" to "wetter" HRU wetness classes. Calibration of discharge at the outlet of the watershed with SWAT-Hillslope was carried out by randomly generating a large number of parameter sets using the Monte Carlo sampling method. The preliminary result shows that SWAT-Hillslope could predict discharge well with Nash-Sutcliffe Efficiency of more than 0.6 and 0.8 for daily and monthly time steps, respectively, and was not affected significantly by reducing the HRU number. As expected, multiple parameter sets could be identified that performed equally well in predicting outlet discharge in the calibration period, but resulted in diverse performances in the validation period. Constraining the parameters further with available spatial information on moisture contents and location of saturated soils reduces equifinality. We expect improved model performance by adjusting the model structure to better represent the landscape and by reducing complexity and equifinality.

American Geophysical Union Fall Meeting
December 14-18, 2015
San Francisco, CA

Realistically Predicting Saturation-Excess Runoff with El-SWAT
Hoang, L., E. M. Schneiderman, T. S. Steenhuis, K. E. Moore, E. M. Owens

Abstract: Saturation excess runoff (SER) is without doubt the major runoff mechanism in the humid well vegetated areas where infiltration rates often exceed the medium rainfall intensity. Despite its preponderance, incorporating SER in the distributed models has been slow and fraught with difficulties. The short term objective of this paper to adjust the generally used Soil and Water Assessment Tool (SWAT) to include SER and test the results in the Catskill Mountains that is the source of most of New York City's

water. The long term goal is to use the adjusted distributed runoff mechanism in water quality models to aid in the design of effective management practices. The current version of SWAT uses information of soil plant characteristics and hydrologic condition to predict runoff and thus is implicitly based on infiltration-excess runoff. Previous attempts to incorporate SER mechanism in SWAT fell short because they were unable to distribute water from a Hydrological Response Unit (HRU) to another. In the current version called El-SWAT, this shortcoming has been overcome by redefining HRU to include landscape position through the topographic or other user-defined index, grouping the newly defined HRU into wetness classes and by introducing a perched water table with the ability to route interflow from "dryer" to "wetter" HRU wetness classes. Mathematically, the perched aquifer is a non-linear reservoir that generates rapid subsurface stormflow as the perched water table rises. The El-SWAT model was tested in the Town Brook watershed in the upper reaches of the West Branch of the Delaware in the Catskill Mountains. The results showed that El-SWAT could predict discharge well with Nash-Sutcliffe Efficiency of 0.69 and 0.84 for daily and monthly time steps. Compared to the original SWAT model, El-SWAT predicted less surface runoff and groundwater flow and a greater lateral flow component. The saturated areas in El-SWAT were concentrated in locations with high topographic index and was in agreement with field observations. With the incorporation of topography characteristics and the addition of the perched aquifer, El-SWAT gives a realistic representation of hydrological processes and will lead to better water quality models where the source of the surface runoff matters.

Evaluation of stochastic weather generators for capturing the statistics of extreme precipitation events in Catskill Mountain watersheds, New York State

Acharya, N., A. Frei, J. Chen, and E. M. Owens

Abstract: Watersheds located in the Catskill Mountains area, part of the eastern plateau climate region of New York, contributes about 90% of New York City's municipal water supply, serving 9 million New Yorkers with about 1.2 billion gallons of clean drinking water each day. The New York City Department of Environmental Protection has an ongoing series of studies to assess the potential impacts of climate change on the availability of high quality water in this water supply system. Recent studies identify increasing trends in total precipitation and in the frequency of extreme precipitation events in this region. The objectives of the present study are: to analyze the probabilistic structure of extreme precipitation based on historical observations, and to evaluate the abilities of stochastic weather generators (WG), statistical models that produce synthetic weather time series based on observed statistical properties at a particular location, to simulate the statistical properties of extreme precipitation events over this region. The generalized extreme value distribution (GEV) has been applied to the annual block

maxima of precipitation for 60 years (1950 to 2009) observed data in order to estimate the events with return periods of 50, 75, and 100 years. These results were then used to evaluate a total of 13 WGs: 12 parametric WGs including all combinations of three different Markov chain (MC) models (1st, 2nd, and 3rd) and four different probability distributions (exponential, gamma, skewed normal and mixed exponential); and on semi-parametric WG based on k-nearest neighbor bootstrapping. Preliminary results suggest that three-parameter (skewed normal and mixed exponential) and semi-parametric (k-nearest neighbor bootstrapping) WGs are more consistent with observations. It is also found that first order MC models perform as well as second or third order MC models.

9. References

Agnew, L.J., S. Lyon, P. Gérard-Marchant, V.B. Collins, A.J. Lembo, T.S. Steenhuis, M.T. Walter, 2006. Identifying hydrologically sensitive areas: Bridging the gap between science and application, *Journal of Environmental Management*, 78: 63-76.

Ailliot, P., D. Allard, V. Monbet, and P. Naveau, 2015: Stochastic weather generators: an overview of weather type models. *Journal de la Société Française de Statistique* 156(1): 101-113.

Anandhi, A., A. Frei, D. C. Pierson, E. M. Schneiderman, M. S. Zion, D. Lounsbury and A. H. Matonse, 2011a. Examination of change factor methodologies for climate change impact assessment. *Water Resources Research*, 47 10p.

Anandhi A, A. Frei, S. M. Pradhanang, M.S. Zion, D. C. Pierson, and E.M. Schneiderman, 2011b: AR4 climate model performance in simulating snow water equivalent over Catskill Mountain watersheds, New York, USA. *Hydrological Processes* 25: 3302–3311.

Anandhi, A., M.S. Zion, P.H. Gowda, D. C. Pierson, D. Lounsbury, and A. Frei, 2013: Past and future changes in frost day indices in Catskill Mountain region of New York. *Hydrologic Processes* 27: 3094–3104.

Apipattanavis, S., G. Podesta, B. Rajagopalan, and R. W. Katz, 2007. A semiparametric multivariate and multisite weather generator, *Water Resources Research* 43, W11401.

Arnold, J.G., P.M. Allen, M. Volk, J.R. Williams, D.D. Bosch, 2010. Assessment of different representations of spatial variability on SWAT model performance, *Transaction of ASABE*, 53 1433-1443.

Arnold, J.G., R. Srinivasan, R.S. Muttiah, J.R. Williams, 1998. Large area hydrologic modeling and assessment part 1: Model development, *JAWRA Journal of the American Water Resources Association*, 34:73-89.

Band, L.E., D. S. Mackay, I. F. Creed, R. Semkin, and D. Jeffries, 1996. Ecosystem processes at the watershed scale: Sensitivity to potential climate change. *Limnology Oceanography* 41, 928–938. doi:10.4319/lo.1996.41.5.0928

Baron, J.S., M.D. Hartman, T.G.F. Kittel, L. E. Band, D. S. Ojima, and R. B. Lammers,1998. Effects of Land Cover, Water Redistribution, and Temperature on Ecosystem Processes in the South Platte Basin. *Ecol. Appl*. 8, 1037–1051, doi: 10.1890/1051-761(1998)008[1037:EOLCWR]2.0.CO;2

Beven, K., and J. Freer, 2001. Equifinality, data assimilation, and uncertainty estimation in mechanistic modelling of complex environmental systems using the GLUE methodology. *Journal of Hydrology* 249, 11–29, doi:10.1016/S0022-1694(01)00421-8

Beven, K., 1986. Runoff Production and Flood Frequency in Catchments of Order n: An Alternative Approach, in: V.K. Gupta, I. Rodríguez-Iturbe, E.F. Wood (Eds.) Scale Problems in Hydrology, Springer Netherlands, pp. 107-131.

Beven, K.J., M.J. Kirkby, 1979. A physically based, variable contributing area model of basin hydrology / Un modèle à base physique de zone d'appel variable de l'hydrologie du bassin versant, *Hydrological Sciences Bulletin*, 24:43-69.

Blöschl, G., S. Ardoin-Bardin, M. Bonell, M. Dorninger, D. Goodrich, D. Gutknecht, D. Matamoros, B. Merz, P. Shand, and J. Szolgay, 2007. At what scales do climate variability and land cover change impact on flooding and low flows? *Hydrologic Processes* 21, 1241–1247. doi:10.1002/hyp.6669

Brantley, S., C. R. Ford, and J.M. Vose, 2013. Future species composition will affect forest water use after loss of eastern hemlock from southern Appalachian forests. *Ecological Appl*. 23, 777–790. doi:10.1890/12-0616.1

Bosch, D.D., J.G. Arnold, M. Volk, P.M. Allen, Simulation of a low-gradient coastal plain watershed using the SWAT landscape model, *Transaction of ASABE*, 53 (2010) 1445-1456.

Boulanger, J.P., F. Martinez, O. Penalba, and E. C. Segura, 2007. Neural Network based daily precipitation generator (NNGEN-P), *Climate Dynamics* 28: 307–324.

Brown, C., W. Werick, W. Leger, and D. Fay, 2011: A decision-analytic approach to managing climate risks: Application to the Upper Great Lakes, *Journal of the American Water Resources Assoc.*, 47(3): 524–534.

Boughton, W., 2004. The Australian water balance model, *Environmental Modelling and Software*, 19:943-956.

Buchanan, B.P., M. Fleming, R.L. Schneider, B.K. Richards, J. Archibald, Z. Qiu, M.T. Walter, 2014. Evaluation of topographic wetness indices across central New York agricultural landscapes, *Hydrology and Earth System Science*, 18:3279-3299.

Buishand T.A., 1978: Some remarks on the use of daily rainfall models. *Journal of Hydrology* 36:295–308.

Buishand, T. A., and T. Brandsma, 2001. Multisite simulation of daily precipitation and temperature in the Rhine basin by nearest-neighbor resampling. *Water Resources Research* 37(11): 2761–2776.

Burns, D.A., J. Klaus, and M. R. McHale, 2007: Recent climate trends and implications for water resources in the Catskill Mountain region, New York, USA. *Journal of Hydrology* 336:155–170.

Chen J., F. Brissette, and P. Zielinski, 2015. Constraining frequency distributions with the probable maximum precipitation for the stochastic generation of realistic extreme events, *Journal of Extreme Events*, DOI: 10.1142/S2345737615500098

Buttle, J.M., P.W. Hazlett, C.D. Murray, I.F. Creed, D.S. Jeffries, R. Semkin, 2001. Prediction of groundwater characteristics in forested and harvested basins during spring snowmelt using a topographic index, *Hydrological Processes*, 15: 3389 - 3407.

Chen J., and F. Brissette, 2014a: Comparison of five stochastic weather generators in simulating daily precipitation and temperature for the Loess Plateau of China. *International Journal of Climatology* 34: 3089–3105.

Chen J., and F. Brissette, 2014b: Stochastic generation of daily precipitation amounts: review and evaluation of different models. *Climate Research* 59:189-206.

Chen, J., F. Brissette, R. Leconte and A. Caron, 2012: A versatile weather generator for daily precipitation and temperature. *Transactions of the American Society of Agricultural and Biological Engineers* 55(3), 895-906.

Cole, T.M., and S.A. Wells, 2013. CE-QUAL-W2: A Two-Dimensional, Laterally Averaged, Hydrodynamic and Water Quality Model, Version 3.71, Department of Civil and Environmental Engineering, Portland State University, Portland, Oregon.

Daly, C., M. Halbleib, J.I. Smith, W.P. Gibson, M.K. Doggett, G.H. Taylor, J. Curtis, P.P. Pasteris, Physiographically sensitive mapping of climatological temperature and precipitation across the conterminous United States, *International Journal of Climatology*, **28** (2008) 2031-2064.

DeGaetano, A. T., and C. M. Castellano, 2013. Recent and future changes in extreme rainfall in the Catskills region of New York. *Annals of the New York Academy of Sciences*, 1298: 43–51.

Doerr, S. M., E. M., Owens, R. K., Gelda, M. T. Auer, and S. W. Effler, 1998. Development and Testing of a Nutrient-Phytoplankton Model for Cannonsville Reservoir. *Lake and Reservoir Management* 14(2-3):301-321.

Dunne, T., and R.D. Black, 1970. Patial area contributions to storm runoff in a small New England watershed, *Water Resource Research* 6:1296-1311.

Dunne, T., L. Leopold, 1978. Water in Environmental Planning, W.H. Freeman: New York.

Easton, Z.M., D.R. Fuka, M.T. Walter, D.M. Cowan, E.M. Schneiderman, T.S. Steenhuis, 2008. Re-conceptualizing the soil and water assessment tool (SWAT) model to predict runoff from variable source areas, *Journal of Hydrology*, 348:279-291.

Gabriel, K.R. and J. Neumann, 1962: A Markov chain model for daily rainfall occurrence at Tel Aviv. *Quarterly Journal of the Royal Meteorological Society* 88: 90–95.

Ganguly, S., R. R. Nemani, G. Zhang, H. Hashimoto, C. Milesi, A. Michaelis, W. Wang, P. Votava, A. Samanta, F. Melton, J. L. Dungan, E. Vermote, F. Gao, Y. Knyazikhin, and R. B. Myneni, 2012. Generating global Leaf Area Index from Landsat: Algorithm formulation and demonstration. *Remote Sens. Environ*. 122, 185–202. doi:10.1016/j.rse.2011.10.032

Ganguly, S., M. A. Schull, A. Samanta, N. V. Shabanov, C. Milesi, R.R. Nemani, Y. Knyazikhin, and R. B. Myneni, 2008. Generating vegetation leaf area index earth system data record from multiple sensors. Part 1: Theory. *Remote Sens. Environ*. 112, 4333–4343. doi:10.1016/j.rse.2008.07.014

Gassman, P.W., M.R. Reyes, C.H. Green, J.G. Arnold, 2007. The Soil and Water Assessment Tool: Historical development, applications, and future research directions, *Transactions of the ASABE*, 50:1211-1250.

Gburek, W.J., C.C. Drungil, M.S. Srinivansan, B.A. Needelman, D.E. Woodward, 2002. Variable-source-area controls on phosphorus transport: Bridging the gap between research and design, *Journal of Soil and Water Conservation*, 57:534-543.

Gelda, R. K., E. M., Owens, S. W. Effler, and J. M. Hassett, 1998. Calibration, Verification, and an Application of a Two-Dimensional Hydrothermal Model [CE-QUAL-W2(t)] for Cannonsville Reservoir. *Lake and Reservoir Management* 14(2-3):186-196.

Gelda, R.K., and S.W. Effler, 2007. Modeling Turbidity in a Water Supply Reservoir: Advancements and Issues. *Journal of Environmental Engineering* 133(2):139-148.

Gelda, R.K., S.W. Effler, F. Peng, E.M. Owens, and D.C. Pierson, 2009. Turbidity model for Ashokan Reservoir, New York: Case Study. *Journal of Environmental Engineering* 135(9):885-895.

Gelda, R.K., S. W. Effler, and F. Peng, 2012. Modeling turbidity and the effects of alum application for a water supply reservoir. *Journal of Environmental Engineering* 138(1):38-47.

Gelda, R.K., S.W. Effler, A.R. Prestigiacomo, F. Peng, A.J.P. Effler, B.A. Wagner, M.G. Perkins, D.M. O'Donnell, S.M. O'Donnell, and D.C. Pierson, 2013. Characterizations and modeling of turbidity in a water supply reservoir following an extreme runoff event. *Inland Waters* 3(3):377-390.

Geng, S., J.S. Auburn, E. Brandstetter, and B. Li, 1988: A Program to Simulate Meteorological Variables: Documentation for SIMMETEO, Agronomy Progress Report 204. Department of Agronomy and Range Science, University of California, Davis.

Grabs, T., J. Seibert, K. Bishop, and H. Laudon, 2009. Modeling spatial patterns of saturated areas: A comparison of the topographic wetness index and a dynamic distributed model. *Journal of Hydrology*, 373(1), 15-23

Green, H.W., and G.A. Ampt, 1911. Studies on soil physics, *The Journal of Agricultural Science*, 4:1-24.

Güntner, A., J. Seibert, and S. Uhlenbrook, 2004. Modeling spatial patterns of saturated areas: An evaluation of different terrain indices, *Water Resources Research* 40, doi:10.1029/2003WR002864.

Gupta, H.V., S. Sorooshian, and P.O. Yapo, 1999. Status of automatic calibration for hydrologic models: Comparison with multilevel expert calibration, *Journal of Hydrologic Engineering*, 4**:**135-143.

Hanson, C.L. and G.L. Johnson, 1998. GEM (Generation of Weather Elements for Multiple Applications): Application in Areas of Complex Terrain. Hydrology, Water Resources and Ecology in Headwaters IAHS 248:27-32.

Harpold, A.A., D. A. Burns, T. Walter, S. B. Shaw, and T. S. Steenhuis, 2010. Relating hydrogeomorphic properties to stream buffering chemistry in the Neversink River watershed, New York State, USA. *Hydrologic Processes* 24:3759–3771. doi:10.1002/hyp.7802

Harpold, A.A., S.W. Lyon, P.A. Troch, and T.S. Steenhuis, 2010. The hydrological effects of lateral preferential flow paths in a glaciated watershed in the Northeastern USA, *Vadose Zone Journal*, 9**:**397-414.

Hazen and Sawyer. 2013. Operations Support Tool development documentation. Contract Cat-330. Catskill Turbidity Control Study - Design services for the development of an operations support tool. Report prepared for New York City Department of Environmental Protection.

Hipsey, M. R., L. C. Bruce, and D. P. Hamilton, 2014. GLM - General Lake Model: Model overview and user information. AED Report #26, University of Western Australia, Perth, Australia. 42pp.

Hjerdt, K.N., J.J. McDonnell, J. Seibert, and A. Rodhe, 2004. A new topograpic index to quantify downslope controls on local drainage, *Water Resource Research*, 40, doi:10.1029/2004WR003130.

Horton, R.E., 1933. The role of infiltartion in the hydrologic cycle, *Transactions of American Geophysical Union* 14:446-460.

Horton, R.E., 1940. An approach toward a physical interpretation of infiltration capacity, *Soil Science Society of America Proceedings* 4:339-417.

Hwang, T., L. E. Band, J. M. Vose, and C. Tague, 2012. Ecosystem processes at the watershed scale: Hydrologic vegetation gradient as an indicator for lateral hydrologic connectivity of headwater catchments. *Water Resources Research* 48, W06514. doi:10.1029/2011WR011301

Iorgulescu, I., and J.P. Jordan, 1994. Validation of TOPMODEL on a small Swiss catchment, *Journal of Hydrology*, 159:255-273.

Ison N.T., A. M. Feyerherm, and L. D. Bark, 1971: Wet period precipitation and the Gamma distribution. *Journal of Applied Meteorology* 10(4): 658–665.

Katz, R.W. 1977: Precipitation as a chain-dependent process. *Journal of Applied Meteorology* 16, 671–76.

King, L. M., A. I. McLeod, and S. P. Simonovic, 2015. Improved Weather Generator Algorithm for Multisite Simulation of Precipitation and Temperature. *Journal of the American Water Resources Association* 51(5): 1305-1320.

Kuo, W.L., T.S. Steenhuis, C.E. McCulloch, C.L. Mohler, D.A. Weinstein, S.D. DeGloria, 1999. Effect of grid size on runoff and soil moisture for a variable-source-area hydrology model, *Water Resources Research*, 35**:**3419-3428.

Lawrence, G.B., G. M. Lovett, and Y. H. Baevsky, 2000. Atmospheric deposition and watershed nitrogen export along an elevational gradient in the Catskill Mountains, New York. *Biogeochemistry* 50, 21–43. doi:10.1023/A:1006332230890

Li, C., V. P. Singh, and A. K. Mishra, 2012. Simulation of the entire range of daily precipitation using a hybrid probability distribution. *Water Resources Research* 48, W03521.

Liang, X., and D.P. Lettenmaier, 1994. A simple hydrologically based model of land surface water and energy fluxes for general circulation models. *Journal of Geophysical Research: Atmospheres* 99:14415-14428.

Liu, Y.B., Y. Li, O. Batelaan, F. De Smedt, 2005. Assessing grid size effects on runoff and flow response using a GIS-Based hydrologic model, in: S.N. Li, V. Tao (Eds.) Proceeding of the 13th International Conference on Geoinformatics, Toronto, Canada.

Lyon, S.W., M.T. Walter, P. Gérard-Marchant, and T.S. Steenhuis, 2004. Using a topographic index to distribute variable source area runoff predicted with the SCS curve-number equation, *Hydrological Processes*, 18**:**2757-2771.

Matonse, A.H., D. C. Pierson, A. Frei, M.S. Zion, A. Anandhi, E, M, Schneiderman, and B. Wright, 2013. Investigating the impact of climate change on New York City's primary water supply. *Climatic Change* 116:437-456.

Matonse, A.H., D. C. Pierson, A. Frei, M. S. Zion, E. M. Schneiderman, A. Anandhi, R. Mukundan, and S. M. Pradhanang, 2011. Effects of changes in snow pattern and the timing of runoff on NYC water supply system. *Hydrologic Processes* 25, 3278–3288. doi:10.1002/hyp.8121

Matonse, A., and A. Frei, 2011. Application of SWAT model to assess snowpack development and streamflow in the Cannonsville watershed, New York, USA. *Hydrological Processes* 25:3268-3277.

Mein, R.G., and C.L. Larson, 1973. Modeling infiltration during a steady rain, *Water Resources Research*, 9**:**384-394.

Molnar, D.K., and P.Y. Julien, 2000. Grid size effects on surface runoff modeling, *Journal of Hydrologic Engineering* 5**:**8-16.

Moore, R., 2007. The PDM rainfall-runoff model, *Hydrology and Earth System Sciences Discussions*, 11**:** 483-499.

Moore, R.D., and J.C. Thompson, 1996. Are Water Table Variations in a Shallow Forest Soil Consistent with the TOPMODEL Concept?, *Water Resources Research* 32**:**663-669.

Moriasi, D.N., J.G. Arnold, M.W. Van Liew, R.L. Bingner, R.D. Harmel, T.L. Veith, 2007. Model evaluation guidelines for systematic quantification of accuracy in watershed simulations, *Transactions of the ASABE* 50**:**885-900.

Nash, J.E., and J. V. Sutcliffe, 1970. River flow forecasting through conceptual models part I — A discussion of principles. *Journal of Hydrology* 10, 282–290. doi:10.1016/0022-1694(70)90255-6

Neitsch, S.L., J.G. Arnold, J.R. Kiniry, and J.R. Williams, 2011. Soil and Water Assessment tool theoretical documentation version 2009, in, Texas Water Resources Institute, Texas.

Nicks A.D., Gander G.A., 1994: CLIGEN: a weather generator for climate inputs to water resource and other model. In Proceedings of the 5th International Conference on Computers in Agriculture. American Society of Agricultural Engineers, St. Joseph, MI, 3–94.

NYSDOH [New York State Department of Health], 2014. New York City Filtration Avoidance Determination. Final Revised 2007 FAD. 99 p. http://www.health.ny.gov/environmental/water/drinking/nycfad/docs/final_revised_2007_fad_may_2014.pdf.

Owens, E.M., R. K. Gelda, S. W. Effler and J. M. Hassett, 1998a. Hydrologic Analysis and Model Development for Cannonsville Reservoir. *Lake and Reservoir Management*, 14(2-3):140-151.

Owens, E.M., 1998b. Development and Testing of One-Dimensional Hydrothermal Models of Cannonsville Reservoir. *Lake and Reservoir Management*, 14(2-3):172-185.

Pradhanang, S. M., A. Anandhi, R. Mukundan, M. S. Zion, D. C. Pierson, E. M. Schneiderman, A. Matonse and A. Frei, 2011. Application of SWAT model to assess snowpack development and streamflow in the Cannonsville watershed, New York, USA. *Hydrological Processes* 25:3268-3277.

Pradhanang, S. M., R. Mukundan, E. M. Schneiderman, M. S. Zion, A. Anandhi, D. C. Pierson, A. Frei, Z. M. Easton, D. Fuka, and T.S. Steenhuis, 2013. Streamflow Responses to Climate Change: Analysis of Hydrologic Indicators in a New York City Water Supply Watershed. *Journal of the American Water Resources Association* 49(6):1308-1326.

Prodanovic, P. and S.P. Simonovic, 2008. Intensity Duration Frequency Analysis under Changing Climatic Conditions. In: *4th International Symposium on Flood Defense: Managing Flood Risk, Reliability and Vulnerability*. S.P. Simonovic and P. Bourget (Editors), Toronto, Canada.

Rathjens, H., N. Oppelt, D.D. Bosch, J.G. Arnold, M. Volk, 2015. Development of a grid-based version of the SWAT landscape model, *Hydrological Processes*, 29**:**900-914.

Report, S.I., 2008. Effects of Forest Harvesting on Ecosystem Health in the Headwaters of the New York City Water Supply , Catskill Mountains , New York Scientific Investigations Report 2008–5057.

Richardson, J.J., L. M. Moskal, and S.-H. Kim, 2009. Modeling approaches to estimate effective leaf area index from aerial discrete-return LIDAR. *Agric. For. Meteorol*. 149:1152–1160. doi:10.1016/j.agrformet.2009.02.007

Rode, M., G. Arhonditsis, D. Balin, T. Kedebe, V. Krysanova, A. Van Griensven, S.E.A.T.M. van der Zee, 2010. New challenges in Integrated Water Quality Modeling, *Hydrological Processes*, 24**:**3447-3461.

Running, S.W., R. R. Nemani, and R.D. Hungerford, 1987. Extrapolation of synoptic meteorological data in mountainous terrain and its use for simulating forest evapotranspiration and photosynthesis. *Canadian. Journal Forest Res.* 17:472–483. doi:10.1139/x87-081

Qian, B., S. Gameda, H. Hayhoe, R. De Jong, and A. Bootsma, 2004. Comparison of LARS-WG and AAFC-WG Stochastic Weather Generators for Diverse Canadian Climates. *Climate Research* 26:175-191

Rajagopalan, B., and U. Lall, 1999: A k-nearest-neighbor simulator for daily precipitation and other weather variables, Water Resources Research 35(10): 3089–3101.

Ray, P. A., and C. M. Brown, 2015. Confronting Climate Uncertainty in Water Resources Planning and Project Design: The Decision Tree Framework. World Bank, Washington, DC.

Richardson C.W., and D.A. Wright DA. 1984. WGEN: a model for generating daily weather variables. Publ. ARS-8, Agricultural Research Service, US Department of Agriculture.

Richardson, C.W. 1981: Stochastic simulation of daily precipitation, temperature, and solar radiation. *Water Resources Research* 17:182–90.

Roldan, J., and D. A. Woolhiser, 1982: Stochastic daily precipitation models. 1. A comparison of occurrence processes. *Water Resources Research* 18:1451–1459.

Rossi, N., L. DeCristofaro, S. Steinschneider, C. Brown, and R. Palmer, 2015. Potential Impacts of Changes in Climate on Turbidity in New York City's Ashokan Reservoir. *Journal of Water Resources Planning and Management*, 10.1061/(ASCE)WR.1943-5452.0000614, 04015066.

Schneiderman, E.M., T.S. Steenhuis, D.J. Thongs, Z.M. Easton, M.S. Zion, A.L. Neal, G.F. Mendoza, and M. Todd Walter, 2007. Incorporating variable source area hydrology into a curve-number-based watershed model, *Hydrological Processes* 21**:**3420-3430.

Seibert, J., K. Bishop, A. Rodhe, and J.J. McDonnell, 2003. Groundwater dynamics along a hillslope: A test of the steady state hypothesis, *Water Resource Research*, 39(1)**:**2-1 - 2-9.

Semenov, M.A., and E. M. Barrow 1997: Use of stochastic weather generator in the development of climate change scenarios. *Climate Change* 35:397–414.

Semenov, M.A., and E. M. Barrow, 2002. LARS-WG, A Stochastic Weather Generator for Use in Climate Impact Studies, User Manual http://www.rothamsted.ac.uk/mas-models/download/LARS-WGManual.pdf

Sharif, M. and D.H. Burn, 2007. Improved k-Nearest Neighbor Weather Generating Model. *Journal of Hydrologic Engineering* 12:42-51.

Sharma, A., D. G. Tarboton, and U. Lall, 1997. Streamflow simulation: A nonparametric approach. *Water Resources Research*, 33(2): 291-308.

Singh, J., H.V. Knapp, and M. Demissie, 2004. Hydrologic modeling of the Iroquois River watershed using HSPF and SWAT, in: Illinois State Water Survey Contract Report 2004-08, Champaign. Available at: www.sws.uiuc.edu/pubdoc/CR/ISWSCR2004-08.pdf.

Sivapalan, M., R.A. Woods, and J.D. Kalma, 1997. Variable bucket representation of TOPMODEL and investigation of the effects of rainfall heterogeneity, *Hydrological Processes*, 11**:**1307-1330.

Soltani, A. and G. Hoogenboom, 2003. A Statistical Comparison of the Stochastic Weather Generators WGEN and SIMMENTO. *Climate Research* 24:215-230, doi:10.3354/cr024215.

Srikanthan, R., McMahon, T., 2001: Stochastic generation of annual, monthly and daily climate data: A review. *Hydrology and Earth System Sciences Discussions*, 5(4): 653-670.

Steenhuis, T.S., M. Winchell, J. Rossing, J.A. Zollweg, and M.F. Walter, 1995. SCS runoff equation revisited for variable-source runoff areas, *Journal of Irrigation and Drainage Engineering* 121**:**234-238.

Stepczuk, C. L., E. M. Owens, S. W. Effler, J.A. Bloomfield, and M. T. Auer, 1998. A Modeling Analysis of THM Precursors for a Eutrophic Reservoir. *Lake and Reservoir Management* 14(2-3):367-378.

Stockle, C.O., G. S. Campbell, and R. Nelson, 1999: ClimGen Manual: Dept. of Biological Systems Engineering, Washington State University, Pullman, WA.

Steinschneider, S., and C. Brown, 2013: A semiparametric multivariate, multisite weather generator with low-frequency variability for use in climate risk assessments, *Water Resources Research* 49:7205–7220.

Tague, C.L., and L. E. Band, 2004. RHESSys: Regional Hydro-Ecologic Simulation System—An Object-Oriented Approach to Spatially Distributed Modeling of Carbon, Water, and Nutrient Cycling. *Earth Interact*. 8:1–42. doi:10.1175/1087-3562(2004)8<1:RRHSSO>2.0.CO;2

Tang, G., T. Hwang, and S. M. Pradhanang, 2014. Does consideration of water routing affect simulated water and carbon dynamics in terrestrial ecosystems? *Hydrol. Earth Syst. Sci*. 18, 1423–1437. doi:10.5194/hess-18-1423-2014.

Tarboton, D.G., 1997. A new method for the determination of flow directions and upslope areas in grid digital elevation models, *Water Resources Research* 33**:**309-319.

Tarboton, D.G., and I.N. Mohammed, 2010. TauDEM 5.1 Quick Start Guide to Using the TauDEM ArcGIS Toolbox.

Todorovic, P., and D. A. Woolhiser, 1975. A stochastic model for n-day precipitation. *Journal of Applied Meteorology* 14(1): 17–24.

Troch, P.A., M. Mancini, C. Paniconi, E.F. Wood, 1993. Evaluation of a distributed catchment scale water balance model, *Water Resource Research* 29**:**1805 - 1817.

Upstate Freshwater Institute, 2013. Implementation of Rondout Reservoir Model in Operation Support Tool. Prepared for New York City Department of Environmental Protection and Hazen & Sawyer, by Upstate Freshwater Institute, Syracuse, NY.

USDA-SCS, National Engineering Handbook, Natural Resources Conservation Service, U.S. Department of Agriculture, 1972.

USDA, 2006. Soil Survey of Delaware County, New York.

Walter, M., V. Mehta, A. Marrone, J. Boll, P. Gérard-Marchant, T. Steenhuis, and M. Walter, 2003. Simple Estimation of Prevalence of Hortonian Flow in New York City Watersheds. *Journal of Hydrologic Engineering* 8**:**214-218.

Walter, M.T., M.F. Walter, E.S. Brooks, T.S. Steenhuis, J. Boll, and K. Weiler, 2000. Hydrologically sensitive areas: Variable source area hydrology implications for water quality risk assessment, *Journal of Soil and Water Conservation* 55**:**277-284.

White, E.D., Z.M. Easton, D.R. Fuka, A.S. Collick, E. Adgo, M. McCartney, S.B. Awulachew, Y.G. Selassie, and T.S. Steenhuis, 2011. Development and application of a physically based landscape water balance in the SWAT model, *Hydrological Processes* 25**:**915-925.

Wigmosta, M.S., and D.P. Lettenmaier, 1999. A comparison of simplified methods for routing topographically driven subsurface flow, *Water Resource Research* 35**:**255-264.

Wilby, R. L., and S. Dessai, 2010: Robust adaptation to climate change, *Weather* 65(7): 180–185.

Wiley, M. W., and R. N. Palmer, 2008: Estimating the impacts and uncertainty of climate change on a municipal water supply system, *Journal of Water Resources Planning and Management* 134(3): 239–246.

Wilks, D. S., and R. L. Wilby, 1999: The weather generation game: A review of stochastic weather models, *Progress Physical Geography* 23, 329–357.

Wilks, D.S. 1992. Adapting stochastic weather generation algorithms for climate change studies. *Climatic Change* 22: 67–84.

Wilks, D.S. 1999: Interannual variability and extreme-value characteristics of several stochastic daily precipitation models. *Agricultural and Forest Meteorology* 93: 153–69.

Wood, E.F., D.P. Lettenmaier, and V.G. Zartarian, 1992. A land-surface hydrology parameterization with subgrid variability for general circulation models, *Journal of Geophysical Research: Atmospheres* 97**:**2717-2728.

Woodbury, J.D., C.A. Shoemaker, Z.M. Easton, and D.M. Cowan, 2014. Application of SWAT with and without Variable Source Area Hydrology in a large watershed, *Journal of the American Water Resources Association* 50**:**42-56.

Yates, D., S. Gangopadhyay, B. Rajagopalan, and K. Strzepek, 2003: A technique for generating regional climate scenarios using a nearest-neighbor algorithm. *Water Resources Research* 39(7)**:**1-14.

Young, K. C., 1994: A multivariate chain model for simulating climatic parameters with daily data. *Journal of Applied Meteorology* 33(6): 661-671.

Zierl, B., H. Bugmann, and C. L. Tague, 2007. Water and carbon fluxes of European ecosystems: an evaluation of the ecohydrological model RHESSys. *Hydrologic Processes* 21, 3328–3339. doi:10.1002/hyp.6540

Zhao, R., X. Liu, and V. Singh, 1995. The Xinanjiang model, *Computer Models of Watershed Hydrology* 215-232.

Zion, M.S., S. M. Pradhanang, D. C. Pierson, A. Anandhi, D. G. Lounsbury, A. H. Matonse, and E. M. Schneiderman, 2011. Investigation and Modeling of winter streamflow timing and magnitude under changing climate conditions for the Catskill Mountain region, New York, USA. *Hydrologic Processes* 25, 3289–3301. doi:10.1002/hyp.8174

Zollweg, J.A., W.J. Gburek, and T.S. Steenhuis, 1996. SmoRMod - A GIS integrated rainfall runoff model, *Transaction of ASAE* 39**:**1299-1307.